Doctoral Dissertation

Estimation of Internal Solitary Waves Parameters and Effects of Long-term Variations using Satellite Data in the Indonesian Seas

インドネシア海域における衛星データを用いた内部波の推定とその長期変動の影響について

March 2026

CHONNANIYAH

Graduate School of Sciences and Technology for Innovation

Yamaguchi University

Acknowledgements

This doctoral dissertation was completed with the support and assistance of many individuals and institutions, to whom I would like to express my sincere gratitude. First and foremost, I express my profound appreciation to Allah SWT and send blessings upon Prophet Muhammad SAW for granting me the strength, patience, and guidance throughout this journey to reach a higher level of knowledge.

I would like to extend my sincere appreciation to my supervisor, Prof. Takahiro Osawa, for his invaluable guidance, unwavering support, and academic mentorship. His profound expertise, insightful feedback, and continuous encouragement played a pivotal role in shaping this research and bringing the dissertation to completion. I am also deeply grateful to my graduate committee members, Prof. Keiji Imaoka, Prof. Koji Asai, Prof. Shinsuke Mochizuki, and Prof. Hidenori Shingin, whose constructive comments and critical insights significantly enhanced the quality and rigor of this work. I am truly thankful to Dr. Abd. Rahman As-syakur for his guidance, supervision, and generous assistance during my research activities in Bali.

I gratefully acknowledge the Japan Society for the Promotion of Science (JSPS) Ronpaku Program for the generous financial support that made it possible for me to pursue and complete my doctoral studies at Yamaguchi University. I also sincerely thank the Institute of Science and Technology of Nahdlatul Ulama Bali (ISTNUBA) for its institutional support and for providing a supportive and stimulating academic environment in which this research could be conducted.

To my beloved family, I owe my deepest and most heartfelt gratitude. Words are insufficient to express my appreciation for your constant prayers, unconditional love, and unwavering patience. Thank you for granting me the freedom to think independently and the courage to explore the world you may never have imagined yet always believed I could reach. Your faith in me has been the greatest source of strength and inspiration throughout this journey.

Finally, I would like to extend my sincere appreciation to all individuals who have contributed, directly or indirectly, to the completion of this dissertation. Each contribution, in its own way, has made this academic milestone both possible and meaningful.

Preface

This dissertation is being submitted to Yamaguchi University, Graduate School of Sciences and Technology for Innovation, in partial fulfilment of the Doctor of Philosophy degree requirements. The dissertation is the author's original contribution, and relevant references are provided in the dissertation itself, wherever the author has used results or data from previous studies.

The publications published during the research which have contributed significantly to the chapters of this dissertation are as follows:

[1] Peer-reviewed Journal Paper

a. **On the Distinction of Seasonal Internal Solitary Waves Characteristics in the Lombok Strait Based on Multi-satellite Data**

   Chonnaniyah, Takahiro Osawa, Abd Rahman As-syakur, I W.G.A. Karang, and Jose C.B. da Silva

   Journal: International Journal of Remote Sensing

   Publication: Vol. 45, Issue 23, 2023, Pages 8742–8757
   https://doi.org/10.1080/01431161.2023.2242592

b. **Surface Manifestation Characteristics of Internal Solitary Waves Observed by GCOM-C/SGLI Imagery**

   Chonnaniyah, Eko Siswanto, Abd. Rahman As-syakur, and Takahiro Osawa

   Journal: Journal of Sea Research

   Publication: Vol. 202, Issue 2024 (102541), Pages 1-12
   https://doi.org/10.1016/j.seares.2024.102541

c. **Estimation of Internal Solitary Waves Propagation Speeds using Long-term Sentinel-1 SAR Data in the Lombok Strait, Indonesia**

   Chonnaniyah, Abd Rahman As-syakur, I Made Dharma Raharja, and Takahiro Osawa

   Journal: IEEE Journal of Selected Topics in Applied Earth Observations and Remote Sensing

   Publication: Vol. 18, 2025, Pages 13770 – 13777
   https://doi.org/10.1109/JSTARS.2025.3568845

[2] Peer-reviewed Conference Paper

a. **Effect of Internal Solitary Waves on Coastal Interaction in The Lombok Strait using Multi-satellite Data**

   Chonnaniyah, Takahiro Osawa, I W.G.A Karang, Abd Rahman As-syakur & Jose C. B. da Silva

   Proceeding: 15th Pan Ocean Remote Sensing Conference (PORSEC) 2022 December 7-8, 2022. Universiti Teknologi Malaysia (UTM), Johor Bahru, Malaysia.

   Publication: Vol. II, 2023.

b. **Seasonal Variability of Internal Solitary Waves Phase Speed in the Lombok Strait Revealed by Sentinel-1 SAR**

   Proceeding: 8th Asia-Pacific Conference on Synthetic Aperture Radar (APSAR) 2023, October 23-27, 2023. Bali-Indonesia

   Publication: IEEE Xplore, 2024
   https://doi.org/10.1109/APSAR58496.2023.10388730

Summary

Internal Solitary Waves (ISWs) are nonlinear internal wave phenomena that propagate within the ocean interior and play a critical role in ocean mixing, nutrient transport, and sediment redistribution. Although they exist primarily below the sea surface, ISWs can significantly influence upper-ocean conditions by modulating surface roughness, temperature, and optical properties. These surface expressions enable their detection using satellite remote sensing. The Indonesian Seas, characterized by strong tidal forcing, complex bathymetry, and pronounced monsoonal variability, represent one of the most active regions globally for ISW generation. Despite their frequent occurrence and large amplitudes, the long-term variability, spatial distribution, and connections between ISWs and large-scale climate oscillations in this region remain insufficiently characterized. This dissertation addresses these gaps through an integrated multi-satellite remote sensing framework to detect, characterize, and quantify ISW properties, with the Lombok Strait as a focal region of intense activity. The originality of this study is based on the integration of optical, thermal, and radar satellite observations spanning nearly a decade to examine ISW surface expressions, propagation characteristics, and seasonal to interannual variability. This long-term, multi-sensor approach provides the first comprehensive assessment of ISW dynamics in the Indonesian Seas and advances understanding of their behavior in a complex tropical environment.

The study first investigates how ISWs manifest at the sea surface and become observable in optical satellite imagery. Using data from the Global Change Observation Mission–Climate (GCOM-C) Second-generation Global Imager (SGLI), ISWs are shown to appear as quasi-linear, alternating bright and dark bands resulting from modulations of surface roughness that affect sunlight reflection. Consistent ISW signatures are identified across multiple spectral products, including top-of-atmosphere radiance, ocean color, and sea surface temperature (SST). This consistency demonstrates that ISWs exert a measurable influence on both optical and thermal satellite-derived parameters. These findings challenge the traditional assumption that internal waves are purely subsurface processes with negligible surface impact. Instead, they demonstrate that ISWs influence upper-ocean thermodynamics and air–sea energy exchange. Consequently, this study underscores the importance of accounting for ISW-related anomalies in ocean color and SST datasets to prevent misinterpretation in large-scale climatological and biogeochemical analyses, particularly in regions of strong internal wave activity.

Building on the characterization of ISW surface manifestations, the dissertation quantifies their propagation characteristics and long-term variability using a nine-year archive of Sentinel-1 synthetic aperture radar (SAR) imagery. The all-weather capability and sensitivity of SAR to surface roughness enable consistent monitoring of ISWs across seasons and years. By integrating SAR detections with tidal model outputs, ISW propagation speeds and occurrence frequencies are estimated. Statistical analyses reveal a

moderate positive correlation between ISW activity and the Indian Ocean Dipole (IOD) ($r = 0.365$) and a moderate negative correlation with the El Niño–Southern Oscillation (ENSO) ($r = -0.30$). These relationships indicate that large-scale climate oscillations modulate ISW generation through variations in ocean stratification and thermocline depth. Spectral analysis further identifies dominant variability at approximately 12- and 54-month periods, corresponding to monsoonal and interannual climate variability, respectively. This provides the first long-term observational evidence that ISW dynamics in the Lombok Strait are influenced by both regional monsoon systems and global climate modes.

To further resolve seasonal contrasts, this study integrates radar and optical observations from Sentinel-1, GCOM-C/SGLI, and Terra/MODIS satellites. Results show that ISWs occur more frequently during the northwest monsoon, often forming multiple solitons within a single wave packet, reflecting enhanced generation under stronger stratification and intensified tidal forcing. During the southeast monsoon, ISWs exhibit longer wavelengths, slower phase speeds, and a higher frequency of double-wave packets. Phase speed estimates derived from satellite observations and theoretical calculations based on the Korteweg–de Vries (KdV) equation consistently indicate faster propagation during the northwest monsoon. This seasonal acceleration is associated with a shallower thermocline and stronger density gradients. Concurrently, optical satellite observations reveal higher chlorophyll-a concentrations and increased turbidity during this season, suggesting that ISW-driven mixing and sediment resuspension significantly modulate surface biogeochemical conditions.

Collectively, these results provide a comprehensive understanding of ISW manifestation, propagation, and variability across multiple spatial and temporal scales. The novelty of this dissertation lies not only in its methodological integration of multiple satellite platforms but also in its conceptual contribution to viewing ISWs as dynamic components of the coupled ocean–atmosphere system. The study provides empirical evidence that ISWs influence satellite-derived environmental parameters, emphasizing the need to consider internal wave effects in ocean color and SST climatology. In summary, this dissertation advances understanding of ISW dynamics in the Indonesian Seas by demonstrating their detectability, quantifiable characteristics, and responsiveness to seasonal and climatic drivers. It highlights the Lombok Strait as a critical region for investigating interactions between internal waves and large-scale ocean–climate processes. The integration of multi-sensor satellite observations and long-term datasets also establishes a foundation for future studies using artificial intelligence and data-driven modeling to improve the detection, characterization, and prediction of ISWs. Through its multidisciplinary approach, this research makes a substantial contribution to the field of ocean remote sensing, particularly in the study of internal wave–climate interactions.

要旨（日本語）

本論文は、インドネシア海域、特にロンボク海峡における海洋内部波（Internal Solitary Waves: ISWs）の長期的な変動、空間的分布、及び気候変動との関連性を、リモートセンシングデータを用いて包括的に研究を行ったものである。ISWs は、海洋内部で発生する非線形波であり、海洋混合、栄養塩輸送、堆積物の再分布などに重要な役割を果たしている。従来、ISWs は主に海中の現象と考えられてきたが、内部波が海面の粗さ、海面温度（SST）、光学特性に影響を与えることで衛星データから検出可能である。第一の研究では、可視域衛星データである GCOM-C 衛星の SGLI センサーを用いて、ISWs が光学画像上で交互に明暗の帯として現れることを明らかにした。これは、海面粗さの変化が太陽光の反射に影響を与えるため、大気上端放射、海色、海面温度など複数のスペクトルに一貫して現れており、ISWs が海面上層の熱力学や大気海洋間のエネルギー交換にも影響を与えていることを示している。ISWs は、海表面に影響を及ぼさないという従来の前提から、大規模な気候解析や生物地球化学的分析においても ISWs の影響を考慮する必要性が示された。第二の研究の研究として、合成開口レーダー（SAR）、Sentinel-1 の画像を用いて、9 年間にわたる ISW の伝播特性と長期変動の定量化と海面祖度から、季節・年次を通じた安定的な ISW の検出が可能となった。又、潮汐モデルとの統合により、ISWs の伝播速度と発生頻度を推定し、インド洋ダイポールモード（IOD）との正の相関（r = 0.365）、エルニーニョ・南方振動（ENSO）との負の相関（r = -0.30）が示された。これらの結果は、気候変動が海洋成層構造や躍層の深さが ISW 生成に影響を与えることを示している。また、スペクトル解析の結果から、約 12 ヶ月と 54 ヶ月の周期的変動が確認され、季節的及び気候的要因が ISW 活動に寄与していることが明らかになった。第三の研究として、Sentinel-1、GCOM-C/SGLI、及び、Terra/MODIS の光学・レーダー観測を統合することで、季節間の ISWs 特性の違いを詳細に解析し、北西モンスーン期には ISWs の発生頻度が高く、1 つの波群に複数のソリトンが含まれることが多くなり、一方、南東モンスーン期には、より長い波長、遅い位相速度、2 波構造の波群が多く観測された。ケーディーブイ（KdV）方程式による理論計算と衛星観測に基づく推定では、北西モンスーン期における伝播速度が速いことが示され、これは浅い躍層と強い密度勾配によるものであることが分かった。また、同時期にはクロロフィル a 濃度と濁度が増加し、ISWs による混合や堆積懸濁物が表層の生物地球化学に影響を与えている可能性が示唆された。

本研究の独自性は、複数の衛星データ（光学・熱赤外・レーダー）を長期間にわたり解析と統合により、ISWs の検出、定量化、変動解析を実施した点にあり、ISWs が大気海洋結合系の大きな構成要素として捉える新たな視点を提供し ISWs の影響を考慮する必要性を提唱

し、インドネシア海域、特にロンボク海峡における ISWs の力学的特性、季節的・気候的変動への応答性を明らかにした。又、本研究は、今後の AI やデータ駆動型モデリングを用いた ISWs の検出・予測精度の向上に向けた基盤を築く研究成果であり、内部波と気候の相互作用に関する海洋リモートセンシングの重要な貢献を示した。

Table of Contents

List of Figures

List of Tables

Abbreviations

ACP	Atmospheric Correction Parameters
ADCPs	Acoustic Doppler Current Profilers
ASF DAAC	Alaska Satellite Facility Distributed Active Archive Center
BATNAS	*Batimetri Nasional*
BIG	*Badan Informasi Geospasial*
CDOM	Colored Dissolved Organic Matter
CHLA	Chlorophyll-a concentration
CTD	Conductivity Temperature Depth
DJF	December-January-February
ENSO	El Niño–Southern Oscillation
FFT	Fast Fourier Transform
GCOM-C	Global Change Observation Mission - Climate
GRD	Ground Range Detected
IOD	Indian Ocean Dipole
IRS	Infrared Scanner
ISWs	Internal Solitary Waves
ITF	Indonesian Throughflow
IWPR	In-Water Parameters
IWs	Internal waves
JAXA	Japan Aerospace Exploration Agency
JJA	June-July-August
JPSS-1	Joint Polar Satellite System-1
KdV	Korteweg-de Vries
MAM	March-April-May
MODIS	Moderate Resolution Imaging Spectroradiometer
MSI	Multispectral Instrument
NIR	Near-Infrared
NWLR	Normalized Water Leaving Radiance

NWM	Northwest Monsoon
OCI	Ocean Color Index
ONI	Oceanic Niño Index
PAR	Photosynthetically Available Radiation
RMSE	Root Mean Square Error
SAR	Synthetic Aperture Radar
SEM	Southeast Monsoon
SGLI	Second-generation Global Imager
SNAP	Sentinel Application Platform
SON	September-October-November
SRGI	*Sistem Referensi Geospatial Indonesia*
SS	Suspended Solid concentration
SST	Sea Surface Temperature
SWIR	Shortwave Infrared
TIR	Thermal Infrared
TMD	Tide Model Driver
TOA	Top of Atmosphere
TSM	Total Suspended Matter
UV	Ultraviolet
VIIRS	Visible and Infrared Imager/Radiometer Suite
VNR	Visible and Near-infrared Radiometer
WOA	World Ocean Atlas

CHAPTER 1

Introduction

1.1 Background

Internal waves are a type of wave motion that occurs within the ocean rather than on its surface. Unlike surface waves that can be seen crashing along the shore, internal waves travel beneath the ocean surface, moving along the boundaries between layers of water with different densities. These density layers naturally arise in the ocean owing to variations in temperature and salinity, creating what scientists refer to as stratified fluid. A helpful analogy is a bottle containing two immiscible liquids (such as oil and water) with different densities. When the bottle is tilted or disturbed, slow and gentle waves propagate along the interface between the two layers (Apel, 2002a).

Internal waves are ubiquitous in the oceans and play a vital role in oceanic mixing, nutrient transport, and energy redistribution (Garrett & Kunze, 2007; Munk & Wunsch, 1998). They are generated primarily by tidal flow over topographic features such as ridges, sills, or continental slopes, or by the interaction of currents with abrupt bathymetric changes (Farmer & Armi, 1999). When these internal waves evolve into large-amplitude nonlinear forms, they are referred to as internal solitary waves (ISWs). ISWs can propagate for hundreds of kilometers with remarkable stability, modulating the thermocline and influencing both biological productivity and subsurface circulation patterns (Apel, Holbrook, et al., 1985; Helfrich & Melville, 2006). To illustrate the fundamental structure of internal waves, Figure 1.1 shows how these waves propagate along the interface between two layers of water with different densities. The upper layer, which consists of low-density water, overlies a denser layer. Internal waves form and travel along this boundary, whereas surface waves continue to oscillate above them. Despite their often-invisible nature from the surface, internal waves can induce observable surface manifestations, such as bands of rough and smooth water, which can be detected using remote-sensing instruments.

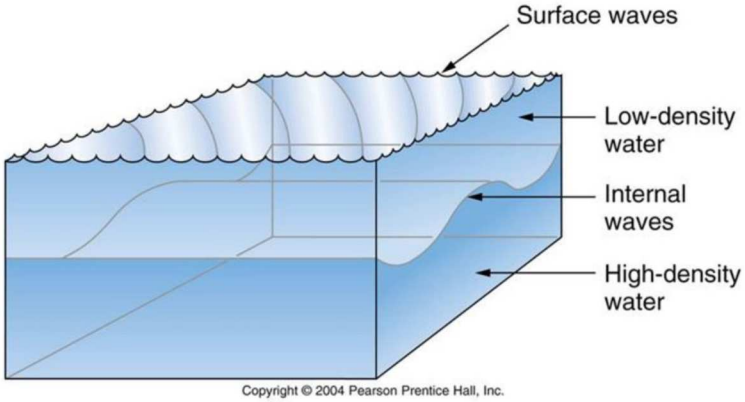

Figure 1.1. Schematic illustration showing surface and internal waves propagating along the interface between layers of low- and high-density water. (Adapted from Pearson Prentice Hall, 2004)

Internal waves have amplitudes that can reach tens to hundreds of meters, far larger than typical surface waves, and wavelengths that can extend over several kilometers. The internal restoring force is gravity acting on the density difference between the two water layers, which means that their dynamics are slower and longer than those of surface waves (Gill, 1982). These waves can be categorized into linear and nonlinear regimes; in strongly stratified regions with large-amplitude oscillations, they exhibit nonlinear behaviors and solitary wave characteristics (Apel, 1988; Shroyer et al., 2010). In tropical archipelagic regions, such as the Indonesian Seas, the generation and propagation of internal solitary waves are enhanced by complex bathymetry and strong tidal currents. The combination of narrow straits, steep topography, and deep basins creates favorable conditions for ISW generation, particularly where strong tidal flows pass through shallow sills or constricted passages (Gordon, 2005; Susanto et al., 2012). These conditions make the Indonesian seas, especially the Lombok, Ombai, and Halmahera Straits, ideal hotspots for studying the dynamics and variability of internal solitary waves.

1.2 Observation and Estimation of Internal Solitary Waves

1.2.1 In-situ Measurements

Traditional approaches to observing internal waves rely on moored instruments, conductivity–temperature–depth (CTD) casts, and Acoustic Doppler Current Profilers (ADCPs). These methods provide detailed vertical profiles of the velocity and density, allowing for the direct observation of the wave amplitude, speed, and structure (Ramp et al., 2004). However, their spatial coverage is limited and sustained multi-year measurements are

expensive and logistically challenging, especially in narrow and deep straits, such as Lombok.

1.2.2 Remote Sensing of Internal Waves

Remote sensing provides an essential means of observing ISWs and their associated surface signatures over vast oceanic regions. Although ISWs propagate beneath the sea surface along density interfaces (pycnoclines), their dynamic coupling with surface layers modulates surface roughness, thermal gradients, and optical reflectance, making them observable from space via satellite. These modulations arise primarily from the convergence and divergence zones formed by internal wave-induced surface currents, which alternately enhance or suppress short gravity-capillary waves (Apel et al., 1985; Klemas, 2012). Consequently, internal waves manifest as quasi-parallel bright and dark bands in radar and optical imagery, representing alternating zones of increased and decreased surface roughness.

Synthetic Aperture Radar (SAR) is one of the most effective tools for internal wave detection because of its ability to image independent of sunlight or cloud cover and its sensitivity to centimeter-scale surface roughness variations (Jackson et al., 2013). The SAR backscatter intensity is modulated by the Bragg scattering mechanism, in which surface roughness elements interact with the radar signal. Regions of surface convergence appear as bright lines owing to enhanced backscatter, whereas divergence zones appear dark because of reduced roughness and wave damping by surface films or surfactants. Sentinel-1, TerraSAR-X, and RADARSAT-2 SAR data have been widely applied to identify internal wave packets, estimate crest length and spacing, and track propagation patterns in coastal and marginal seas (Lund et al., 2013).

Optical and thermal sensors, such as MODIS, GCOM-C/SGLI, and Landsat 8, provide complementary observations in cloud-free conditions. ISWs can modulate optical signals by altering light reflectance and sea surface color due to the redistribution of suspended particles, chlorophyll, and surfactants, or by modifying surface slopes that influence sun glint intensity (Jackson & Alpers, 2010). In thermal infrared imagery, ISWs appear as alternating warm and cool streaks resulting from vertical advection and mixing. These signatures are particularly useful for studying the biological and biogeochemical responses to ISW-induced mixing in tropical seas.

Klemas (2012) emphasized that multi-sensor approaches, combining radar, optical, and thermal imagery, greatly improve the detection and characterization of internal waves.

The integration of different datasets enables a more complete representation of ISW behavior, allowing for the estimation of the wavelength, amplitude, propagation speed, and crest orientation. Furthermore, when coupled with in-situ observations and numerical models such as MITgcm and CROCO, satellite-based methods provide insights into generation mechanisms, energy fluxes, and the relationships between surface manifestations and subsurface stratification (Muacho et al., 2015; Shroyer et al., 2010; S. Zhang et al., 2023).

However, the remote sensing of internal waves is constrained by several factors, including sensor geometry, sea surface wind speed, and environmental conditions. SAR detectability decreases under very low wind conditions (<2 m/s), when Bragg scattering is weak, or under high winds (>10 m/s), which obscure ISW signatures owing to wave breaking and background clutter (Klemas, 2012). Optical visibility is similarly affected by cloud cover, the solar zenith angle, and the degree of surface glint. Consequently, successful ISW detection requires careful selection of satellite data based on the wind and illumination conditions, sensor configuration, and local stratification patterns.

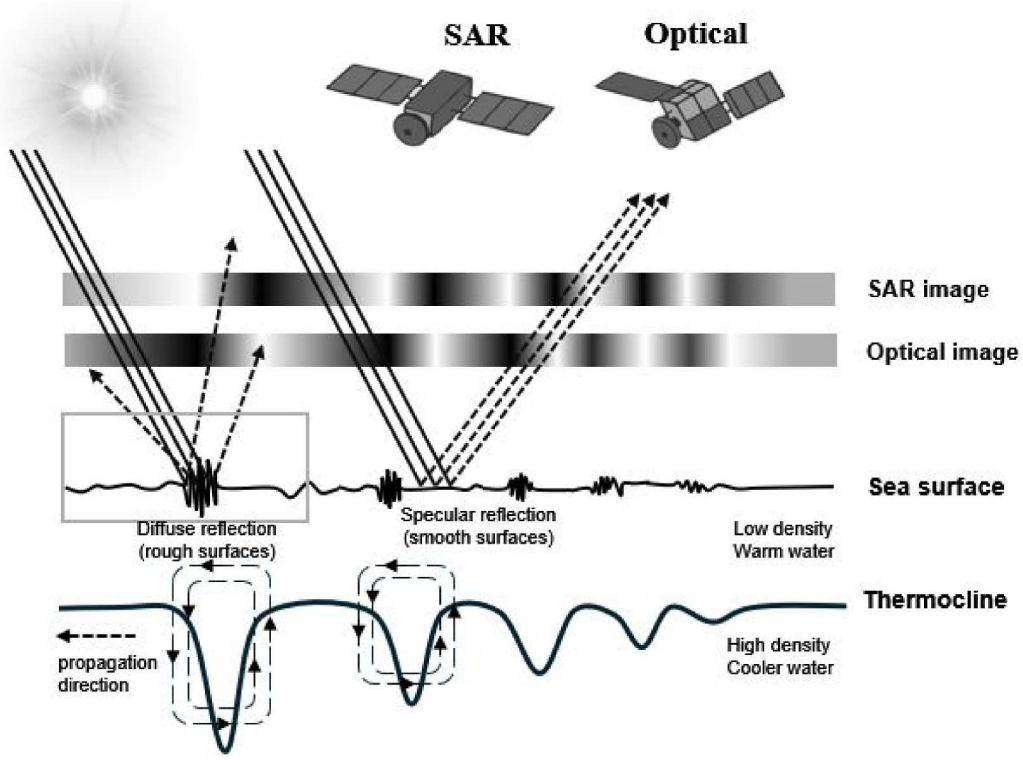

Figure 1.2. Conceptual diagram showing the principles of remote sensing observations of ISWs using SAR and optical sensors. SAR detects variations in surface roughness through radar backscatter, whereas optical systems capture changes in reflectance and color associated with ISW-induced surface modulations (modified from Klemas, 2012).

Figure 1.2 schematically illustrates the remote sensing principles of internal waves using SAR and optical systems. Tidal flow interacting with topographic features generates ISWs that propagate along the pycnocline and modulate sea surface roughness and brightness. SAR sensors record diffuse backscatter from rough surfaces, whereas optical sensors capture specular reflections and variations in brightness owing to surface slope and particulate redistribution. Together, these techniques enable a comprehensive assessment of the internal wave dynamics in the Indonesian Seas.

1.2.3 Parameter Estimation from Surface Signatures

Quantitative retrieval of ISW parameters from satellite imagery remains challenging because surface manifestations indirectly respond to subsurface dynamics. Analytical relationships derived from weakly nonlinear theory (e.g. the Korteweg–de Vries equation) link wave speed and amplitude to stratification and layer depth (Helfrich & Melville, 2006). The estimation of ISW parameters from satellite surface signatures provides crucial insights into their geometric and dynamical characteristics of ISWs. SAR imagery captures the surface roughness variations induced by internal wave-induced surface current modulations, allowing for the quantitative derivation of key ISW properties. As illustrated in Figure 1.3, the bright and dark alternating bands correspond to the convergence and divergence zones at the sea surface, which serve as indicators of the internal wave crests and troughs.

In this analysis, several parameters were derived from the SAR image intensity profile along a transect (***S–S′***) across the wave packets. The soliton number (***a–g***) represents the number of distinct bright lines detected in a packet, which, in this example, corresponds to seven solitons. The first crest length (***D***), measured along the leading bright line (***A–B***), defines the extent of the first internal wavefront and is approximately 100 km. The wavelength (***k***) is determined as the distance between adjacent crests within a single packet, estimated to be approximately 3 km. The propagation direction (***α***) indicates the angle between the crest orientation and the north direction, with an average of approximately 30°, implying a predominant northward propagation pattern toward the Bali Sea.

The phase speed (v) of an ISW packet was estimated using the relation $v = T/L$, where L denotes the distance between the leading solitons of two consecutive packets and T is the semidiurnal tidal period (12.42 hours). This formulation assumes that consecutive packets are generated by successive tidal cycles that interact with the Lombok Strait sill. The estimated parameters collectively describe the ISW morphology and dynamics, linking surface manifestations to subsurface processes such as stratification, tidal forcing, and

throughflow modulation. Moreover, when integrated with in-situ or modelled water column data, these parameters facilitate a comprehensive understanding of the energy flux and wave evolution within the Lombok Strait.

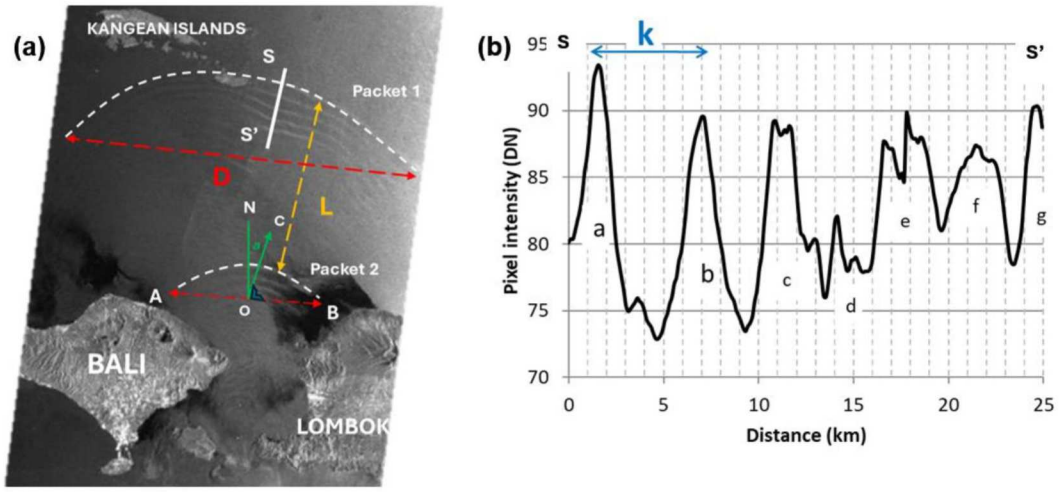

Figure 1.3. Estimation of ISW parameters derived from Sentinel-1 SAR imagery in Lombok Strait. (a) The figure illustrates the crest length (**D**), wavelength (**k**), soliton number (**a–g**), propagation direction (**α**), and phase speed (**v**). (b) The graph shows the pixel intensity variation along transect **S–S′**, which is used to identify soliton structures and measure characteristic parameters. The equation defines the group velocity of wave packets based on the distance (***L***) between consecutive solitons and the semidiurnal tidal period (T = 12.42 h).

1.3 Internal Solitary Waves in the Indonesian Seas

The Indonesian Seas constitute a highly complex network of narrow straits and deep basins that form a critical gateway between the Pacific and the Indian Oceans. Among the most significant features of this region is the ITF, a major low-latitude water mass exchange driven by pressure and density gradients between the Pacific and Indian Oceans (A. Gordon, 2005; Sprintall et al., 2014). As this vigorous flow interacts with steep bathymetric slopes, sills, and constricted passages, combined with strong semidiurnal tides, it leads to the generation of energetic internal tides and their subsequent transformation into nonlinear ISWs (Susanto et al., 2005).

Previous observational and remote-sensing studies have documented frequent ISW activity in several key passages of the Indonesian archipelago, including the Lombok, Ombai, and Lifamatola Straits (Karang et al., 2019b; Purwandana et al., 2023). These solitary waves are understood to play a major role in the vertical mixing and cross-strait exchange of heat, salt, and biogeochemical constituents, thereby influencing the thermocline structure and energy redistribution across the region (Purwandana et al., 2021). However,

despite their importance, comprehensive long-term studies that systematically quantify ISW parameters (e.g. amplitude, phase speed, and occurrence frequency) using satellite remote-sensing archives remain relatively scarce, a gap that this dissertation aims to address.

1.4 The Lombok Strait: A Key Region for ISWs

1.4.1 Geometry and Oceanography of the Lombok Strait

The Lombok Strait is one of the most important passages in the Indonesian Seas, serving as a major pathway for the ITF, which transports warm Pacific Ocean water into the Indian Ocean (Gordon et al., 2010; Sprintall et al., 2014). Located between the Bali and Lombok Islands, the strait spans approximately 35 km in width, with a north–south orientation that connects the deeper Flores Sea in the north to the Indian Ocean in the south. Its complex bathymetry, steep slopes, and constricted topography make it a highly dynamic region where strong tidal currents interact with the seabed, creating favorable conditions for the generation of ISWs (Susanto et al., 2012; Nugroho et al., 2018). Figure 1.4 shows the bathymetric map of the Lombok Strait, highlighting the presence of a pronounced sill located near the southern entrance, where the depth rises abruptly to approximately 300 m before descending into deeper waters. This sill plays a critical role in modulating the flow of the ITF, acting as a generation site for internal tides and solitary waves when strong tidal currents from the Indian Ocean and Flores Sea interact with steep topography (Gordon et al., 2010; Kida & Wijffels, 2012). The inset map provides the regional context of the strait within the Indonesian archipelago, illustrating its connectivity to the Pacific and Indian Oceans.

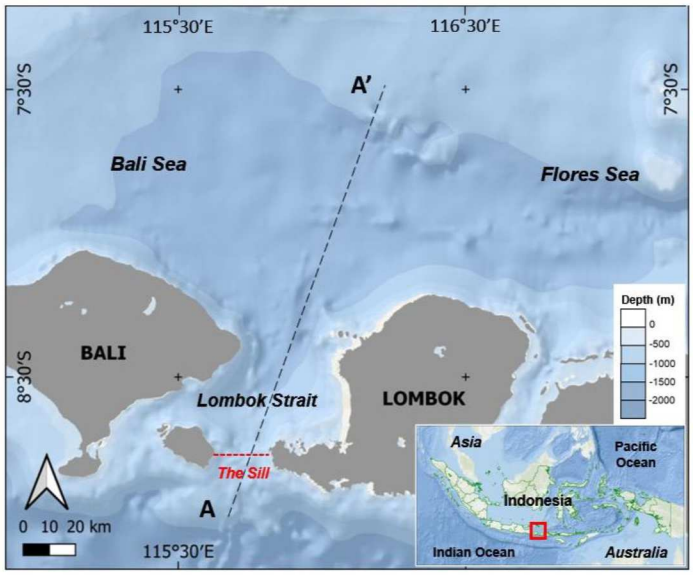

Figure 1.4. Bathymetric map of the Lombok Strait showing cross-section A–A′ across the sill region. The inset map indicates the location of the strait within the Indonesian Sea.

Figure 1.5 presents a vertical cross-section of the Lombok Strait along the A–A′ transect, corresponding to the dashed line in Figure 1.4. The sill near the southern entrance (approximately 20–40 km from the Indian Ocean) is a key topographic feature that influences water mass exchange and internal wave dynamics. The elevation profile illustrates how the pycnocline, representing the density interface, extends across the strait and is often displaced by tidal forces. The interaction between the northward-propagating ITF and southward-moving Kelvin waves from the Indian Ocean can generate strong baroclinic tides that subsequently evolve into nonlinear internal solitary waves (Atmadipoera et al., 2009). These waves often propagate northward into the Flores Sea, where they are observed as surface manifestations in satellite imagery.

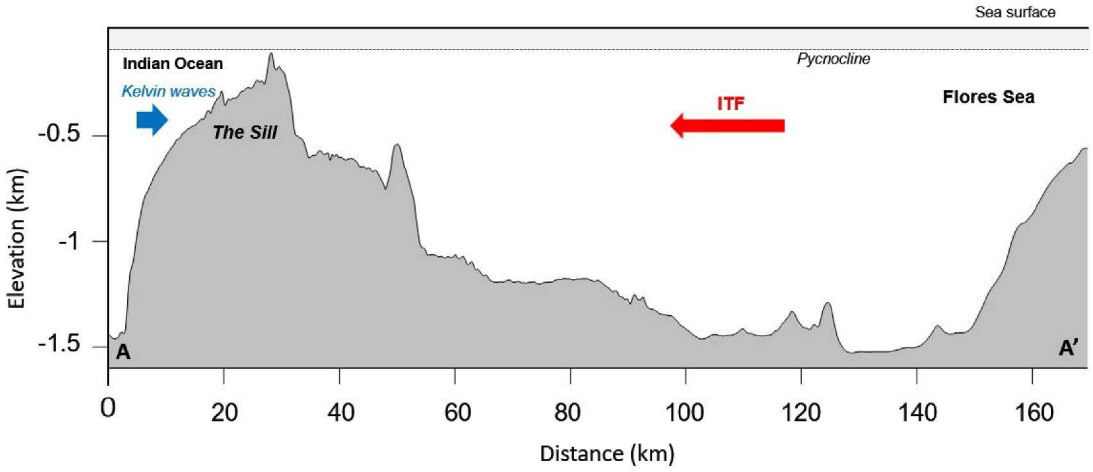

Figure 1.5. Bathymetric cross-section along the A–A′ transect of the Lombok Strait showing the sill, pycnocline, and schematic directions of ITF and Kelvin waves.

The combination of complex topography and energetic tidal forcing makes the Lombok Strait a hotspot for internal wave activity. The sill acts as a natural generation site where barotropic tidal energy is converted into baroclinic internal waves, contributing significantly to local mixing processes and vertical transport in the region (Purwandana et al., 2021). These physical interactions not only affect the regional thermohaline structure but also play an essential role in the redistribution of oceanic energy within the Indonesian Throughflow system.

1.4.2 ISWs Observed in the Lombok Strait

The generation of ISWs in the Lombok Strait is primarily governed by the interaction between semidiurnal tidal currents and the complex bathymetric structure of the strait, particularly in the sill region, under ITF modulation. When strong tidal flows traverse the topographic features of sills, ridges, and steep slopes, barotropic tidal energy is efficiently

converted into baroclinic internal tides that steepen nonlinearly into solitary wave packets propagating northward and southward (Aiki et al., 2011; Lukman et al., 2024; Matthews et al., 2011; Ningsih et al., 2010; Purwandana et al., 2021). These internal waves typically originate near the sill and propagate into both the Bali and Flores Seas, with their amplitudes and phase speeds modulated by background stratification and throughflow variability.

Early satellite-based investigations using SAR imagery revealed distinct packet-like ISW signatures emerging from the sill region of the Lombok Strait (Matthews et al., 2011). Subsequent in-situ measurements and numerical modelling further characterised the generation and evolution processes, identifying strong baroclinic conversion zones and enhanced turbulent mixing within the sill region (Purwandana et al., 2021; Syamsudin et al., 2019). A recent field study by Lukman et al. (2024) demonstrated the initial stages of nonlinear wave formation, showing that the energy transfer between internal tides and solitary waves plays a critical role in shaping the wave amplitude and packet structure. These findings align with other regional observations of nonlinear internal tides and solitary waves in the Indonesian Seas, suggesting that similar mechanisms operate throughout the archipelagic passage.

The seasonal variability of ISWs in the Lombok Strait is strongly influenced by the monsoonal cycles. During the southeast monsoon (SEM), upper-layer stratification is strengthened by solar heating and reduced precipitation, creating a shallower and more stable thermocline that favors the generation of high-amplitude waves. Conversely, during the northwest monsoon (NWM), weaker stratification and altered flow regimes tend to suppress solitary wave activity or reduce their phase speeds (Chonnaniyah et al., 2025; Chonnaniyah et al., 2023; Chonnaniyah et al., 2021; Karang et al., 2019; Ningsih et al., 2010). In addition to the monsoon, large-scale climatic oscillations, such as the Indian Ocean Dipole (IOD) and El Niño–Southern Oscillation (ENSO), exert secondary but significant control on ISW occurrence. These phenomena influence the depth and intensity of the thermocline, as well as the strength of the ITF, thereby modulating the background conditions for ISW generation (Feng et al., 2018).

Modern multi-satellite observations have advanced the detection and quantification of ISW characteristics in the Lombok Strait, Indonesia. High-resolution sensors, such as Sentinel-1 SAR, GCOM-C/SGLI, MODIS, Landsat-8, and Himawari-8, provide detailed surface manifestations of ISWs that enable the estimation of wave crest length, number of solitons, propagation direction, and phase speed (Karang et al., 2019; Chonnaniyah et al., 2023). When integrated with numerical simulations using models such as CROCO,

MITgcm, and CFD-FEM, these optical and radar datasets permit a robust assessment of ISW dynamics and energy fluxes (Gong et al., 2022; Wang et al., 2025). For instance, Karang et al. (2019) reported northward-propagating solitary waves with mean phase speeds of approximately 2.05 m s^{-1} based on Landsat-8 imagery, whereas Sentinel-1 SAR analyses confirmed the repeated occurrence of multi-crest packets originating from the sill zone.

Numerical experiments have been particularly valuable in elucidating the mechanisms controlling ISW generation and evolution in the Lombok Strait. Aiki et al. (2011) used nonhydrostatic simulations to show that the interaction between semidiurnal tides and background throughflow results in asymmetric wave amplitudes between northward and southward-propagating solitons. Gong et al. (2022) further demonstrated that local bathymetric variations cause spatial asymmetries in wave amplitude and phase speed, with the northern branch exhibiting faster decay owing to shallower and rougher terrain. These modelling results agree with observational findings from SAR imagery and moored observations, confirming that bathymetry, stratification, and ITF intensity jointly determine the strength and spatial pattern of the ISW activity (Kida & Wijffels, 2012; Matthews et al., 2011).

1.5 Research Motivation

ISWs are powerful underwater waves that play a significant role in ocean mixing, nutrient transport and coastal dynamics. Despite occurring beneath the ocean surface, ISWs have visible surface manifestations that are detectable via satellite remote sensing. In regions such as the Lombok Strait, one of the key conduits for the ITF, the presence of these eddies is both persistent and dynamic. However, many questions remain regarding their long-term behavior, seasonal variability, and the influence of climate oscillations on their dynamics. There is a growing need to develop accurate and efficient methods for monitoring ISWs, especially those that use freely available satellite data. Understanding how these waves interact with the sea surface, affect satellite-derived oceanographic products, and responding to broader climatic events is essential for understanding the ocean. These insights have implications for marine ecosystem management, climate research and navigation safety.

1.6 Research Problem

Although numerous studies have documented the existence of internal solitary waves in Indonesian waters, several key challenges remain.

1. Surface manifestation uncertainty: The mechanisms behind the appearance of ISWs in optical imagery (e.g. ocean color or temperature anomalies) are not yet fully understood, particularly in complex tropical environments such as the Lombok Strait.
2. Temporal and spatial coverage gaps: Although radar data (SAR) can provide detailed spatial resolution, it suffers from limited temporal resolution. Conversely, optical data offers a higher revisit frequency but is often affected by clouds or sun glint.
3. Lack of integrated analysis: Most studies have examined SAR or optical data independently, with limited multi-sensor integration to comprehensively analyze ISW behavior across different timescales and seasons.
4. Climate influence: The relationship between ISW dynamics and large-scale climate events, such as ENSO and IOD, has been observed but not thoroughly quantified in the Lombok Strait.

To address these challenges, the present study developed a multi-satellite framework for detecting, tracking, and characterizing ISWs over extended periods, focusing on the Lombok Strait as a representative Indonesian passage.

1.7 Research Scope and Objectives

1.7.1 Scope

This study focused on the observation, analysis, and interpretation of ISWs in the Lombok Strait using multi-satellite remote sensing data, including Sentinel-1 SAR, GCOM-C/SGLI, Terra/MODIS, and other auxiliary datasets. It covers both short-term seasonal variations and long-term trends, with an emphasis on the interactions between ISWs, climate oscillations, and coastal processes.

1.7.2 Overall Objective

To estimate the key parameters of internal solitary waves and assess their seasonal and long-term variations using satellite remote sensing in the Indonesian seas, with an emphasis on the Lombok Strait.

1.7.3 Specific Objectives

1. To identify the surface manifestations of ISWs using GCOM-C/SGLI optical imagery and describe their morphological characteristics.
2. To estimate the propagation speeds and occurrence frequency using long-term Sentinel-1 SAR imagery through feature-tracking methods.

3. To distinguish seasonal differences in ISW behavior in the Lombok Strait using multi-satellite datasets.
4. To analyze potential long-term trends in ISW parameters and discuss their relationship with background oceanographic conditions.

1.7.4 Research Questions

1. What are the spatial and temporal characteristics of the ISW surface signatures in the Indonesian seas?
2. How do ISW propagation speeds and occurrence vary seasonally in the Lombok Strait?
3. What factors govern long-term variations in ISW activity, and can they be inferred from satellite records?

1.8 Research Structure and Outline

This dissertation is structured into five main chapters to present a comprehensive investigation of ISWs in the Lombok Strait and the surrounding Indonesian Seas. Chapter 1 introduces the research background, motivation, problem formulation, objectives, and overall framework of the study. Chapter 2 examines the surface manifestation characteristics of ISWs as observed from GCOM-C/SGLI optical imagery, emphasizing their influence on ocean color and sea surface temperature (SST) variability. Chapter 3 focuses on the estimation of ISW propagation speeds and occurrences derived from long-term Sentinel-1 SAR data, including methodological developments for wave detection and the assessment of temporal trends concerning large-scale climate indices. Chapter 4 analyzes seasonal variations in ISW characteristics using multi-satellite datasets, highlighting their connections with thermocline dynamics and sediment transport processes in the Lombok Strait. Finally, Chapter 5 presents the conclusions drawn from the study, synthesis the main findings, and proposes directions for future research on satellite-based ISW monitoring, parameterization, and numerical modelling. The organization of the dissertation is illustrated in Figure 1.6, which summarizes the logical flow of the research from the introductory concepts to the analytical and concluding stages.

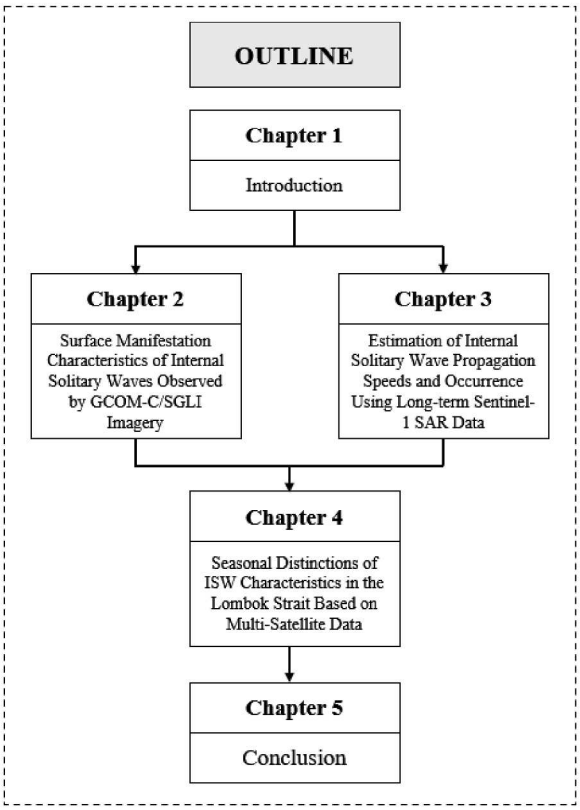

Figure 1.6. Outline of the dissertation

1.9 Scientific Significance and Contribution

This dissertation provides the following contributions:

1. This study presents a comprehensive, long-term satellite analysis of ISWs in the Indonesian seas, which is one of the first of its kind in the region.
2. A methodological framework for integrating SAR and optical remote sensing in ISW studies.
3. Insights into the seasonal and interannual variability of ISWs in a critical oceanographic gateway improve the understanding of nonlinear internal wave dynamics within the ITF system.
4. Contributions relevant to operational oceanography include forecasting internal wave occurrence for marine navigation and offshore safety.

CHAPTER 2

Surface manifestation characteristics of internal solitary waves observed by GCOM-C/SGLI imagery

2.1 Introduction

Internal waves (IWs) are global phenomena generated by the interactions between stratification, bathymetry, and tidal flow. They are characterized by fine mesoscale structures and strong vertical shears. IWs play a crucial role in the exchange of energy between large-scale tides and small-scale mixing (Jackson, 2007; Klemas 2012). IWs manifest in various forms depending on stratification, generation mechanisms, and external forces. Internal tides, the first form of IWs, occur at tidal frequencies. Internal solitary waves (ISWs) are IWs characterized by non-sinusoidal, nonlinear, isolated, and large-amplitude waves. The surface manifestation of ISWs is often observed as alternating bands of bright and dark strips resulting from ocean surface roughness variations (Alpers, 1985; Osborne & Burch, 1980). Ocean surface roughness induced by ISW activity can be detected by the naked eye and remote sensing (Apel, 2002a; Klemas, 2012; Mitnik, Alpers, Chen, et al., 2000).

Remote sensing technologies have revolutionized the study of ISWs by enabling the detection and analysis of these phenomena over vast oceanic areas. Remote sensing can provide details of the two-dimensional spatial structures of ISWs that cannot be easily observed in situ (Alpers, 2014; Helfrich & Melville, 2006; Robinson, 2010). Synthetic aperture radar (SAR) has become an important tool for detecting ISW, as it can measure very small changes in sea surface roughness in the centimeter to decimeter wavelength range (Jackson et al., 2013). Although SAR has its own advantages, such as all-weather, day and night imaging capabilities, optical sensors offer distinct advantages in terms of spatial and spectral resolution, ocean color analysis, temperature detection, and ease of interpretation. Optical sensors detect ISWs based on ocean surface roughness in the sun glint area (Apel et al., 1975). The characteristics of ocean surface roughness inferred from optical sensors are vital in calm waters at the point of specular reflection.

The Lombok Strait is a strait in the southern Indonesian seas where high-amplitude ISWs occur (Susanto et al., 2005). This strait plays a crucial role as an exit pathway for trans-oceanic water transport, known as the Indonesian Throughflow (ITF). The characteristics and dynamics of ISWs in the Lombok Strait have been studied based on in-situ observations

(Purwandana et al., 2021; Susanto et al., 2005; Syamsudin et al., 2019), numerical simulations (Gong et al., 2022; Ningsih et al., 2010), and remote sensing data (Chonnaniyah, Osawa, et al., 2023; Karang et al., 2019b; Lindsey et al., 2018; Matthews et al., 2011; Mitnik et al., 2000; Susanto et al., 2005). Several studies have used sun glint imagery to detect and analyse ISW dynamics in the Lombok Strait. Lindsey et al. (2018) utilized data from Himawari-8, a geostationary satellite, to measure the spatial and temporal attributes of ISWs in the Indonesian seas, including the Lombok Strait. Karang et al. (2019) monitored and analyzed various parameters of ISWs in the Lombok Strait using data from Landsat 8.

The surface manifestation of ISWs provides valuable insights into their behavior and dynamics. The interaction between surface waves and IWs has been widely studied using numerical simulations (Craig et al., 2012; Hao & Shen, 2020). Craig et al. (2012) presents a theoretical framework for understanding the influence of internal wave dynamics on surface features, while Hao et al. (2020) emphasizes the significance of local wave geometry and energy dynamics. Their work underscores the complexity of surface-internal wave interactions and the importance of using different modelling approaches to capture these phenomena. Numerical simulations capture the dynamics of ISWs at the surface and subsurface, whereas remote sensing allows the observation of the evolving behavior of ISWs as they move across different regions. ISW manifestations on the sea surface detected by satellite sensors have not been studied in detail, and previous studies have employed these patterns to reveal ISW dynamics (Chonnaniyah, Osawa, et al., 2023; da Silva et al., 2002; Kim et al., 2018; C. Wang et al., 2019). Surface roughness heterogeneity can affect the physical properties of the near-surface, such as the atmosphere (Ortiz-Suslow et al., 2019), surface roughness heterogeneity can affect the physical properties of the near-surface (da Silva et al., 2002; Farrar et al., 2007), and the bulk properties of ISW (Colosi et al., 2018; Vrećica et al., 2022). These studies have provided valuable insights into IW dynamics; however, they also revealed the limitations of relying solely on point measurements.

The Global Change Observation Mission - Climate (GCOM-C) satellite, equipped with the Second-generation Global Imager (SGLI), offers a unique capability to observe ISWs through its wide spectral range and high spatial resolution, which is up to four times higher than that of previous optical sensors for ocean color. The SGLI sensor, which includes visible, near infrared, and thermal infrared channels, allows for comprehensive monitoring of sea surface conditions, capturing both optical and thermal manifestations of ISWs. This study focused on the surface manifestation characteristics of ISWs in the Lombok Strait, as observed by GCOM-C/SGLI imagery. By analyzing both Level-1B radiance and Level 2

ocean color products, this study aims to clarify the interactions between ISWs and sea surface properties in this dynamic region. The ISW manifestation patterns in SST data are an important finding. This is particularly important because of the potential impact of SST modulation on air-sea exchange and the atmospheric boundary layer. The findings contribute to a better understanding of ISW dynamics in the Lombok Strait and offer broader implications for the study of internal waves in other stratified oceanic environments.

2.2 Material and methods

2.2.1 Research location

This study focused on the analysis of ISW patterns detected by the SGLI sensor on 9 January 2019 at 10.35 GMT+8 in the Lombok Strait areas (Figure 2.1). The Lombok Strait is a channel that separates the Bali and Lombok islands in Indonesia. This allows Pacific Ocean water to flow into the Indian Ocean through an east-west running sill at a depth of 250 m (Susanto et al., 2005). The Lombok Strait experiences two distinct monsoonal wind patterns. The southeast monsoon peaks in June-July-August, whereas the northwest monsoon peaks in December-January-February (Susanto et al., 2007). ISWs in the Lombok Strait are frequently observed during the northwest monsoon (Karang et al., 2019a; Matthews et al., 2011). The peak of the northwest monsoon in January is characterized by relatively low sea levels in the northern part of the Lombok Strait and relatively high sea levels in the southern part, causing a net surface current moving towards the north.

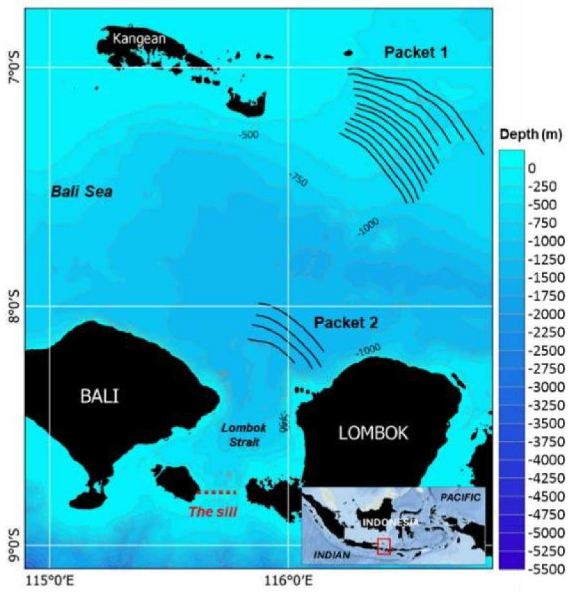

Figure 2.1. The map of the Lombok Strait areas with topography inferred from BATNAS with the dashed red line representing the sill location and black curve lines representing ISW pattern extraction detected by GCOM-C/SGLI on 9 January 2019 at 10.35 GMT+8

2.2.2 Remote sensing data

The Japan Aerospace Exploration Agency (JAXA) launched an Earth-observing satellite named the Global Change Observation Mission for Climate (GCOM-C), which carries an optical sensor called the Second Generation Global Imager (SGLI), on 23 December 2017 (Murakami et al., 2022). The SGLI consists of two sensors: a visible and near-infrared radiometer (SGLI-VNR) and an infrared scanner (SGLI-IRS). The SGLI-VNR has 13 different observation channels from ultraviolet (UV) to near-infrared (NIR) wavelengths, and two of them have polarimetric, multi-directional observation functions. The SGLI-IRS has four shortwave infrared (SWIR) and two thermal infrared (TIR) channels. The SGLI collects a complete picture of the Earth every 2–3 days with a spatial resolution of 250 m (Hori et al., 2018). The nadir-looking channels of the VNR regions (VN1-VN11) and SWIR channel SW3 (1.63 μm) have a spatial resolution of 250 m. In contrast, the other SWIR (SW1, 2, and 4) and slant-viewing polarization channels (P1-P2) have a ground resolution of 1 km. The TIR channels (T1-T2) have a standard spatial resolution of 500 m, but SGLI can acquire 250 m resolution data for T1-T2 channels if needed.

The SGLI Ocean Level 2 products are organized into three categories comprising seven distinct products. The atmospheric correction category includes normalized water-leaving radiance (NWLR), Atmospheric Correction Parameters (ACP: aerosol optical thickness 670), and Photosynthetically Available Radiation (PAR). Atmospheric correction for ocean color uses Level-1B top-of-atmosphere (TOA) radiance data from the visible (VN) and shortwave infrared (SW) bands captured during the daytime. The NWLR and ACP are estimated using an iterative algorithm that bypasses the black-pixel assumption. The SGLI algorithm introduces advanced features, such as absorptive aerosol correction using the 380 nm band (VN1) and high-turbidity water correction using three NIR bands (VN7, VN9, VN10) to accurately estimate the NWLR in turbid waters. PAR was calculated using an algorithm similar to those utilized by SeaWiFS and MODIS. The in-water parameters (IWPR) category includes chlorophyll-a concentration (CHLA), Suspended Solid concentration (SS or TSM), and the absorption coefficient of colored dissolved organic matter (CDOM). The IWPR category relies on the NWLR data as input. CHLA was estimated using the Ocean Color Index (OCI) algorithm, which improves accuracy in areas with low chlorophyll concentrations. TSM was estimated using three NIR bands, whereas CDOM was derived from the detritus absorption coefficient and the Inherent Optical Property (IOP). The last category is the Sea Surface Temperature (SST), which was derived

from Level-1B TOA radiance data collected during both daytime and nighttime using the T1 and T2 bands. Notably, this process operates independently of atmospheric correction (Ogata et al., 2017).

The Level-1B TOA radiance products from GCOM-C/SGLI include data across 19 channels ranging from 380 nm to 12.0 µm. Seven Level 2 Ocean products were obtained from G-Portal JAXA (https://gportal.jaxa.jp/gpr/). These products, available in the GeoTIFF format, were converted and geometrically corrected for accurate analysis. On 9 January 2019 at 10.35 GMT+8 (Figure 2.1), GCOM-C/SGLI detected two packets of internal solitary waves (ISWs) moving northward in Lombok Strait. To validate the presence of these ISWs, Sentinel-1B Synthetic Aperture Radar (SAR) data were used, which were captured earlier on 9 January 2019 at 05.51 GMT+8, five hours and 16 minutes before the SGLI data were recorded. Additionally, high-resolution multispectral data from the Sentinel-2 Multispectral Instrument (MSI) provided information on sea surface conditions at the time the ISW patterns were observed. The data was available on 8 January 2019 at 10.20 GMT+8, one day before the SGLI data were recorded. Moderate Resolution Imaging Spectroradiometer (MODIS) data from the Terra and Aqua satellites, collected on 8 January 2019 at 11.05 GMT+8 and 13.55 GMT+8, respectively, further supplemented the analysis with cloud-free imagery.

2.2.3 Analysis method

A total of 26 SGLI products (Figure 2.2) in GeoTIFF format were collected and cropped into the area of interest in the Lombok Strait. The data were cropped and visualized using the Sentinel Application Platform (SNAP). For a detailed analysis, transect lines were placed over the observed ISW patterns in the images. The Collocation Tool in SNAP was used to align spatially overlapping products for consistency. Level-1B products were combined into a single file, and pixel values along the transect lines were extracted for further analysis. Similarly, Level 2 products were combined with transect lines set at the same locations as the Level-1B data. For the Level-1B data, two transect lines were set along the two detected ISW packets, whereas for the Level 2 data, only one transect line was set on the detected ISW packet in the northern part of the Lombok Strait.

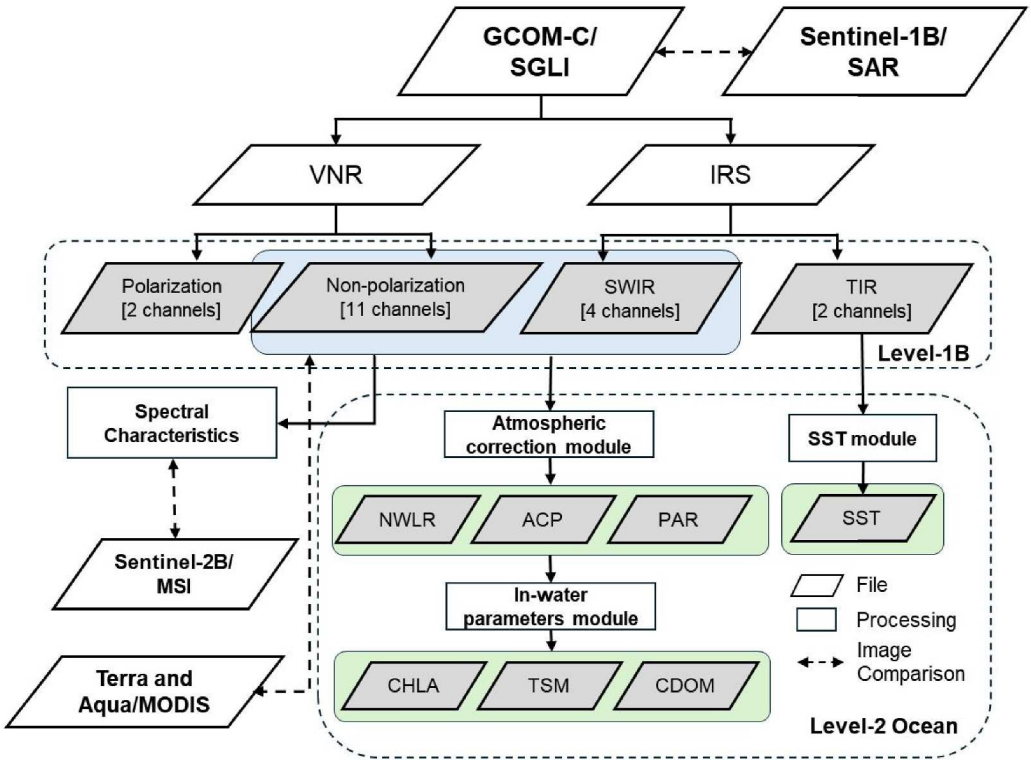

Figure 2.2. Flowchart of the comprehensive method used in this study. The gray-out files are SGLI channels and products analyzed in this study, adapted from Ogata et al. (2017). The blue box represents the TOA radiance for the spectral characteristics, and the green boxes represent ocean color products.

The method integrates data from various sensors on the GCOM-C/SGLI satellite, as well as other satellite platforms, such as Sentinel-1B SAR, Sentinel-2B MSI, Terra/MODIS, and Aqua/MODIS. By integrating these datasets, researchers can validate their findings across different sources, increase the resolution and accuracy of their observations, and develop a more complete understanding of ISW behavior. In this context, a comprehensive method refers to the use of all available data to achieve a thorough and detailed understanding of ISWs, from their basic characteristics to their broader implications in oceanographic research. This comprehensive method enables a detailed analysis of ISWs using the full spectrum of data available from the GCOM-C/SGLI satellite, providing insights into their dynamics, impacts, and potential applications in oceanography.

2.3 Results

ISWs detected in the Lombok Strait are believed to result from the interaction between semidiurnal tides and the rough topography (sill) in the southern part of the Strait, specifically between the Nusa Penida and Lombok Islands. Two ISW occurrences were

observed in the vicinity of the Lombok Strait and the northern part near Kangean Island, approximately 200 km from the generation site. This observation was captured by GCOM-C/SGLI imagery on 9 January 2019 at 10:35 GMT+8. The appearance of short-period ISWs during the northwest monsoon in this area is an interesting subject for further research. The first ISW occurrence (Packet 1) was detected in the Lombok Strait at a depth of approximately 500-700 meters, whereas the second occurrence (Packet 2) was observed further north in the Lombok Strait at a depth of approximately 1000 m (Figure 2.1). It is assumed that Packet 1 was generated earlier than Packet 2, which was likely produced during a later tidal event. The visible channel of the TOA radiance Level 1 product, VNR-01, with a wavelength of 380 nm, clearly revealed the pattern of both ISW occurrences (Figure 2.3(a)).

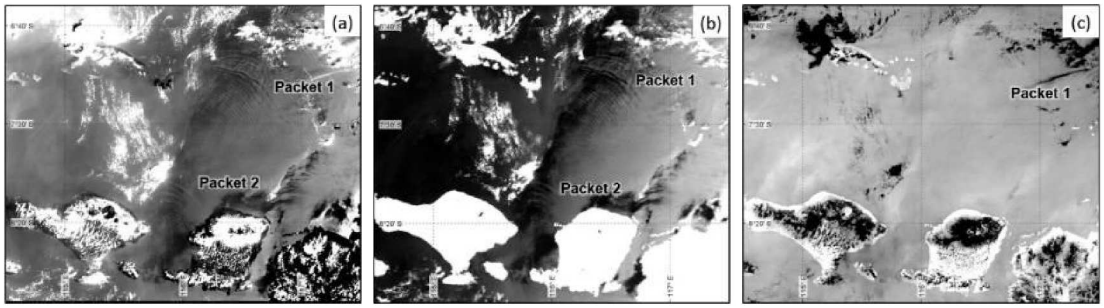

Figure 2.3. The observed ISWs surface manifestation by GCOM-C/SGLI Level-1B VNR TOA radiance on 9 January 2019 at 10.35 GMT+8 for the channel (a) VNR-01 at wavelength 380 nm with 250 m spatial resolution, (b) SW-1 at wavelength 1050 nm with 1000 m spatial resolution, and (c) T-1 at wavelength 10800 nm with 500 m spatial resolution.

The manifestation of ISWs in optical images, particularly in the visible channel, occurs because of the modulation of sea surface roughness caused by ISW activity beneath the surface. This modulation affects the optical reflectivity and absorption of light, which is captured by the sensor. ISW manifestation patterns were detected not only in non-polarization channels (Figure 2.4) but also in polarization channels, specifically in Stokes I and Q components (Figure 2.5). Light becomes polarized when interacting with each surface in a system; however, significant effects will appear if there is absorption or scattering in the medium (Clavano, 2008). The detection of ISW manifestation patterns in the polarization channel in this study is attributed to the significant effect of absorption and scattering on rough sea surfaces caused by ISWs.

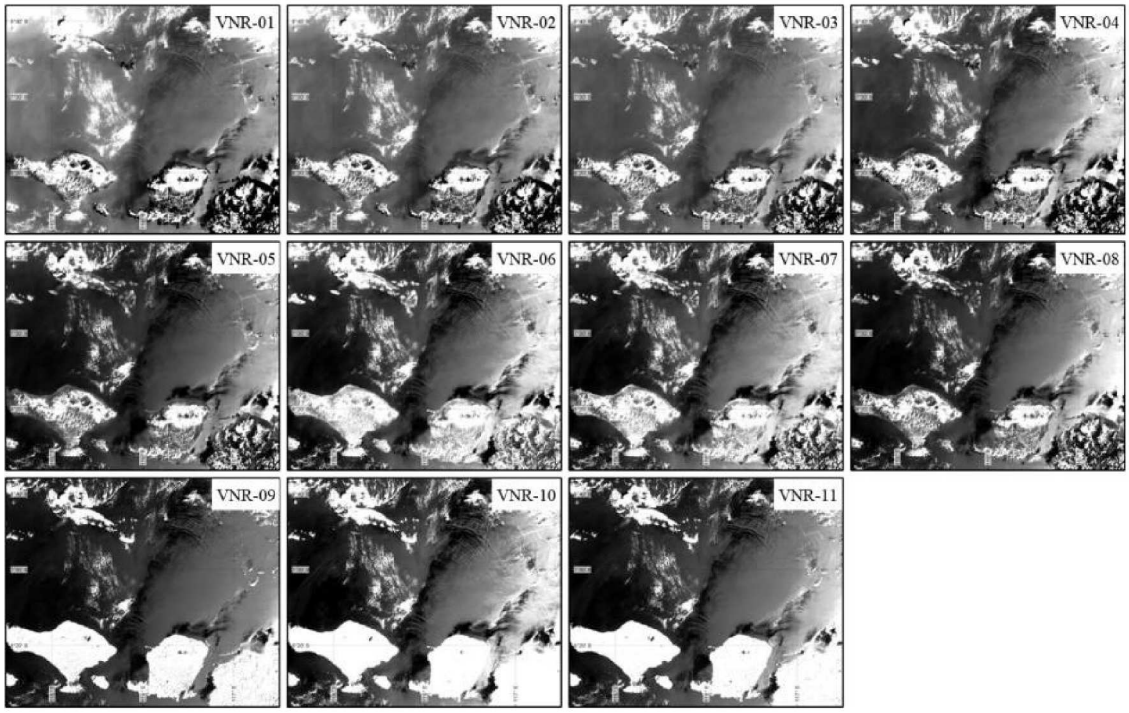

Figure 2.4. Manifestation of ISWs on the surface by GCOM-C/SGLI Level-1B VNR TOA radiance for the non-polarization channel on 9 January 2019 at 10.35 GMT+8 from channel VNR-01 to VNR-11.

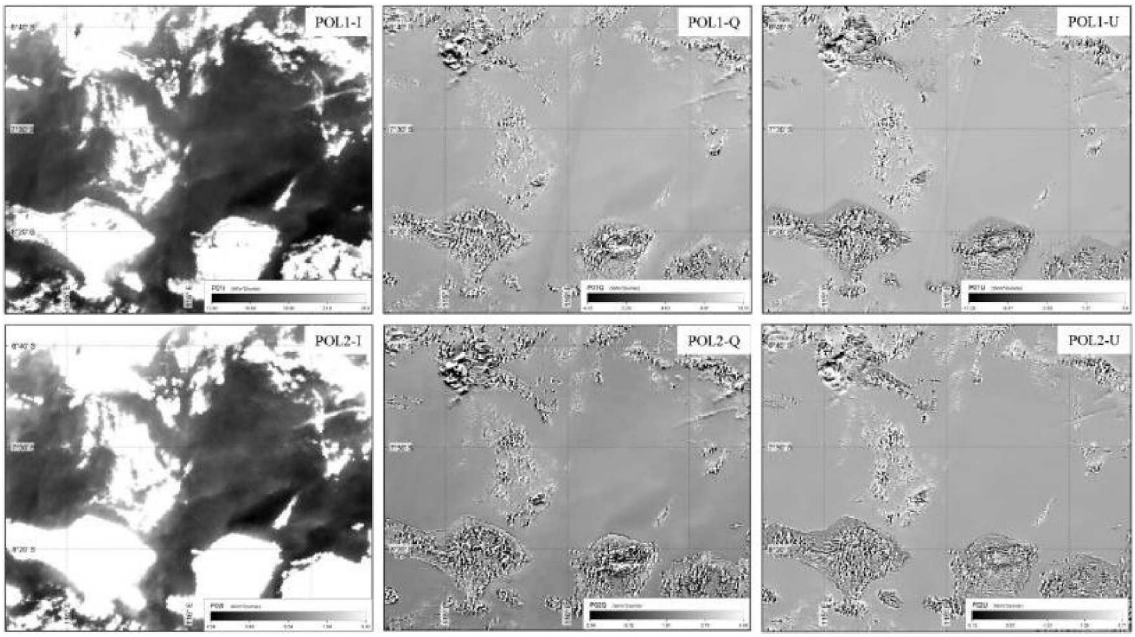

Figure 2.5. GCOM-C/SGLI Level-1B VNR TOA radiance for the polarization channel (1 km spatial resolution) on 9 January 2019 at 10.35 GMT+8 from channel POL1 to POL2 with the Stokes parameters (I, Q, and U).

The presence of ISW can be observed in the short-wave infrared (SWIR) channel of the TOA radiance data. Figure 2.3(b) shows that the ISW patterns of the two features are

visible in the SWIR images at a wavelength of 1050 nm, similar to what is seen in Figure 2.3(a) in the visible spectrum. The surrounding waters show different color contrasts on both sides of the image, with dark colors indicating a relatively calm sea surface and light colors representing areas close to the sun glint. The SWIR channel on the SGLI includes four bands at different wavelengths; however, one of these, the SW-2 band at 1380 nm, does not capture the ISW pattern. The SW-2 band was specifically designed for cloud detection with a spatial resolution of 1000 km (Figure 2.6). The thermal infrared (TIR) channel can still detect patterns consistent with those seen in the VNR and SWIR, although the ISW patterns are less visible and only detect Packet 1 (see Figure 2.3(c)). The TIR channel on the SGLI has two bands with different wavelengths (10.8–12.0 μm), but these two channels (T-1 and T-2) only detect the ISW pattern for Packet 1 (Figure 2.7). Further clarification is provided by the cross-sectional profile along the ISW propagation direction.

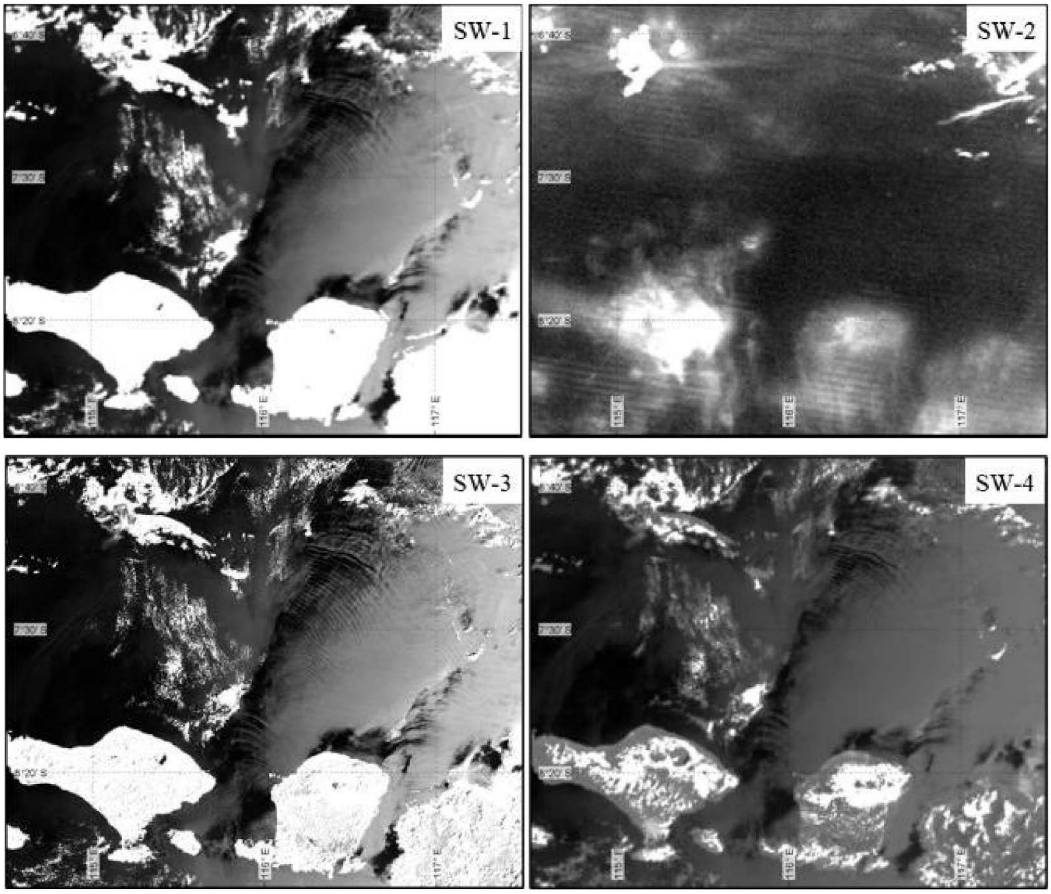

Figure 2.6. GCOM-C/SGLI Level-1B Infrared Scanner (IRS) TOA radiance for shortwave infrared (SWI) channel on 9 January 2019 at 10.35 GMT+8 from channel SW-1 to SW-4.

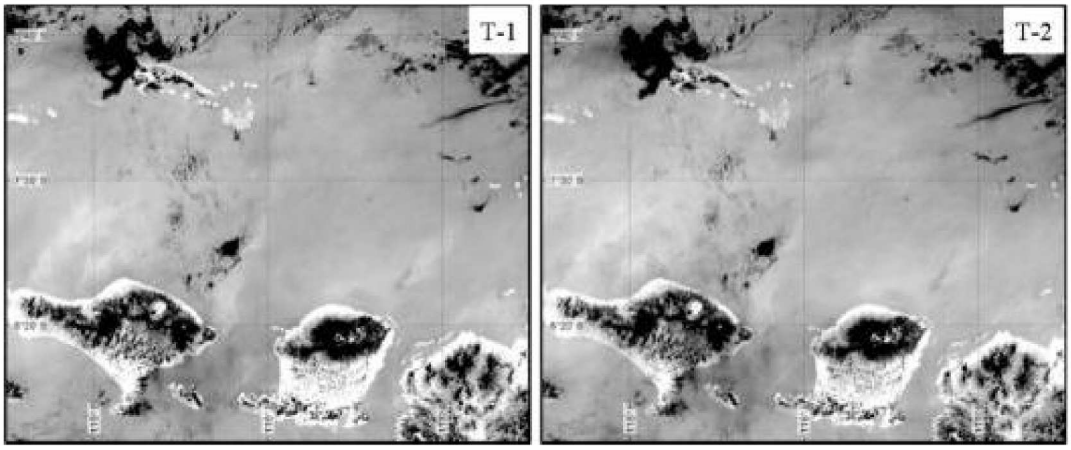

Figure 2.7. GCOM-C/SGLI Level-1B Infrared Scanner (IRS) TOA radiance for thermal infrared (TIR) channel on 9 January 2019 at 10.35 GMT+8 from channel T-1 and T-2.

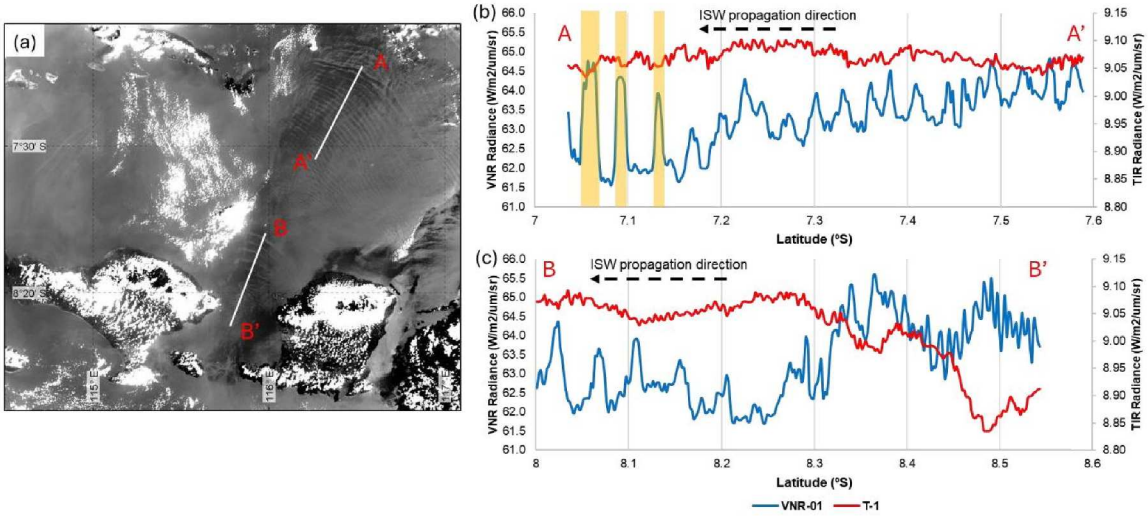

Figure 2.8. (a) Level-1B VNR TOA radiance channel VNR-01 product on 9 January 2019 at 10.35 GMT+8. White lines represent a cross-section starting from label A-A' for the northern part of the Lombok Strait and B-B' for the Lombok Strait, (b) TOA radiance profile A-A' of VNR-01 at wavelength 380 nm compared with thermal infrared radiance T-1 at wavelength 10800 nm, and (c) TOA radiance profile B-B.'

Figure 2.8(a) shows the cross-sectional profiles of two different transects that represent ISW manifestations in the TOA radiance channels Packet 1 and Packet 2. Transect A-A' (Figure 2.8(b)) displays the profile of ISW Packet 1. The cross-sectional profile in the visible and thermal channels showed that the radiance values varied by approximately 2.5 $W.m^{-2}.\mu m^{-1}.sr^{-1}$ at the crest of Packet 1 and decreased towards the rear. This variation reflects the impact of smooth and rough stripes on the sea surface caused by ISW. Transect B-B' (Figure 2.8(c)) shows the profile of ISW Packet 2. In this profile, the radiance value at the first crest was approximately 2.0 $W.m^{-2}.\mu m^{-1}.sr^{-1}$, with a decrease observed at the rear of the wave.

Packet 2 is not detected on the thermal channel. The data indicate that Packet 1 exhibited greater variation in radiance values, which is related to sea surface roughness and causes interference in the thermal data. This interference results in inconsistent patterns between the thermal and visible channels of the spectrum. Specifically, the radiance in the visible channel increased by 2.5 $W.m^{-2}.\mu m^{-1}.sr^{-1}$ corresponds to a decrease in the radiance value in the thermal channel by approximately 0.04 $W.m^{-2}.\mu m^{-1}.sr^{-1}$.

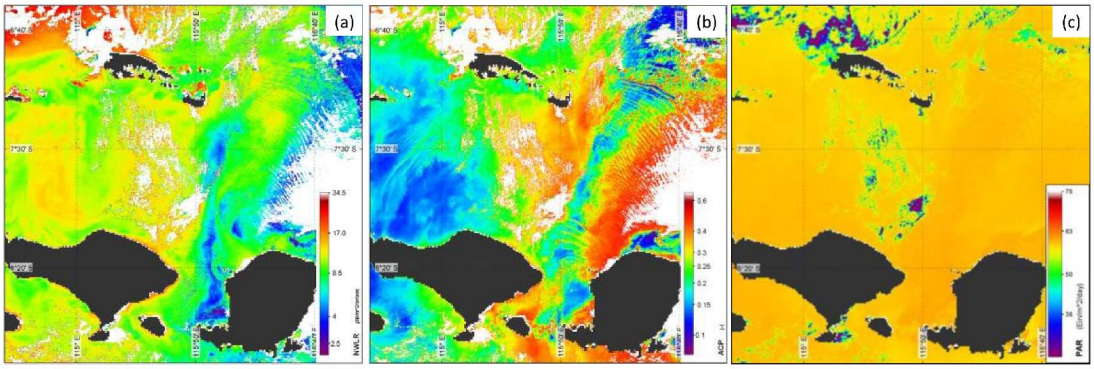

Figure 2.9. SGLI Level 2 Ocean products for atmospheric correction category on 9 January 2019 at 10.35 GMT+8, (a) normalized water-leaving radiance (NWLR), (b) atmospheric correction parameter (ACP), and (c) photosynthetically available radiation (PAR)

The ISW manifestation pattern was detected in both the Level-1B product and Level 2 ocean data. The three categories of ocean color products at Level 2 Ocean consistently detected ISW patterns similar to those found in the Level-1B products. According to the atmospheric correction algorithm used to generate Level 2 ocean data, Level-1B TOA radiance products from the VNR and SWIR channels were utilized as inputs to estimate the NWLR, ACP, and PAR products (Ogata et al., 2017). Figure 2.9(a) shows the NWLR product, which detects both ISW manifestation patterns (Packets 1 and 2), with the first crest pixel values being lower than the surrounding background pixel values. The ACP product (Figure 2.9(b)) reveals the ISW pattern in more detail, with the first crest of the ISW showing higher values than that of the background. The striking differences on both sides of the ISW propagation area are assumed to be due to the influence of the sun glint effect. The PAR product (Figure 2.9(c)) also shows an ISW pattern, although it is slightly faint because the value differences compared to the background are less pronounced. Nonetheless, the detected pattern was consistent with that of the other products. Variations in PAR values influenced by ISW manifestations were lower at the first crest of the ISW than at the surrounding background values.

The next Level 2 Ocean product is an in-water parameter (IWPR) product that uses data input from the NWLR product. The IWPR category includes three products: CHLA, TSM, and CDOM (Figure 2.10). Both ISW patterns (packets 1 and 2) were detected in all three products. The CHLA product shows the ISW manifestation pattern at the first crest with a lower value than the surrounding background (Figure 2.10(a)). Similarly, the TSM product detected the ISW pattern with values lower than the surrounding background (Figure 2.10(b)). In contrast, the CDOM product detected the ISW manifestation pattern at the first crest with a higher value than the surrounding background (Figure 2.10(c)).

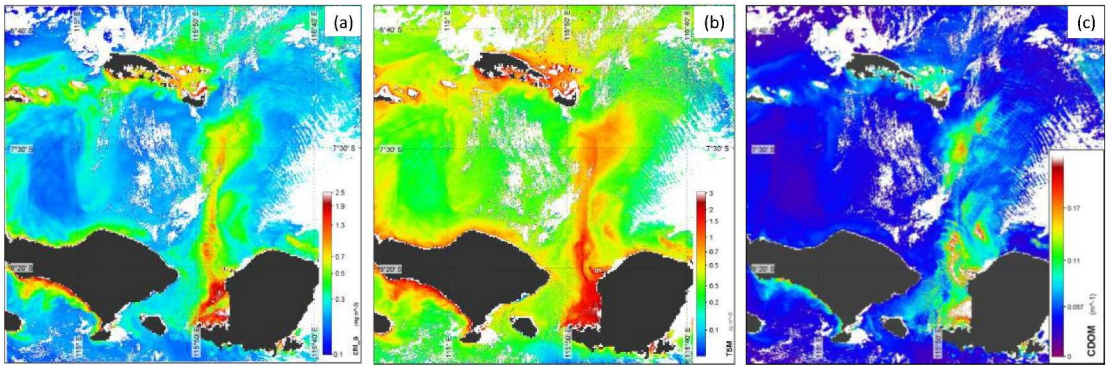

Figure 2.10. SGLI Level 2 Ocean products for in-water parameters category on 9 January 2019 at 10.35 GMT+8 (a) chlorophyll-a concentration (CHLA), (b) suspended solid concentration (TSM), and (c) colored dissolved organic matter (CDOM)

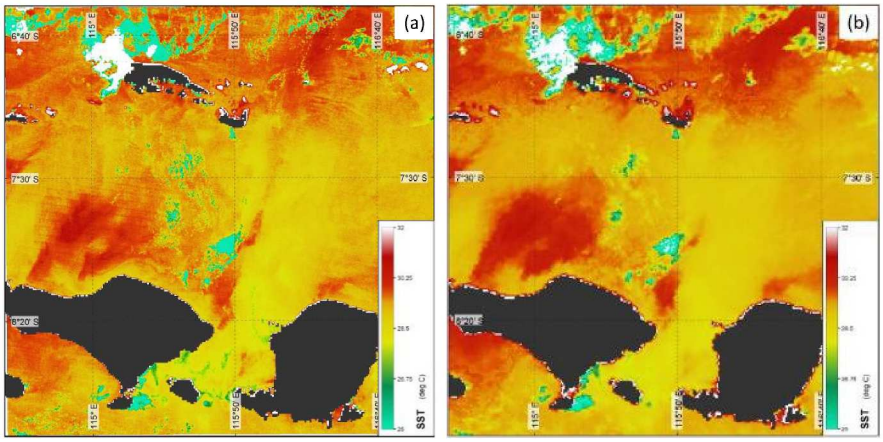

Figure 2.11. Sea surface temperature (SST) products on 9 January 2019 at 10.35 GMT+8 (a) Version 2, (b) Version 3

The SST product was derived using data from the Level-1B TOA radiance on the TIR channel. Figure 2.11 presents the SST product, which identifies ISW manifestation patterns consistent with those observed in the TOA radiance data in the TIR channel (Figure 2.3(c)). Two versions of the SST product were estimated using different atmospheric correction processes. Figure 2.7(a) shows the result of Version 2, where the ISW manifestation pattern

in Packet 1 is evident. In contrast, Figure 2.11(b) shows the results of Version 3, which includes improvements in atmospheric correction. The enhancements in Version 3 involved refining the cloud mask process and adding an L1B filtering process to remove stripe noise (Kurihara et al., 2021). Although the SST product in Version 3 appears smoother and free of striped noise, the ISW manifestation pattern is less prominent. However, the cross-sectional profile along the ISW manifestation pattern still reveals a consistent up-and-down pattern, similar to that observed in the TOA radiance data.

2.4 Discussion

The mechanism for detecting ISW manifestation patterns in SGLI products is discussed in detail by validating these findings using data from other sensors. SAR data are particularly important for ISW detection. Fortunately, a SAR image from Sentinel-1B was captured within a short time frame of the SGLI image. The Sentinel-1B/SAR image taken on 9 January 2019 at 05:51 GMT+8 detected an ISW manifestation pattern consistent with that observed in the SGLI product. There was a 4-hour and 44-minute time gap between the two images, with the Sentinel-1B image captured in the morning before the SGLI image. Figure 2.12(a) shows the Sentinel-1B/SAR image, which reveals three ISW packets propagating in the northward direction. Despite the time gap of 4 h and 44 min, the SGLI product continued to detect packets 1 and 2. Transect lines (Line C-C') were used to examine the backscatter profile on the Sentinel-1B SAR image, and these profiles were subsequently compared with the TOA radiance and ocean color product profiles from SGLI data.

Cross-sectional profile analysis along the direction of ISW propagation revealed that the first crest (Packet 1) was detected by the Sentinel-1B SAR imagery at approximately 7.3 °S latitude. Later, the SGLI imagery located this crest at 7.05 °S, suggesting that the ISW crest had moved approximately 30 km during this time. A comparative analysis of the cross-sectional profiles of the SGLI TOA radiance and ocean color products (Figure 2.12(c)-(d)) showed a consistent pattern between the visible channel and ocean color products ACP and CHLA: when the radiance value was high (smooth surfaces), the ACP and CHLA values also increased. Conversely, the TIR channel and SST products showed a consistent pattern but inversely proportional to the visible channel; when the radiance value in the visible channel was high (smooth surface), the TIR radiance and SST values decreased. The in-situ data from the Lombok Strait (Purwandana et al., 2021, 2023) strongly support the results of the present study. Both studies by Purwandana et al. (2021, 2023) highlight the significant role of ISWs in the region, their impact on sea surface conditions, and the underlying dynamics driving

these phenomena. The consistency across these observations and models strengthens the validity of the present study's findings, particularly in understanding the interaction between internal tides and seabed topography in generating and propagating ISWs in the Lombok Strait and surrounding areas.

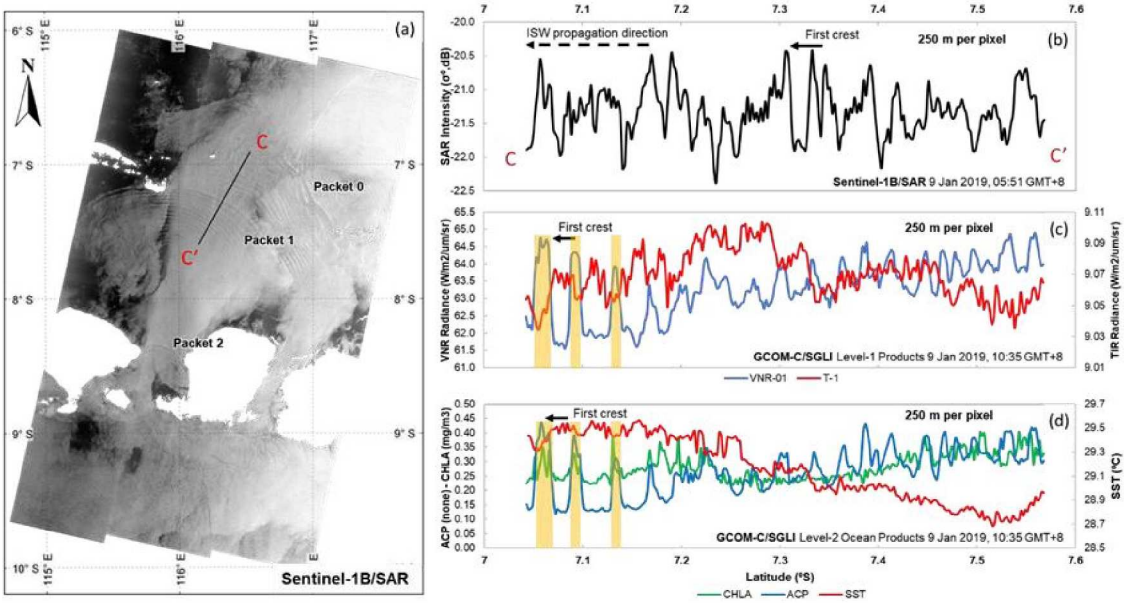

Figure 2.12. (a) The observed ISWs surface manifestation by Sentinel-1B/SAR images on 9 January 2019 at 05.51 GMT+8, and the cross-section profile of ISWs manifestation for the A-A' transect in Figure 2.8(a) for (b) SAR intensity, (c) comparison of VNR and TIR radiance Level-1B products of SGLI, and (d) Level 2 Ocean of SGLI for the ACP, CHLA, SST products

One possible explanation for this phenomenon is the modulation of the sea surface by ISWs, which induces areas with rough and smooth surfaces. Rough sea surfaces scatter and absorb sunlight, causing these areas to appear darker than the sensor. Conversely, smooth sea surfaces reflect sunlight more effectively, resulting in brighter areas. The increased opacity in rough areas disrupts light penetration, whereas smooth surfaces allow better retrieval of ocean color information. This explains why the ISW pattern detected by the ocean color products aligned with the TOA radiance product, whereas the thermal channels and SST data showed different patterns.

The detection of ISW patterns in thermal channels and SST images can be attributed to the impact of ISWs on the mixed layer depth, where cooler water is brought closer to the surface than warmer water. Packet 1, which has propagated further and become shallower, exhibits a higher amplitude compared to Packet 2, which remains at a depth of around 1500 meters in the Lombok Strait area. The amplitude of the ISWs in Packet 1 was sufficient to

elevate the cooler water layer closer to the surface, resulting in lower thermal emissions detected by the sensor over the smooth surface (Figure 2.13). Previous studies have also detected the sea surface thermal manifestation of IWs (Farrar et al., 2007; Marmorino et al., 2004; Walsh et al., 1998). The mechanism proposed in this study is consistent with that of Farrar et al. (2007), who concluded that the signal in SST data is due to IWs affecting upper ocean mixing by changing the depth of the diurnal warm layer. However, an additional mechanism that may contribute significantly to the observed manifestations of ISWs is the net particle transport induced by ISW. This process involves the movement of materials within the water column, where ISWs lift cooler water from deeper layers to the surface of the water. Satellite sensors, which capture snapshots of the sea surface, can precisely detect these cooler water masses when they are elevated to the upper ocean layer by ISW. The cooler water brought to the surface by ISWs may descend again, but the momentary lifting captured by satellites contributes to the observed ISW patterns in SST and other remote sensing data.

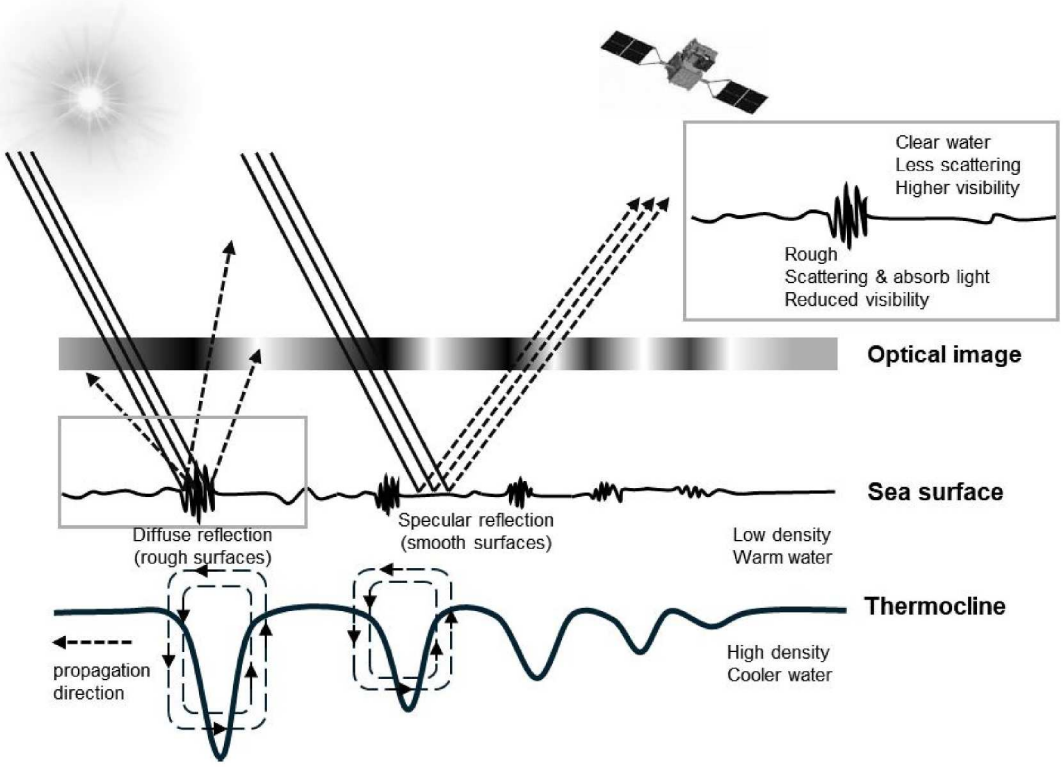

Figure 2.13. Imaging process of ISWs using an optical sensor consisting of depression solitons with decreasing amplitude. The sea surface roughness due to ISW activity below the surface affects the visibility and characteristics of the sea surface recorded by optical sensors

When comparing the findings of Craig et al. (2012) and Hao & Shen (2020) with the results of the present study, several key points emerge regarding the influence of IW dynamics on surface features and the importance of local wave geometry and energy dynamics. Craig et al. (2012) and Hao and Shen (2020) focused on theoretical and numerical modelling approaches. This study provides empirical data from satellite imagery, allowing for the direct observation of ISW behavior across different regions. This empirical evidence complements theoretical models by offering real-world examples of these dynamics in action. Vrećica et al. (2022) utilized high-resolution infrared imagery from a helicopter to observe shoaling and breaking IWs, capturing fine spatial details and identifying areas where waves were breaking. In contrast, the current study employed satellite-based remote sensing data from SGLI to detect and analyze ISWs. Nonetheless, the satellite data confirmed the presence of ISW patterns, showing consistency in the manifestation of ISWs across different imaging channels. Both studies highlight the complex interactions of internal waves with the ocean surface, but they do so from different perspectives and scales. Vrećica et al. (2022) provided detailed high-resolution observations of wave breaking and spatial variability, which are crucial for understanding local IW dynamics. The current study complements these findings by using satellite data to observe ISW patterns over broader spatial scales, demonstrating how these patterns manifest and influence the surface properties.

The Sentinel-2B MSI detected the ISW manifestation pattern a day before the SGLI imagery was recorded. By combining six views from Sentinel-2B/MSI imagery, wide area coverage was achieved, revealing three ISW packages. Newly generated ISW packets were observed near their generation area (indicated by box 3 in Figure 2.14(a)). Analysis of the spectral information from Sentinel-2B/MSI and GCOM-C/SGLI showed a consistent pattern of high reflectance values in the violet band (380-443 nm). There was no significant difference in the spectral characteristics between the bright and dark areas influenced by ISWs on the sea surface. The spectral characteristics of these bright and dark lines in the ISW patterns observed in the northern part of the Lombok Strait are consistent (Figure 2.14(c)-(d)).

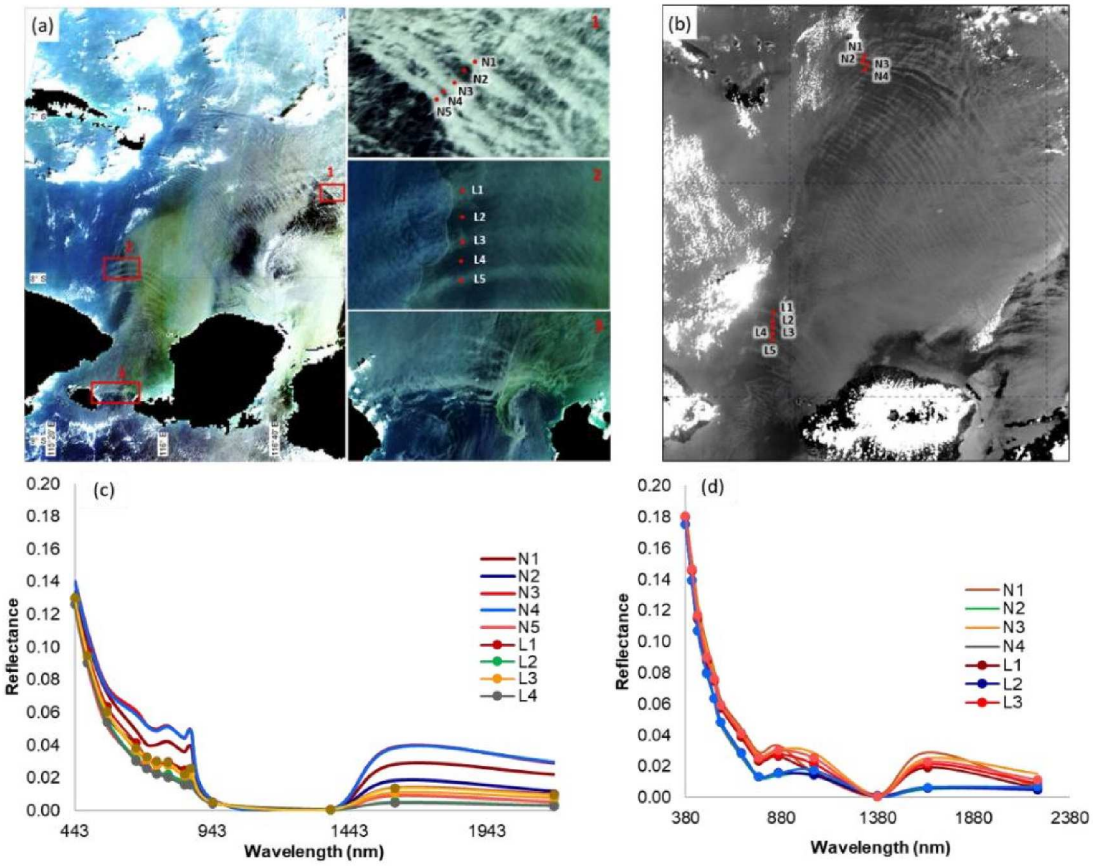

Figure 2.14. (a) True-color images of Sentinel-2B/MSI on 8 January 2019 at 10.20 GMT+8 with details of ISWs surface manifestation, (b) TOA reflectance of GCOM-C/SGLI on 9 January 2019 at 10.35 GMT+8, (c) spectral reflectance information of the bright and dark areas of ISWs manifestation by the Sentinel-2B/MSI, and (d) spectral reflectance information of the bright and dark areas of ISWs manifestation by the GCOM-C/SGLI.

The MODIS optical sensors on the Terra and Aqua satellites also captured the ISW manifestation pattern, but on the day before the SGLI image was captured. The absence of MODIS imagery on the same day as SGLI was due to the limited satellite paths through the Lombok Strait and the cloud cover. The ISW manifestation pattern detected in MODIS images for both Terra and Aqua showed a consistent pattern with Sentinel-2B/MSI on the same day, with a recording time difference of approximately 45 min (Figure 2.15).

Nevertheless, some uncertainties remain in this study, particularly concerning the processes occurring below the surface that influence the reflectance and emissions of the sea surface. The results of this analysis have not been validated using ground-truth data, and the validation process is essential for ensuring the accuracy of these findings. However, due to the challenges and high costs associated with data collection in the open sea, as well as the non-linear occurrence pattern of ISW, it is rarely carried out. In future studies, it would be beneficial to validate the findings by comparing them with field data, such as using an

Echosounder or Acoustic Doppler Current Profiler (ADCP), as conducted by Susanto et al. (2005) and Purwandana et al. (2021). Consequently, this study contains some biases, and improvements are necessary for future research.

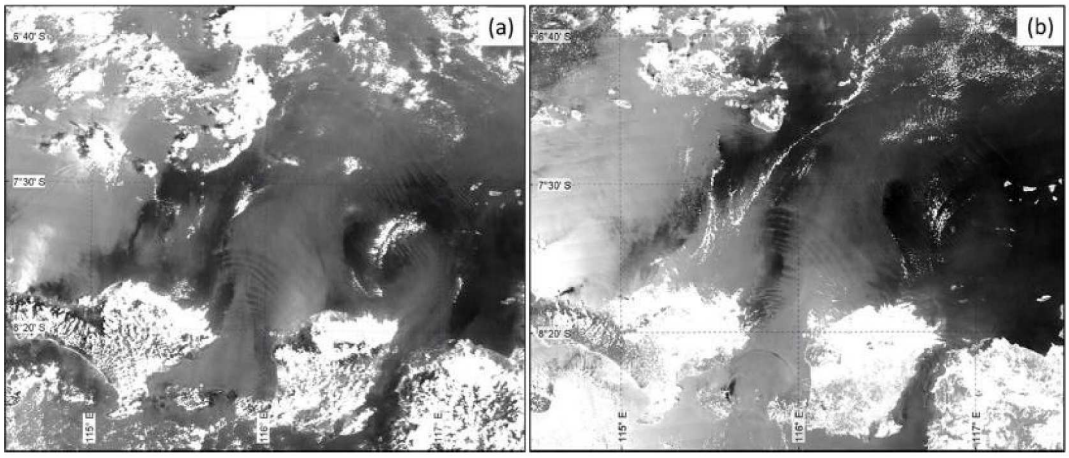

Figure 2.15. The observed ISWs surface manifestation by (a) Terra/MODIS image on 8 January 2019 at 11.05 GMT+8 and (b) Aqua/MODIS image on 8 January 2019 at 13.55 GMT+8

2.5 Conclusions

The interaction between light and matter, especially at the ocean surface, is an important topic in remote sensing. Small-scale phenomena that are sometimes ignored can accumulate and create anomalies that are often missed in the analysis. ISWs are small-scale phenomena that are often neglected because of their complexity and nonlinear characteristics. ISWs are the most frequently appearing type of internal waves and have been discussed in remote sensing research because of their unique characteristics, which allow them to be differentiated from other phenomena above the sea surface. The interaction between ISWs and surface waves causes changes in sea surface roughness that can be detected using sensors. The detection of ISWs using optical sensors has been widely used to analyze ISW dynamics based on patterns detected in images. A comprehensive analysis of optical sensor products has never been conducted. GCOM-C/SGLI, which has a high spatial resolution and consists of two sensors, a visible-near infrared radiometer and an infrared scanner, comprehensively reveals the characteristics of ISW manifestations through products derived from different scanning techniques.

A comparison between Level-1B data and Level 2 Ocean products on SGLI indicated that ISW patterns affect ocean color parameters and thermal channel data. The consistent manifestation pattern of ISW detected in TOA radiance and ocean color products is assumed

to be due to the impact of ISW on the sea surface, creating rough and smooth surfaces. Rough sea surfaces scatter and absorb sunlight, causing the sensor to record these areas as darker. Conversely, smooth sea surfaces reflect sunlight, causing the sensor to record these areas as brighter owing to specular reflection. The manifestation of ISWs in the thermal channels and SST is due to the modulation of the mixed layer depth by ISWs. This modulation lifts the cold-water layer near the surface, causing the emissions recorded by the sensors to be consistent with the pattern of ISW manifestation at the sea surface. Sentinel-2B/MSI and GCOM-C/SGLI reflectance spectral information showed a consistent pattern of high reflectance values in the violet band (380-443 nm). There was no significant difference in the spectral characteristics between the bright and dark areas owing to the manifestation of the ISW on the surface.

These findings confirm that ISWs influence both optical and thermal sensor data, with implications for understanding ocean surface dynamics and improving the accuracy of remote-sensing applications. The ability to detect ISWs using multiple sensors provides valuable insights into their formation, propagation, and impact on the sea surface, contributing to more accurate monitoring and analysis of oceanographic processes in the future.

CHAPTER 3

Estimation of Internal Solitary Waves Propagation Speeds and Occurrence using Long-term Sentinel-1 SAR Data in the Lombok Strait, Indonesia

3.1 Introduction

Internal Solitary Waves (ISWs) are significant oceanographic phenomena observed worldwide in various straits and coastal regions (Apel, 2002b). These waves, generated by tidal forces and influenced by various climatic and oceanic factors, play a crucial role in the distribution of energy and nutrients in oceans (Klemas, 2012). Understanding the dynamics of ISWs, particularly their occurrence frequency and propagation speed, is essential for marine navigation, ecological studies and climate research (Woodson, 2018).

The Lombok Strait, located between the islands of Bali and Lombok in Indonesia, is an essential region for studying ISWs because of its unique geographical and oceanographic characteristics (Susanto et al., 2005, 2007). The strait is part of the Indonesian Throughflow (ITF), a significant ocean current that transports water from the Pacific Ocean to the Indian Ocean. The generation and propagation of ISWs in this region are influenced by complex interactions between tidal currents, ocean stratification, and climatic phenomena such as the El Niño-Southern Oscillation (ENSO) and Indian Ocean Dipole (IOD) (Matthews et al., 2011).

Sentinel-1 Synthetic Aperture Radar (SAR) images are valuable tools for observing and analyzing ISWs, offering high-resolution data that can reveal detailed patterns of wave dynamics over time. Researchers have used ERS SAR images in the Strait of Messina to demonstrate that Internal Wave (IW) features are more frequently detected during summer when the thermocline is clearly defined (Brandt et al., 1997). In the South China Sea, Meng et al. (2003) and Zheng et al. (2007) documented interannual and seasonal changes in IW detection using ERS SAR. Seasonal patterns of IW activity generation, penetration, and location have been observed in the Mozambique Strait using ENVISAT SAR (da Silva et al., 2009). Sentinel-1 has a SAR C-band instrument similar to ERS-1/2 and ENVISAT ASAR, with an improved temporal resolution. ISW observations using Sentinel-1 SAR time series images have been conducted in the Timor Sea over six years, showing the variability and characteristics of the detected ISWs (Zhang et al., 2023). Tao et al. (Tao et al., 2022)

published a public dataset of SAR images using Sentinel-1 SAR images, which can be used as internal wave observation datasets using machine learning.

ISW observations in the Lombok Strait utilizing time-series data from SAR images have been conducted previously. Matthews et al. (2011) statistically investigated the frequency of ISW occurrences propagating north and south of the Lombok Strait using PALSAR and ERS-1/2 data. This study suggests long-term modifications of the monsoon-induced throughflow in the Lombok Strait. Karang et al. (2011) also investigated the interannual occurrence frequencies of ISWs in the Lombok Strait using PALSAR data over five years, demonstrating that ISWs were observed frequently in April. Zheng et al. (Zheng et al., 2007) statistically analyzed the occurrence of internal waves in the South China Sea and introduced a de-weighted factor to normalize SAR working days, which are typically not evenly distributed in each annual and monthly period.

Chonnaniyah et al. (2021) provided valuable insights by estimating the ISW phase speed in the northern part of the Lombok Strait based on a comprehensive analysis of Sentinel-1 SAR images and Himawari-8 data. This study revealed a decrease in the ISW propagation speed as these waves traversed shallow waters in the northern part of the strait. Furthermore, the variability of ISW detection in the Lombok Strait was investigated over six years, as detailed in a separate study (Chonnaniyah et al., 2021).

Previous studies have indicated that ISW occurrences in the Lombok Strait are closely associated with tidal currents from the Indian Ocean (Mitnik, Alpers, & Hock, 2000; Susanto et al., 2005). Previously, propagation speed estimation relied on the distance between packets and tidal timing (Tensubam et al. 2021). If an ISW packet is assumed to have a critical phase with semidiurnal tides, it is possible to estimate the average propagation speed of the ISW packet by ascertaining the generation location and highest tide data at that location. This study proposes combining information from Sentinel-1 images with tidal predictions from a model to estimate the propagation speed of ISWs in the Lombok Strait using a nine-year time series of Sentinel-1 SAR images. However, the relative influence of ENSO and IOD on these occurrences and propagation speeds remains a topic of ongoing research.

This study demonstrates the utility of remote sensing techniques, such as SAR, in detecting ISW surface signatures, although biases remain compared to in situ measurements owing to limitations in temporal resolution and environmental factors. These findings contribute to a deeper scientific understanding of the mechanisms driving ISW generation and propagation, with implications for oceanographic modelling and forecasting in the region.

3.2 Data and Methods

3.2.1 Sentinel-1 SAR

SAR data have become the most critical remote sensor for detecting ISW occurrence in the ocean. Sentinel-1 SAR missions distribute free open-access data and provide the opportunity to analyze ISW dynamics using high-resolution imagery over long periods. A pair of polar-orbiting satellites collected sentinel-1 SAR data using available day and night C-band SAR imagery. The Ground Range Detected (GRD) Level 1 product was used to analyze the occurrence frequencies and propagation speed estimation in the Lombok Strait areas. The interferometry wide-swath mode on the GRD Level 1 product offers comprehensive area coverage of 250 × 200 km in a single scene. Sentinel-1 SAR data covering nine years, from January 2015 to December 2023, were collected from the Alaska Satellite Facility's Distributed Active Archive Centre (ASF DAAC). A total of 578 images were available from different days in the Lombok Strait area for the ascending and descending orbits of Sentinel-1A and Sentinel-1B (Figure 3.1). A total of 372 SAR images detected the ISW pattern, and 273 SAR images focused on the northward-propagating ISW for the analysis of the propagation speed estimation.

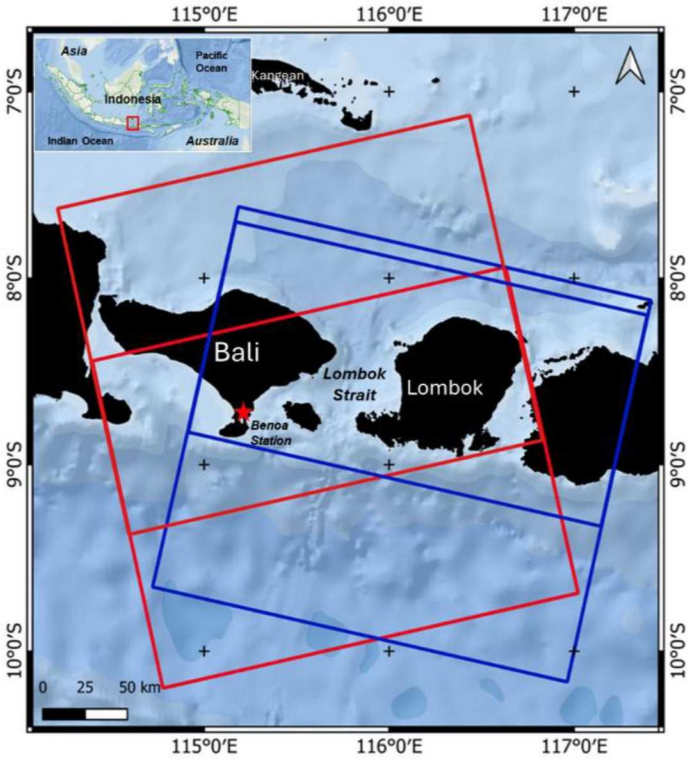

Figure 3.1. Map of the Lombok Strait. The red boxes represent the Sentinel-1 swath for the ascending (red boxes) and descending (blue boxes) orbits. The red star indicates the location of the tidal data validation.

3.2.2 Tidal Elevation

The predicted tidal elevation and zonal and meridional current components were obtained from the Tide Model Driver (TMD) – TPXO-9. This model utilizes 22 tidal components (M_2, S_2, N_2, K_2, K_1, O_1, P_1, Q_1, M_m, M_f, M_4, MN_4, MS_4, $2N_2$, S_1, $2Q_1$, J_1, L_2, M_3, MU_2, NU_2, and OO_1) and has a resolution of approximately about 1/30°. The TMD provides tidal elevation data at 10-minute intervals; however, for this study, the data were filtered to one-hour intervals. TPXO-9 is a global ocean tide model that provides accurate predictions of tidal elevation and currents across oceans. Recent research on ISW in the central Andaman Sea has used the TPXO-9 model to observe the behavioral characteristics of ISW (Sun et al., 2024).

Before utilizing the tidal elevation data from TMD, validation was conducted by comparing the TMD data with real-time tidal elevation data from the *Sistem Referensi Geospatial Indonesia* (SRGI), developed by *the Badan Informasi Geospatial* (BIG). This validation was performed at Benoa Station (red star in Figure 3.1). Tidal elevation data from 1 May to 31 May 2024 recorded at one-hour intervals, were used for this validation.

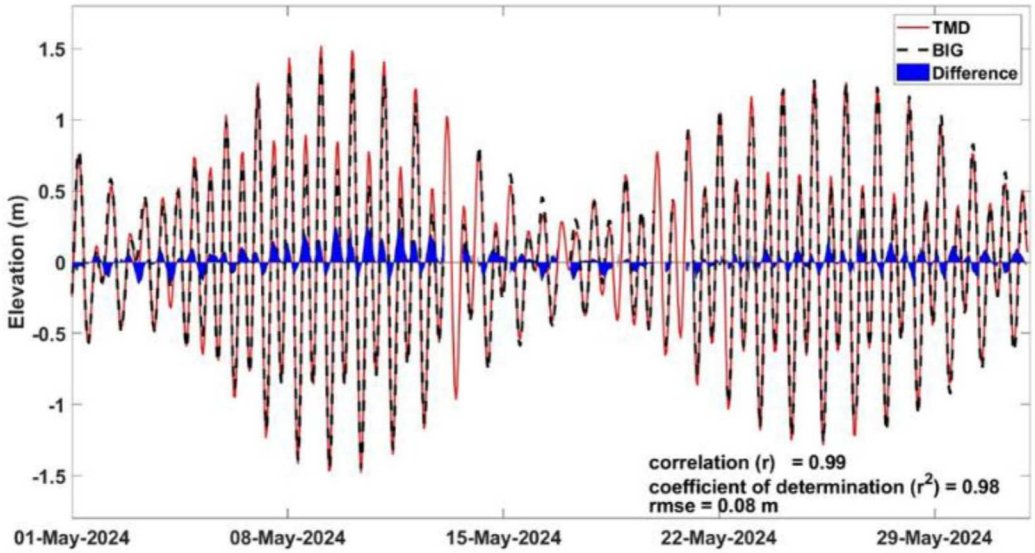

Figure 3.2. Validation of tidal elevation at Benoa Station, Bali.

The validation results for the tidal elevations at Benoa and Bali are presented in Figure 3.2. The comparison between the model and observed data indicated a high correlation (r) of 0.99 and a coefficient of determination (r^2) of 0.98. Additionally, the Root Mean Square Error (RMSE) was 0.08 m (8 cm). Overall, the tidal elevation model closely matched the observed data, indicating that it accurately represented the actual field conditions.

3.2.3 Statistical Analysis

The occurrence frequency distribution of ISW events in the Lombok Strait for nine years from 2015 to 2023 was analyzed using statistical methods similar to those used in previous research on the northern South China Sea (Zheng et al., 2007). Previous research has applied a de-weighting factor for the irregular distribution of Sentinel-1 images annually. The annual distribution of ISW detection frequency observed by Sentinel-1 SAR is determined as (1)

$$p_i = q_i \left(\frac{N_i}{\sum_j N_j} \right) \tag{1}$$

q_i represents the de-weighted factor for annual distribution, described as (2)

$$q_i = \frac{D_{\min}}{D_i} \tag{2}$$

D_i is the Sentinel-1 mission working days in the ith year (24 (2015), 27 (2016), 55 (2017), 101 (2018), 99 (2019), 88 (2020), 80 (2021), 50 (2022), and 54 (2023)). N_i (N_j) denotes the total number of days for detected ISW in Sentinel-1 SAR images and represents the total number of days for detected ISW in Sentinel-1 SAR images. The Sentinel-1 SAR working days in 2015 were minimal (D_{min}); therefore, the de-weighted factor for 2015 was assigned to a value of 1. The same calculations were performed for the seasonal and monthly distributions.

The occurrences of Sentinel-1 SAR are categorized into four distinct seasons: December-January-February (DJF) represents the northwest monsoon or boreal winter; March-April-May (MAM) represents the transition season or mid-autumn; June-July-August (JJA) represents the southeast monsoon or boreal summer; and September-October-November (SON) represents the spring intermediate (Susanto et al., 2007).

3.2.4 Phase Speeds Estimation

ISWs in the Lombok Strait are generated by interactions between stratified water, tidal flow, and complex bottom topography (Susanto et al., 2005). Previous research estimated the ISW propagation speed using two ISW packets detected in SAR images. This approach assumes that the time difference between two packets is approximately equivalent to the tidal period, which is similar to the tidal period (Mitnik, Alpers, & Hock, 2000; Susanto et al., 2005). Tides in the Lombok Strait are generated by tidal waves propagating from the

Indian Ocean with a dominant M_2 semidiurnal period of 12.4 h (Purwandana et al., 2021). The method proposed in this study for estimating the ISW propagation speed involves the use of a Sentinel-1 SAR image scene that detects a single ISW packet only and then combines it with information about the closest high tide time to the SAR image acquisition time (Figure 3.3).

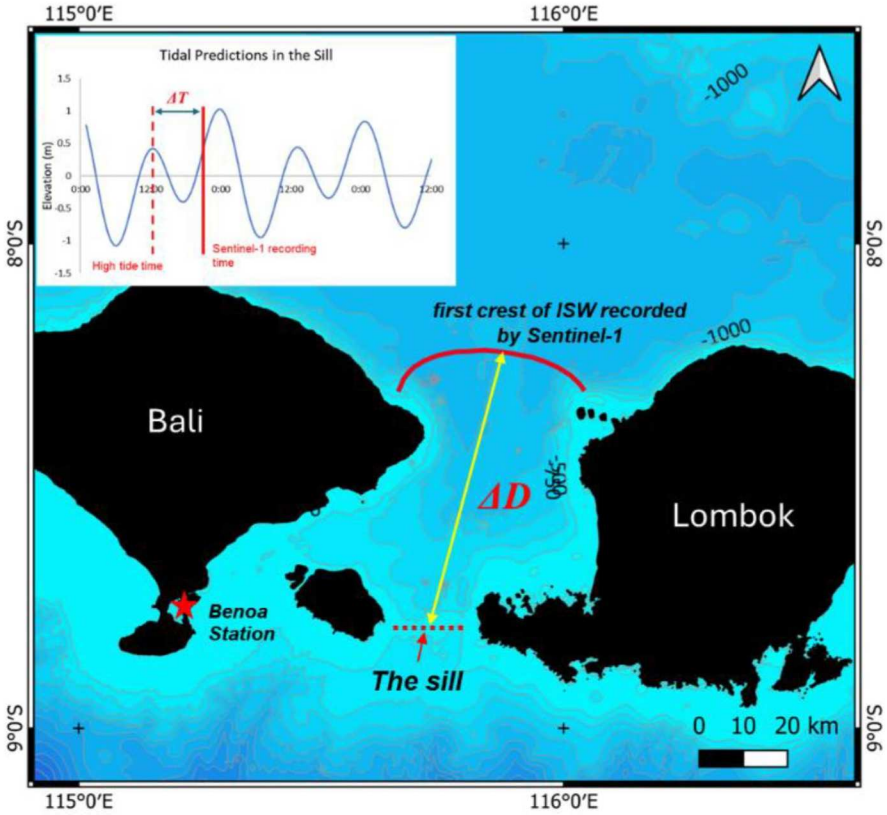

Figure 3.3. The ISW propagation speed estimation methodology combines the distance of the first ISW crest detected in the Sentinel-1 image to the sill (ΔD), the high tide interval, and the recording time of the Sentinel-1 image (ΔT). The red asterisk indicates the location of tidal data validation.

ISW propagation speed utilizing Sentinel-1 SAR image (C_{SAR}) and tidal data is estimated by (3)

$$C_{SAR} = \frac{D_{Sill-ISW}}{T_{SAR} - T_{Tidal}} = \frac{\Delta D}{\Delta T} \qquad (3)$$

Where $D_{sill\text{-}ISW}$ is the distance between the sill location (dashed red line) measured in meters (m) and the first ISW crest recorded by the Sentinel-1 SAR image (Figure 3.3), T_{SAR} represents the Sentinel-1 SAR image recording time, and T_{tide} is the high tide time closest to the SAR image recording time measured in seconds (s). C_{SAR} is the ISW propagation speed measured in meters per second (ms^{-1}).

3.3 Results

ISW packets are typically observed as alternating bright and dark bands in SAR images. An ISW packet consists of several individual waves with different amplitudes and speeds. Typically, the wave with the greatest amplitude is located at the front, with the amplitudes decreasing towards the rear of the wave packet (Alpers et al., 2011). The spatial distribution of the first crest of the ISW across the Lombok Strait was mapped using Sentinel-1 SAR images from 2015 to 2023 (Figure 3.4). A total of 273 SAR images with the detection of ISW patterns propagating northward were concentrated in the Lombok Strait area at Latitude 8-9ºS. In this study, the ISW packets detected in the Sentinel-1 SAR imagery were predominantly located in the transition zone from shallow to deep water, ranging from 500 to 1500 m.

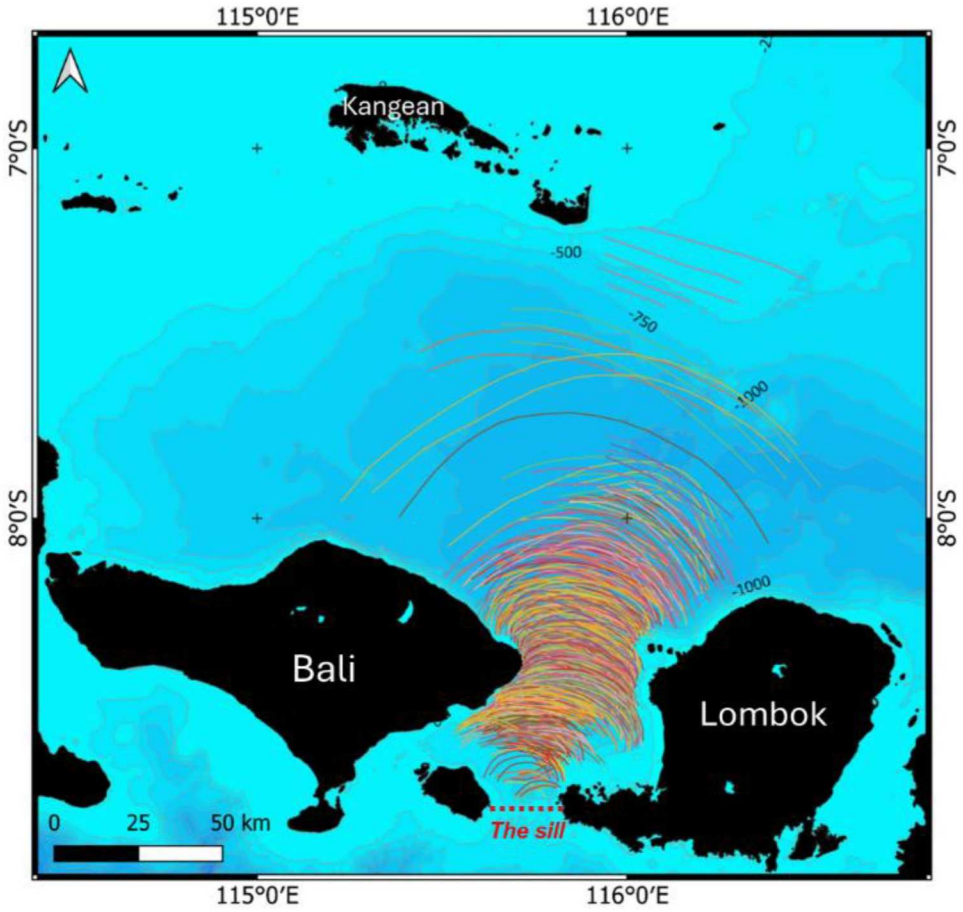

Figure 3.4. Spatial distribution of ISW occurrence observed by Sentinel-1 SAR in the Lombok Strait area from 2015 to 2023. The colored curved line delineates the first crest of the ISW detected in the Sentinel-1 SAR imagery.

An analysis of long-term Sentinel-1 SAR data revealed distinct patterns in the monthly occurrence of ISWs in the Lombok Strait. Over the nine-year study period from 2015 to

2023, ISWs were detected every month, with their frequency varying significantly during the year. Figure 3.5 shows the monthly distribution time series of the ISW occurrence frequency and propagation speed, as observed in the Sentinel-1 SAR images. The highest number of ISW was observed during the transitional period, specifically in October, with an average of 9%. The ISW activity was relatively low at the beginning of the southeast monsoon in June, with an average activity of 5%. The average ISW propagation speed across the entire dataset was estimated to be approximately 2.36 ms^{-1}, which is consistent with previously reported values for the Lombok Strait. The highest propagation speeds were observed in December, averaging 2.72 ms^{-1}. The ISW propagation speed decreased by an average of 2.23 ms^{-1} in October.

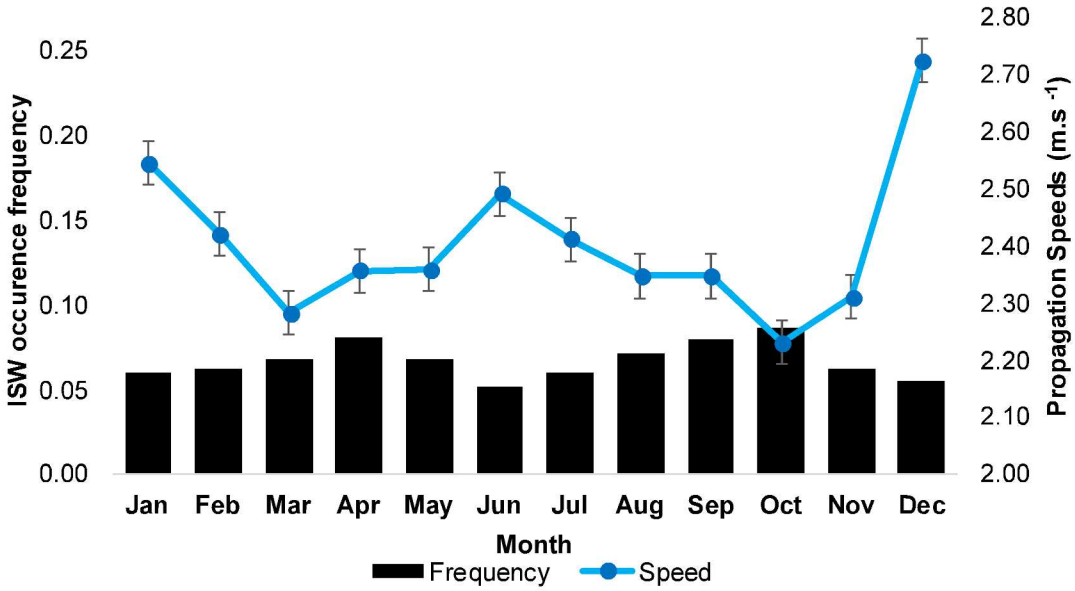

Figure 3.5. Monthly average distribution of ISW occurrence frequency and propagation speed estimation in the Lombok Strait observed by Sentinel-1 SAR during the period 2015-2023.

Seasonal analyses provided additional insights into the influence of regional climatic and oceanographic processes on ISW activity. The highest number of ISW occurrences was observed during the transitional periods of SON, with an average of 27%, and the lowest was observed in DJF, with an average of 21% (Figure 3.6). The highest propagation speeds were observed in DJF, averaging 2.56 ms^{-1} and the lowest were observed in SON, averaging 2.29 ms^{-1}. The results of the monthly and seasonal analyses were consistent and reliable.

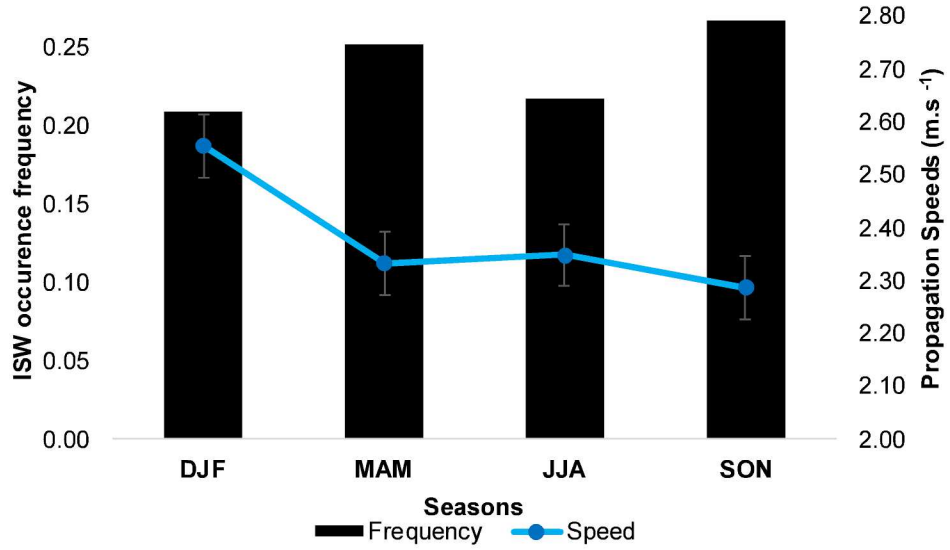

Figure 3.6. Seasonal distribution of ISW occurrence frequencies and propagation speed estimation in the Lombok Strait observed by Sentinel-1 SAR during 2015-2023.

Figure 3.7 shows the annual distribution of ISW occurrence frequencies in the Lombok Strait, indicating significant variability across the years. The peak occurrence was in 2015, accounting for 5% of all observed ISWs, whereas 2020 exhibited the lowest frequency of only 3%. Although wave activity fluctuated, the propagation speed exhibited a distinctly different pattern. The highest average speed was recorded in 2021, with ISWs traversing the strait at 2.53 ms^{-1}, whereas 2023 displayed the lowest average speed of 2.22 ms^{-1}.

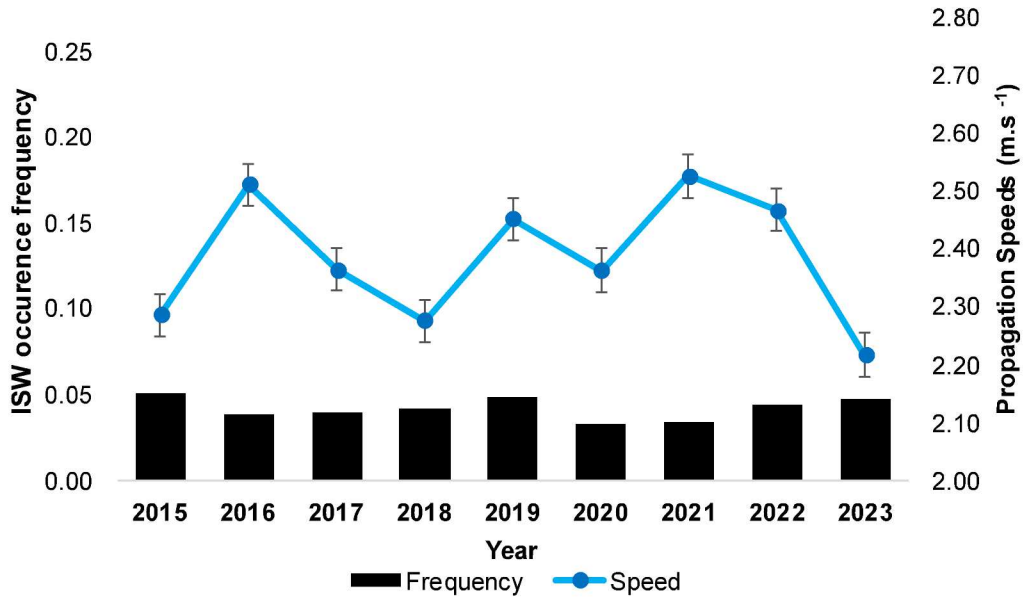

Figure 3.7. Annual distribution of ISW occurrence frequencies and propagation speed estimation in the Lombok Strait observed by Sentinel-1 SAR during 2015-2023.

The analysis of the monthly distribution time series data for ISW occurrence frequency in the Lombok Strait overlaid with the ENSO and IOD indices revealed an average occurrence frequency of 5% per month. Figure 3.8 shows that the correlation coefficient between the ISW occurrences and the IOD index is 0.365, indicating a moderate relationship. This suggests that fluctuations in IOD influence ISW activity in the Lombok Strait. In contrast, the correlation coefficient between the ISW occurrence and ENSO index was -0.006, indicating a negligible relationship. This implies that ISW occurrences in the Lombok Strait are not significantly associated with the ENSO cycle.

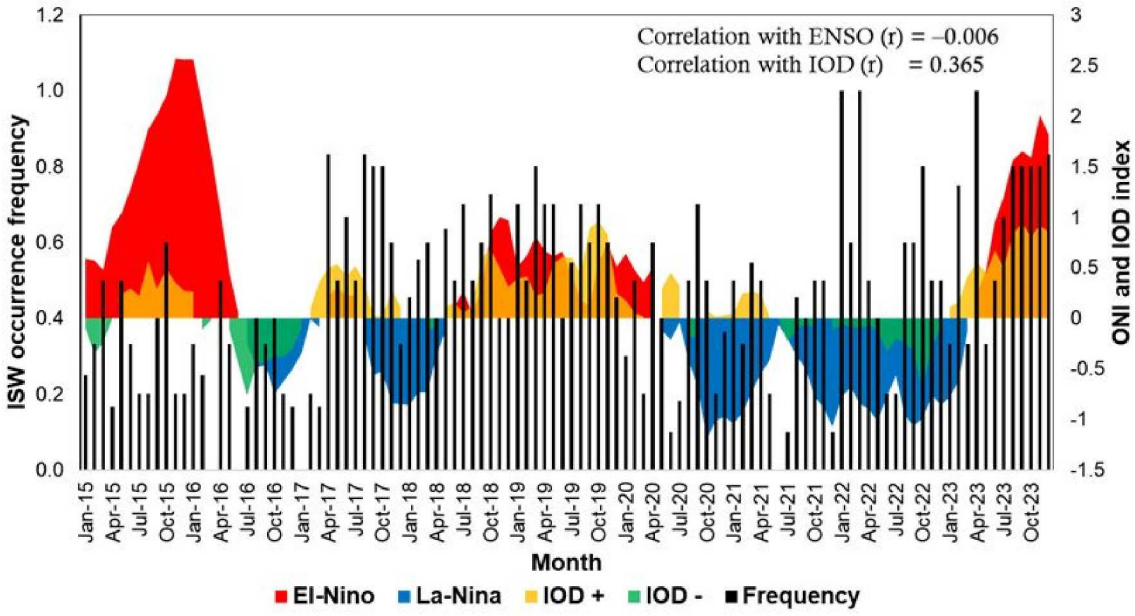

Figure 3.8. Monthly distribution time series of ISW occurrence frequencies observed by Sentinel-1 SAR from January 2015 to December 2023. The red and blue shaded areas represent ENSO events. The yellow and green shaded areas represent IOD events.

The time series analysis of the ISW propagation speed data revealed an average speed of 2.4 ms^{-1}, ranging from 1.6 ms^{-1} to 3.5 ms^{-1}. The standard deviation of 0.32 ms^{-1} indicates moderate variability in the speed over the observed period. Figure 3.9 shows the correlation coefficient between the ISW propagation speeds and ENSO index, which was found to be -0.30. This negative correlation indicates a moderately inverse relationship between the two variables. This suggests that ISW propagation speeds may be affected by ENSO fluctuations. The correlation between the ISW propagation speed and IOD index was -0.18, indicating a weak negative relationship. Although this correlation is less pronounced than that with ENSO, it suggests that variations in the IOD may influence ISW speeds.

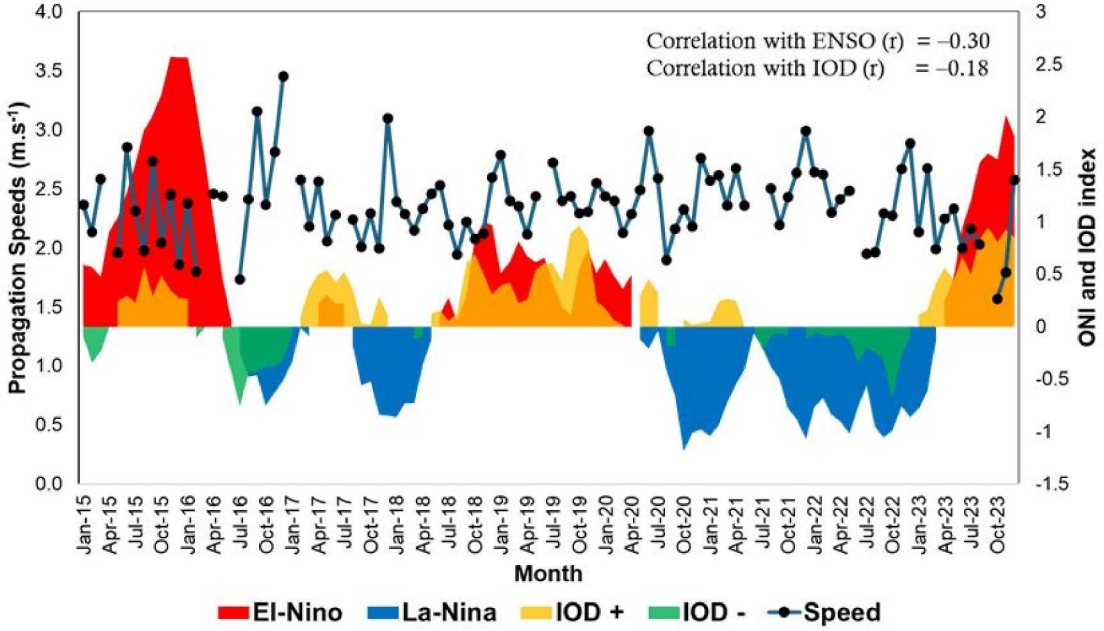

Figure 3.9. Monthly distribution time series of ISW propagation speeds estimated using Sentinel-1 SAR and tidal data from January 2015 to December 2023. The red and blue shaded areas represent ENSO events. The yellow and green shaded areas represent IOD events.

Further analysis to identify periodic patterns in ISW occurrence and propagation speed was conducted using the Fast Fourier Transform (FFT), a mathematical algorithm that converts time-domain signals into frequency-domain representations. By analyzing the frequency components of the data, FFT facilitates the identification of dominant cycles in the ISW activity. The period of these cycles can be obtained by taking the inverse of the frequency; specifically, the period is calculated as $P = 1/f$, where P is the period and f is the frequency. Figure 3.10 shows the FFT analysis based on long-term Sentinel-1 SAR data, indicating a dominant cycle with a period of approximately 54 months. ISW occurrence in the Lombok Strait followed a long-term periodic trend, with increased activity approximately every 4.5 years. This pattern is associated with climate oscillations, such as the IOD, which influences the oceanographic conditions in the Lombok Strait.

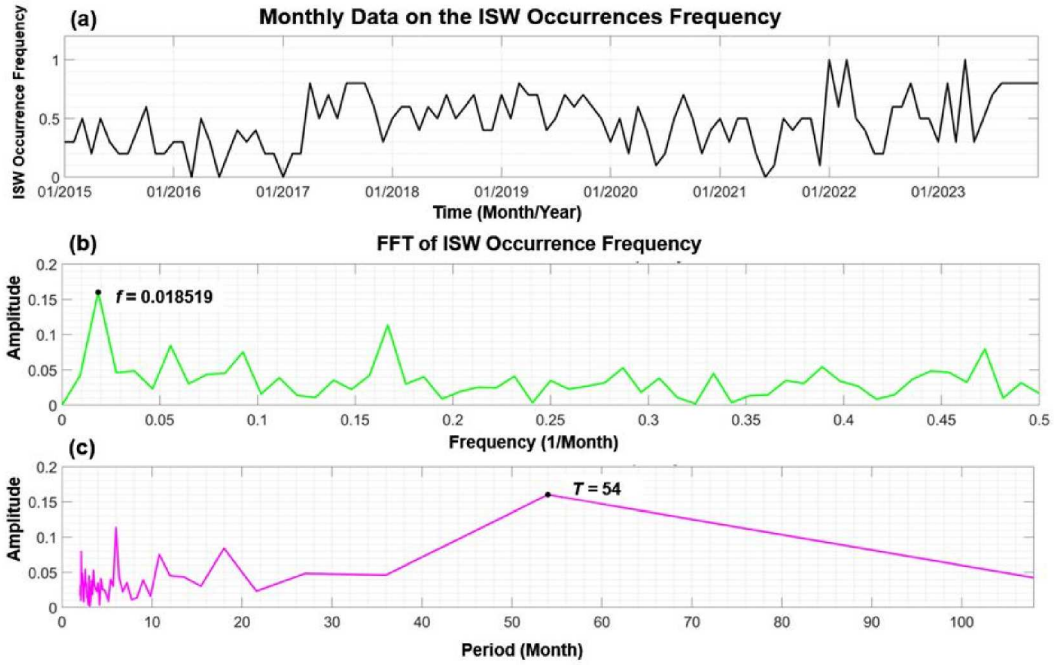

Figure 3.10. FFT results of ISW occurrence frequency using monthly time-series data. (a) Original data, (b) frequency domain, (c) period.

Figure 3.11 shows that the FFT analysis revealed a prominent spectral peak corresponding to a 12-month period, indicating significant seasonal variability in the ISW propagation speed. For the analysis, no months with missing data were assigned a value of zero in the original dataset.

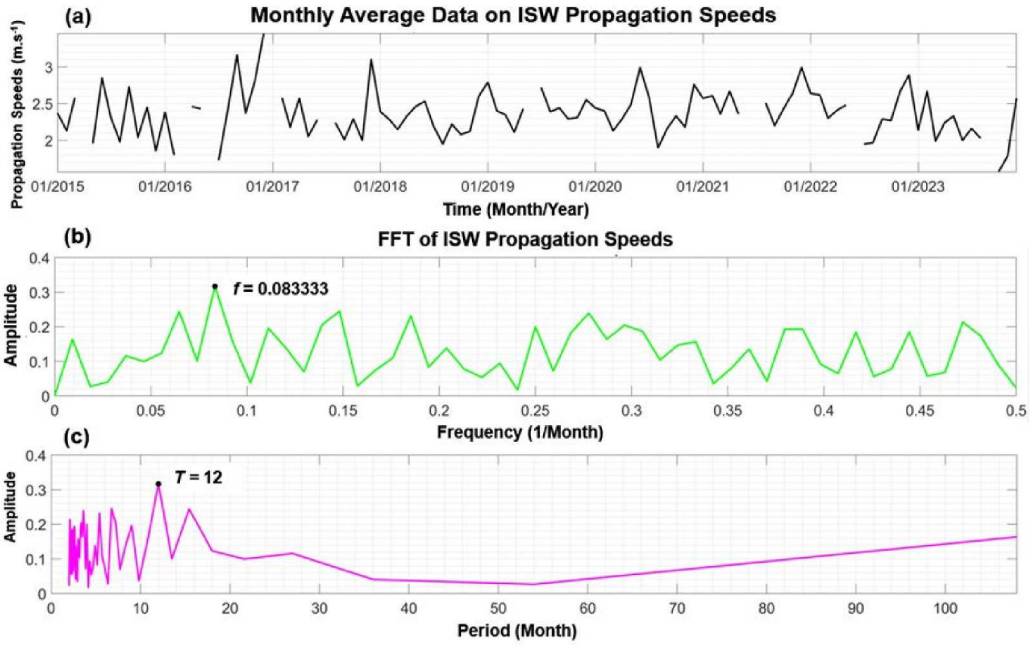

Figure 3.11. FFT results of ISW propagation speeds using monthly average time-series data. (a) Original data, (b) frequency domain, (c) period.

3.4 Discussion

The distinct monthly and seasonal patterns of ISW occurrence observed in the Lombok Strait are the result of complex interactions among tidal dynamics, stratification and atmospheric conditions. The peak ISW occurrence frequency occurred during the monsoon transition of the SON, and lower ISW occurrence occurred during the DJF. This study revealed that the ISW occurrences detected in Sentinel-1 SAR images were primarily influenced by stratification conditions during each season. In the transition season (SON and MAM), the thermocline tended to be stable, whereas in DJF, it became deeper. The deepening of the thermocline affects the ISW manifestations at the surface, diminishing their detectability and making them less significant for detection by SAR. Furthermore, ISW occurrences are less frequent in JJA because of the presence of a net surface current south of the Lombok Strait, which impedes the generation of ISW to the north (Susanto et al., 2007). Additionally, the intrusion of Kelvin waves from the Indian Ocean during the transition season contributed to the increased detection of ISW events. Kelvin wave intrusion strengthens the tidal current flowing northward through the Lombok Strait, intensifying the ISW generation in the northern part of the strait (Syamsudin et al., 2004). The lowest frequency of ISW occurrence in June can be attributed to the southward strengthening of the tidal current driven by intensified ITF transport during the southeast monsoon, which affects the release of ISW (Susanto et al., 2007).

The distribution of propagation speeds differed from the frequency of ISW occurrences, with the highest average propagation speed in December (boreal winter), when ITF transport weakened, and the lowest in October. The monthly variability of ISW propagation speeds in the Lombok Strait exhibited an inverse trend compared to the frequency of ISW occurrence. The highest propagation speed occurred during the DJF season, whereas it remained relatively constant during the other seasons. These seasonal distribution results suggest that variations in ITF transport, rather than changes in the thermocline, influence ISW propagation speeds in the Lombok Strait. Matthews et al. (2011) conducted numerical simulations of the dynamics of ISWs in the Lombok Strait, examining monsoonal variations with and without ITF transport. Their study revealed that ITF transport during the southeast monsoon weakened the current gradient, resulting in slower ISW propagation. The analysis in this study is consistent with that of Matthews et al. (Matthews et al., 2011) in terms of monthly and seasonal distributions, demonstrating that ISW propagation speeds are faster during the northwest monsoon. However, the annual

distribution analysis showed some inconsistencies, likely due to interannual modifications influenced by ENSO and IOD. However, the combination of El Niño and a positive IOD yielded contradictory results (Sprintall et al., 2019), with a higher frequency of detected ISW occurrences and increased propagation speed.

Correlation analysis revealed a moderate positive relationship between ISW occurrences and the IOD index (0.365), whereas the ENSO index had a negligible influence (-0.006). During positive IOD phases, cooler sea surface temperatures can cause the thermocline to become shallower, contributing to a higher frequency of ISW occurrences. Conversely, negative IOD phases are associated with warmer sea surface temperatures, which can influence the thermocline to deepen, resulting in a decrease in ISW occurrence (Ng et al., 2014). ISW propagation speeds were moderately negatively correlated with ENSO (-0.30) and weakly negatively correlated with IOD (-0.18), suggesting that ENSO-related changes in ocean stratification have a stronger impact on ISW propagation. The discrepancy in the correlation between the ISW occurrence frequencies and propagation speed estimates can be attributed to the assumption that ISW generation in the Lombok Strait occurs when the water is stratified. This finding is consistent with Zhu and Wang (2024), who posited that ENSO plays an essential role in upper layer transport in Indonesian waters, while IOD plays a crucial role in lower layer transport. The ISW propagation speed is closely related to the thermocline, which influences the ENSO. The ISW propagation speed during La Niña was higher than that during El Niño because of variations in the thermocline depth. During El Niño, the thermocline conditions in Indonesian waters become shallow, and ITF transport is reduced, causing the current gradient to weaken (Matthews et al., 2011).

FFT analysis identified a 54-month cycle in ISW occurrence and a 12-month cycle in propagation speed, thereby elucidating the effects of long-term climatic oscillations and seasonal patterns on ISW dynamics. This observation indicates that, in addition to short-term seasonal influences, long-term climatic oscillations, such as the IOD and other multi-year cycles, significantly influence ISW generation over an extended period. While time-series analysis provides detailed insights into the short-term variability of ISW behavior, FFT analysis reveals the underlying long-term cycles that govern ISW activity. The correlation analysis corroborated these findings, demonstrating a moderate positive relationship between ISW occurrence and the IOD index, emphasizing the role of long-term climate variability. In contrast, the ENSO index showed a negligible correlation with ISW occurrences, although it moderately impacted the propagation speeds, as suggested by both time series and FFT analyses. Therefore, the utilization of a long-term dataset is crucial for

a comprehensive analysis; however, this study utilized only a nine-year dataset, which limits its ability to fully establish the statistical significance of the observed cycles. Despite this limitation, this study offers valuable preliminary insights into the importance of long-term observations for understanding the impact of climate oscillations on the dynamics of ISW. This finding is in line with previous studies that stated that long-term trend analysis, especially those covering multi-year cycles, such as ENSO and IOD, requires data spanning more than a decade to significantly distinguish between natural oscillations and random fluctuations (Norel et al., 2021). Extending the dataset would not only deepen the understanding of the critical role of climate variability in shaping ISW dynamics but also make important contributions to the modelling and prediction of regional ocean dynamics.

ISW detection using remote sensing techniques still contains considerable bias compared to in situ measurements. Observations using SAR imagery focus solely on detecting surface roughness signatures caused by ISW activity beneath the ocean surface. The modulation of sea surface roughness by ISWs is primarily influenced by environmental conditions, which can lead to misclassification or missed events when the ISW surface signatures are not well defined. Additionally, ISW detection using Sentinel-1 SAR is prone to bias owing to its limited temporal resolution, which means that ISWs may occur but go undetected by Sentinel-1 SAR. The long-term implications of this study focus only on detecting the surface signatures of ISWs under the influence of monsoon, ENSO, and IOD variability in the Lombok Strait. Further research is needed to observe variations in the detected ISW properties, such as soliton number, wavelength, and first-crest length.

3.5 Conclusion

This study provides important insights into the occurrence and propagation of ISWs in the Lombok Strait using long-term Sentinel-1 SAR data. The occurrence frequencies of ISWs observed in Sentinel-1 SAR images demonstrated a higher correlation with IOD than ENSO. This suggests that tidal currents from the Indian Ocean, which are predominantly influenced by the IOD, play a substantial role in ISW generation in the Lombok Strait. During positive IOD phases, cooler sea surface temperatures can cause the thermocline to become shallower, contributing to a higher frequency of ISW occurrences. Conversely, negative IOD phases are associated with warmer sea surface temperatures, which can influence the thermocline to deepen, resulting in a decrease in ISW occurrence. ISW propagation speeds were negatively correlated with ENSO and IOD indices, with ENSO having a more significant impact. During La Niña conditions, propagation speeds increase,

whereas during El Niño conditions, they decrease because of variations in the thermocline depth and ITF transport.

The monthly distribution of ISW occurrences reached its maximum in October and minimum in June, influenced by the stratification conditions during each season and increased ITF transport. Propagation speeds were highest in December (boreal winter), when ITF transport weakened, and lowest in October, exhibiting an inverse relationship with ISW frequencies. Annually, the highest ISW frequency was observed in 2015, coinciding with El Niño conditions, whereas frequencies decreased during La Niña conditions, demonstrating a more decisive and substantial IOD influence over ENSO. The highest average propagation speed was recorded in 2021, and the lowest was recorded in 2023, highlighting the annual variability in ISW dynamics. The results indicated that ISW activity exhibits both seasonal and multi-year variability, as evidenced by the FFT analysis, which identified a 54-month cycle in occurrence and a 12-month cycle in propagation speed. The moderate positive correlation between ISW occurrence and the IOD index suggests that climatic oscillations, particularly the IOD, play a significant role in influencing ISW activity. In contrast, the negligible correlation with the ENSO index highlights its limited impact on ISW occurrence, although ENSO-related changes in ocean stratification appear to influence the propagation speed, as demonstrated by the moderate negative correlation with ENSO. However, the utilization of only nine years of data constrains the ability to thoroughly establish the statistical significance of the observed cycles. Consequently, future research should incorporate longer datasets to enhance the robustness of these results.

The complex transport dynamics through the Lombok Strait resulted in varying average distributions of ISW occurrence and propagation speeds in the different months. This complexity necessitates further investigation, including external boundary condition data and numerical simulations, to better understand the parameters influencing the appearance of ISWs in SAR images. Additional observations using in-situ data and more comprehensive numerical simulations are essential to confirm these findings and provide a deeper understanding of ISW dynamics in the Lombok Strait. This study contributes to the expanding body of knowledge on ISW dynamics and their broader implications for ocean circulation and climate systems in the Lombok Strait and similar regions.

CHAPTER 4

On the Distinction of Seasonal Internal Solitary Waves Characteristics in the Lombok Strait Based on Multi-Satellite Data

4.1 Introduction

Internal solitary waves (ISWs) are among the easiest oceanographic phenomena to identify using remote-sensing data. The naked eye, optical sensors, and radar satellite sensors can observe the interaction between the ISW-induced surface roughness and the distinctive pattern of light and dark lines on the sea surface. The combination of radar and optical sensors can effectively determine the generation, propagation, and dynamic parameters of ISWs. Synthetic aperture radar (SAR), which can be used to measure very small changes in sea surface roughness in the centimeter-to-decimeter wavelength range, is the most effective instrument for detecting ISWs from space (Alpers, 2014). The dynamics of oceanic internal waves remain a mystery and require considerable investigation before the interaction between the ocean and atmosphere can be fully understood. These waves are crucial determinants of various oceanic processes, including sediment transport, nutrient dispersion, and ecosystem dynamics. Understanding the behavior and characteristics of ISWs is essential for accurately predicting and managing these processes, and therefore has practical implications for coastal engineering, fisheries management, and marine environmental monitoring.

The Lombok Strait is an essential pathway for the transoceanic transport of water. The current that crosses the Indonesian Seas, known as the Indonesian Throughflow (ITF), plays a role in the transfer of warm water masses from the Pacific Ocean to the Indian Ocean. The ISWs in the Lombok Strait are the most energetic ISWs in the Indonesian Seas, and their large amplitudes have been studied extensively (Susanto et al., 2005). Previous studies have used remote sensing data (Chonnaniyah et al., 2021; Karang et al., 2012, 2019; Matthews et al., 2011; Mitnik, 2008; Susanto et al., 2005), in situ measurements (Purwandana et al., 2021; Syamsudin et al., 2019), and numerical simulations (Gong et al., 2022; Ningsih et al., 2008). The generation and propagation of ISWs can modify currents that affect sea surface roughness (Alpers, 1985). ISW activity below the sea surface can displace the thermocline vertically and generate internal currents that result in convergence and divergence (Klemas, 2012). When the ISW crests pass below the surface, water on the surface flows down the crest sides and pools into the trough sides of the ISWs. because the sea surface is converging

(diverging) over the ISW crests (troughs), biological material and natural oils on the surface are alternately dispersed and concentrated in a similar wave pattern (da Silva et al., 2002).

The seasonal thermocline significantly affects the manifestation and characteristics of internal waves detected at the sea surface. Brandt et al., (1997) who observed the behavior of internal waves detected at the sea surface in the Strait of Messina, showed that they spread locally to the south of the strait, where they produced stronger manifestations than those propagated northwards. This pattern reveals the influence of seasonality on the direction of propagation and the properties of internal waves. The presence of seasonality and interannual influences on the properties of internal ocean waves have been thoroughly examined in numerous regions (da Silva et al., 2009; Zheng et al., 2007). Matthews et al. (2011) have extensively studied the characteristics of ISWs in the Lombok Strait using satellite imagery and numerical modelling. They identified two main types of ISWs in the strait: arc-like ISWs, which propagate towards the northern part of the strait, and irregularly propagating ISWs, which are found in the southern part of the generation site. In this study, we distinguished the characteristics of ISWs in the Lombok Strait between the two distinct monsoon seasons, the southeast monsoon (SEM) and the northwest monsoon (NWM).

The SEM is characterized by a strong southward throughflow between May and October. In contrast, the NWM, which typically occurs from November to March, exhibits more variable throughflow patterns and may even show a reversal to a northward direction. Past research has primarily focused on examining the features of identified ISW types during both monsoon seasons without further investigating the dynamic parameters estimated from the observed ISW patterns. We investigated these parameters in this study by utilizing multi-satellite data to acquire more comprehensive information about ISW parameters, including soliton numbers, wavelengths, and phase speeds in distinct seasons.

This study used a multi-satellite approach based on SAR and optical sensors to distinguish the characteristics of ISWs detected in different seasons in the Lombok Strait. We used SAR and optical images to estimate ISW dynamic parameters (soliton number, wavelength, and phase speed) in different seasons based on the detected ISW patterns. We also used ocean color products from three different sensors to identify ISW patterns and the possibility that ISW activity affected the conditions in the surrounding waters. This study provided multi-satellite observation data that could be used to highlight recent progress in understanding how ISWs affect coastal interactions in the Lombok Strait.

4.2 Data and methods

4.1.1 Remote sensing data

Multi-satellite radar and optical images can reveal differences in the ISW patterns and estimated characteristics of ISW dynamics in the Lombok Strait. SAR data, the most effective tool, has been used extensively to estimate and detect the dynamic characteristics of ISWs. In this study, we used open-access Sentinel-1 SAR data, which included day and night C-band SAR imagery from two polar-orbiting satellites. We used Level 1 Ground Range Detected (GRD) products to detect the ISWs in the Lombok Strait. Specifically, we used the interferometric wide-swath mode of the Level 1 GRD products, which covers a wide area of 250 km × 200 km in a single scene. The IW mode has the advantage of combining two sequential scenes to create a larger research area with linear dimensions of up to 400 km, thereby expanding the scope of the study.

Optical sensors are another type of instrument that can detect ISW patterns. They have the advantage of high temporal resolution, although their observations are confined to daylight hours and require cloud-free conditions to be effective. This study focused on the analysis of ISW patterns using optical images from various instruments, including the Second-generation Global Imager (SGLI) sensor obtained from the Global Change Observation Mission-Climate (GCOM-C), the Moderate Resolution Imaging Spectroradiometer (MODIS) sensor onboard the Terra satellite, and the Visible and Infrared Imager/Radiometer Suite (VIIRS) sensor onboard the Joint Polar Satellite System-1 (JPSS-1) satellite. The investigation of ISW patterns and surrounding water conditions involved the use of the visible-near infrared band and ocean color products such as chlorophyll-a concentration (Chl-a), sea surface temperature (SST), and aerosol optical thickness (AOT). This study used visible band products to observe and estimate the detected ISW patterns, which were then compared with SAR images for validation. Ocean color products from three different sensors were also used to identify ISW patterns and explore the potential influence of ISW activity on ocean color observations. This study incorporated data from the Sentinel-2A multispectral instrument (MSI) to further support the observed phenomenon.

To confirm the variations in the ISW patterns and dynamic parameters in the Lombok Strait, we used satellite data captured during different seasons. The inferred surface geostrophic transport analysis through the strait revealed significant variability across intra-seasonal and interannual time scales (Susanto et al., 2007). In this study, we concentrated on the two main seasons in the Lombok Strait region: the SEM from June to November and the

NWM from December to May. The selection of satellite data was based on the proximity of optical images detecting ISW patterns, which aligned with the ISW patterns detected by SAR. Table 4.1 summarizes the relevant information regarding the satellite data used in this study.

Table 4.1. Summary of used satellite data

Satellite/ Sensor	Date, Time (hh: mm, local)	Spatial resolution (m)	Products	Data Source
Sentinel-1/ SAR	October 25, 2018, 18:25 January 5, 2019, 18:41 January 9, 2019, 05:53 January 11, 2019, 18:41	20 20 20 20	Level 1 Ground Range Detected (IW Mode)	Copernicus Open Access Hub (https://scihub.copernicus.eu/)
GCOM-C/SGLI	October 26, 2018, 10:19 January 5, 2019, 10:41 January 9, 2019, 10:35	250 250 250	Visible and ocean color	G-Portal JAXA (https://gportal.jaxa.jp/gpr/)
Terra/ MODIS	October 26, 2018, 10:25 January 8, 2019, 11:05 January 9, 2019, 10:10	250, 1000 250 1000	Visible and ocean color	Ocean Color Web (https://oceancolor.gsfc.nasa.gov/)
JPSS-1/ VIIRS	October 26, 2018, 13:54 January 9, 2019, 13:48	750 750	Ocean color	Ocean Color Web (https://oceancolor.gsfc.nasa.gov/)
Sentinel-2A MSI	January 8, 2019, 10:20	10	True color image	Copernicus Open Access Hub (https://scihub.copernicus.eu/)

Our study focused on the northern area of the Lombok Strait near Kangean Island (6.5–9ºS and 114.5–117ºE). The bathymetric relief data used in this study were obtained from the Indonesian National Bathymetry (BATNAS). For the analysis, Sentinel-1/SAR data were collected from two scenes, one from the ascending and the other from the descending acquisitions, as shown in Figure 4.1(a). The months for the study were selected based on salinity variations; October and January were chosen to represent the conditions during the SEM and NWM, respectively. Salinity reaches a maximum in October and a minimum in March (Atmadipoera et al., 2009). Conditions during October 2018 and January 2019 were chosen for analysis because the similarity of the Oceanic Niño Index (ONI) during those months allowed us to ignore the impact of the El Niño Southern Oscillation (ENSO). The vertical temperature profiles derived from the World Ocean Atlas 2023 (WOA) climatology dataset provided monthly spatial data for October 2018 (SEM) and January 2019 (NWM). These profiles indicated the presence of a thermocline at a depth of approximately 100–125 m (Figure 4.1(b)). This study also used daily northward ocean current velocity data from the Global Ocean Physics Reanalysis product obtained from the Copernicus Marine Service. The analysis revealed distinct characteristics in the depth profiles of current velocity (Figure

4.1(c)). During the SEM (NWM), the ISW exhibited weak southward (strong northward) current velocity.

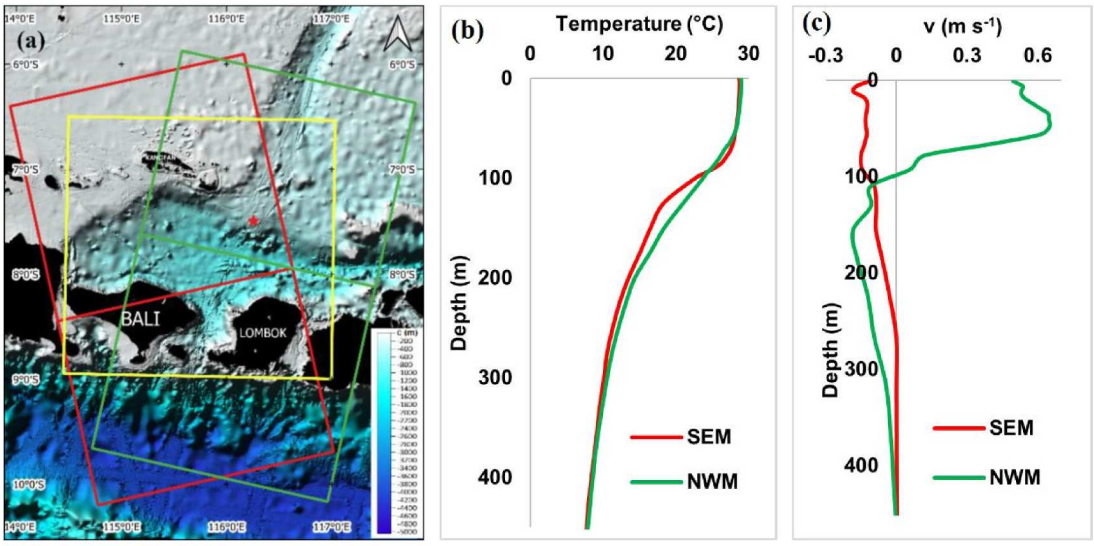

Figure 4.1. (a) Bathymetry map of the Lombok Strait area. The red, green, and yellow squares represent the Sentinel-1 SAR image swath for the ascending orbit mode (SEM), descending orbit mode (NWM), and research location focus, respectively. The red stars represent the locations of the vertical temperature profiles. (b) Vertical temperature profile. (c) Vertical northward ocean current velocity.

4.1.2 Methods

The manifestation of ISWs in satellite images results from interactions between ISW-induced surface roughness, which generates variations in roughness on the sea surface. Variations in sea surface roughness are usually apparent as smooth and rough surfaces that appear as dark and light bands in satellite images. Under favorable meteorological and hydrodynamic conditions, rich information about internal waves can be obtained from SAR images because variations in surface roughness reflect the characteristics of internal waves (Alpers, 1985). Radar and optical images provide quantitative estimations of ISW parameters such as phase speed, wavelength, soliton number, first crest length, and propagation direction. The first crest (leading soliton) is the front of the soliton in a package and usually has the brightest intensity. The soliton number is described as several bright/dark lines in a packet. The average wavelength between solitons in one packet is the distance between two adjacent, bright bands.

The parameters of ISW were determined or estimated across different seasons using Synthetic Aperture Radar (SAR) from Sentinel-1 and optical imagery from SGLI and MODIS. Ocean color products facilitated the identification of anomalies potentially

coinciding with the ISW patterns observed during these periods. We conducted a comparative analysis of the phase speed estimates using data from multiple satellites, given the significant importance of the phase speed in this study. Our comparison of phase speeds estimated using the Korteweg-de Vries (KdV) equation was similar to the previous comparisons made by Karang et al. (2020) in the Flores Sea. The KdV equation considers the effects of nonlinearity and dispersion, which can cause waves to exhibit interesting phenomena, such as soliton solutions. A stable configuration of solitary waves from the KdV equation can be obtained if the effects of nonlinearity and dispersion are in equilibrium. Under stable conditions, one of the coefficients of the solution of the KdV equation can be used to estimate the nonlinear ISW phase speed (*Cp*), as given by Equation (1):

$$C_{\mathrm{P}} = C_0\left[1+\frac{\eta_0\left(h_2-h_1\right)}{2h_1h_2}\right] \tag{1}$$

where C_0 is the linear phase speed of the corresponding two-layer model, h_1 is the upper layer thickness, h_2 is the lower layer thickness, and η_0 is the maximum amplitude of the solitary wave (Osborne & Burch, 1980).

4.3 Results

4.3.1 ISW dynamics from multi-satellite images

Manifestations of ISWs at the sea surface are groups or packets of oscillations with several cycles that vary from very few to several dozen, depending on the age and distance from the generation site (Apel 2002). The influence of seasonal effects on wave properties has been previously recognized (Matthews et al., 2011). We used Sentinel-1/SAR, GCOM-C/SGLI, and Terra/MODIS sensors to observe the characteristics of ISWs in the Lombok Strait during two distinct seasons. The combination of radar and optical sensors has proven effective in determining the generation, propagation, and dynamic parameters of ISWs.

Two consecutive images of Sentinel-1/SAR were acquired during two different seasons in the Lombok Strait. The first image (Figure 4.2(a)), which was recorded on 25 October 2018 at 18:25 WITA (Central Indonesian Time) during the SEM period, shows packets of ISWs propagating both northward and southward. The second image (Figure 4.2(b)), which was recorded on 9 January 2019 at 05:53 WITA during the NWM period, showed only packets of ISW propagating northward. This variation in the seasonal propagation behavior of ISWs in the Lombok Strait could be explained by the results of numerical modelling using a non-hydrostatic, incompressible Boussinesq model. Model

simulations revealed that during the SEM period, strong southward currents restricted the northward movement of tides from the Indian Ocean, particularly near the surface. This limited northward influx inhibited the generation of embryonic waves and led to a relatively weak release of ISWs in the strait (Matthews et al., 2011).

Figure 4.2(c) shows the ISW patterns extracted from the Sentinel-1/SAR images that overlapped with bathymetric relief. The ISW pattern extracted during the SEM period (red lines) showed two packets of ISWs, one propagating northward and the other propagating southward. The northward-propagating ISW detected 3 – 5 solitons clearly, with the first crest varying with the width of the strait, which was getting wider in the northern part of the strait approaching Kangean Island. The wavelengths for the packet near Kangean Island were approximately 6.47 km, and the packet near the strait was approximately 6.92 km. ISW pattern extraction in the NWM period (green lines) shows three packets northward; only two packets in the north were detected owing to the limited image coverage area. The packet that was detected near Kangean Island had 13 solitons, while those still in the Lombok Strait area had seven solitons. The first crest detected varied based on the width of the strait and could be up to 175 km. The wavelengths for the packet near Kangean Island were approximately 3.27 km, and the packet near the strait was approximately 4.55 km. The difference in the wavelength value in the packet that approached Kangean Island was higher than that when the packet was still detected in the Lombok Strait. The wavelengths of the ISW packets were higher when approaching Kangean Island than when detected in the Lombok Strait.

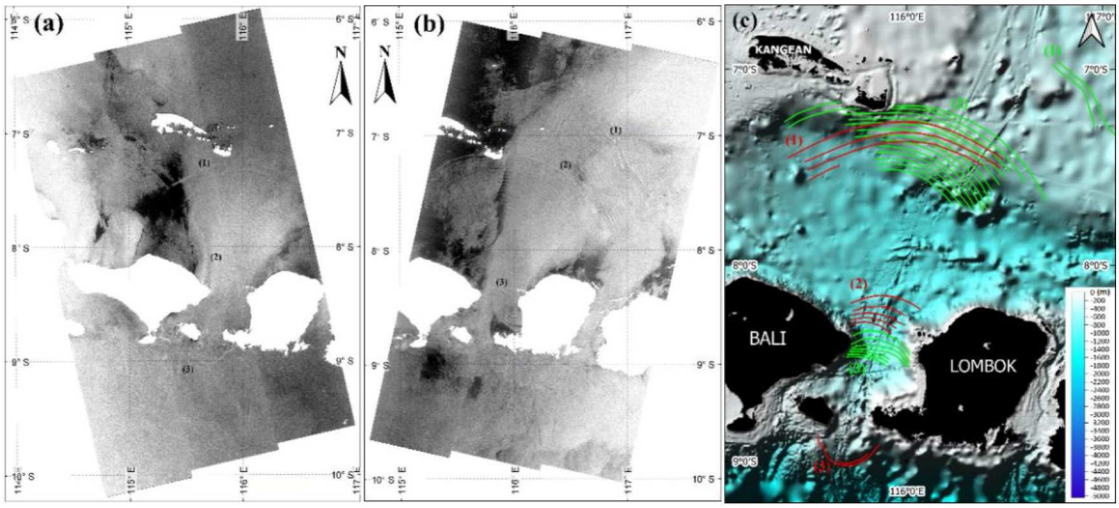

Figure 4.2. Sentinel-1/SAR images with ISW patterns detected during (a) the SEM period, (b) the NWM period, and (c) ISW pattern extraction from Sentinel-1/SAR images overlaid from (a) and (b). The red and green lines represent the ISW packets during the SEM and NWM periods, respectively.

Additionally, the wavelengths observed during the SEM period were longer than those observed during the NWM period. The differences in the wavelengths may be attributed to variations in the phase speed, which will be discussed in further detail. The findings of this study align with previous research conducted in the East/Japan Sea, which demonstrated seasonal variations in the intensity of internal tide generation and energy propagation, along with corresponding changes in wavelengths during different seasons (Jeon et al., 2014).

During the SEM period, the SGLI and MODIS sensors captured visible band imagery (at 673 and 645 nm, respectively) in the Lombok Strait. In Figure 4.3(a), the SGLI imagery detected more than 13 solitons in packets near Kangean Island, with a wavelength of approximately 6.31 km, whereas in the Lombok Strait area, more than five solitons were detected in packets with a wavelength of approximately 7.03 km. Similarly, Figure 4.3(b) shows the MODIS imagery in the SEM period, where more than 13 solitons were detected in packets near Kangean Island, with a wavelength of approximately 6.20 km, and more than three solitons were observed in packets within the Lombok Strait area, with a wavelength of approximately 7.30 km. The time difference between the SGLI and MODIS images during the SEM period was 3 h and 35 min.

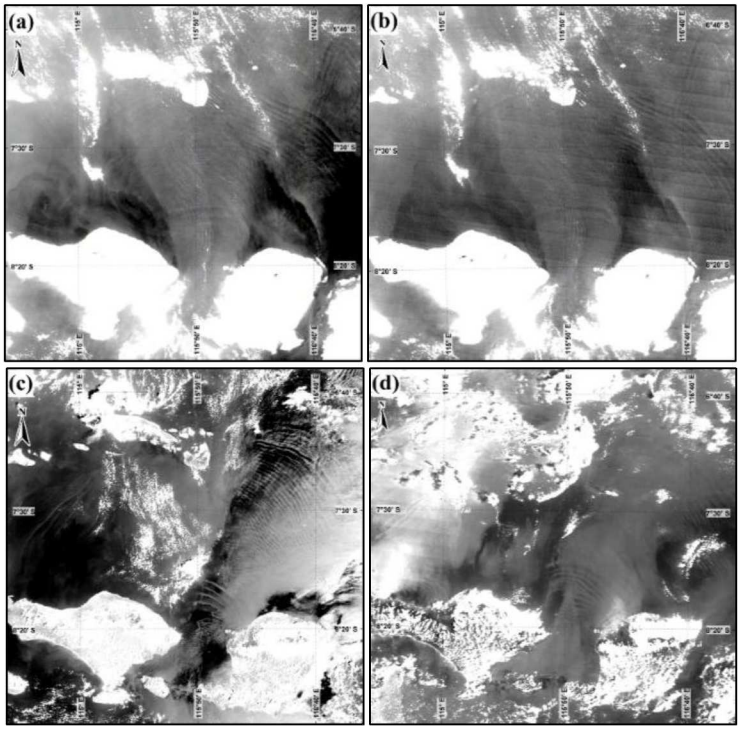

Figure 4.3. (a) SGLI 673 nm visible band with ISW patterns detected on 26 October 2018 at 10:19 WITA during SEM period, (b) MODIS 645 nm visible band on 26 October 2018 at 13:54 WITA during SEM period, (c) SGLI 673 nm visible band with ISW patterns detected on 9 January 2019 at 10:35 WITA during NWM period, (d) MODIS 645 nm visible band on 8 January 2019 at 11:05 WITA during NWM period.

Both visible band images from two different sensors have the same variation of ISW parameters detected as in the Sentinel-1/SAR imagery, except that there is a difference in the number of solitons detected owing to differences in the sensor imaging mechanisms. Figure 4.3(c) shows an SGLI image in the NWM period, which identifies more than 25 solitons in packets near Kangean Island with wavelengths ranging from 3.85 to 5.30 km and more than five solitons in packets in the Lombok Strait area with wavelengths of approximately 5.00 km. Figure 4.3(d) shows a MODIS image in the NWM period which identifies more than 20 solitons in packets near Kangean Island with wavelengths ranging from 2.96 to 5.11 km and more than three solitons in packets still in the Lombok Strait area with wavelengths of approximately 5.32 km. The SGLI and MODIS images in this NWM period had a time difference of 25 h and 20 min, respectively, owing to the limited cloudy MODIS images on the same date. The difference in wavelength variation in the same soliton was caused by the difference in the pattern detected due to the shallowing of the bathymetry in the eastern part and the complete absence of the ISW arc-like pattern. In addition, the seasonal variation of the ISW wavelength in the Lombok Strait is closely related to the seasonal variation in the thermocline depth and density differences between the two layers (Ningsih et al., 2008).

Table 4.2. ISW phase speed estimation results from multi-satellite images and the KdV equation.

	Satellite estimation (m s^{-1})			KdV equation (m s^{-1})
	Sentinel-1/SAR	**GCOM-C/SGLI**	**Terra/MODIS**	
SEM	2.23	2.12	2.11	2.18
NWM	2.91	2.68	2.52	2.23

A comparison between theoretical and multi-satellite estimations is necessary for one of the crucial parameters, phase speed. Fan et al. (2015) describe the ISW phase speeds as a function of maximum wave amplitude (η_0), linear wave coefficients (c_0), and water depths (Equation (1)). The estimated distance between packets in the multi-satellite phase speed estimation was divided by the semi-diurnal dominant tidal period in the Lombok Strait. The maximum wave amplitudes in the Lombok Strait during the SEM and NWM periods were assumed to be ~70 m (h_1 ~ 100 m) and ~63 m (h_1 ~125 m), respectively (Ningsih et al., 2010). The average density in the surface layer ρ was 1022.95 kg m^{-3}, and the density difference $\Delta\rho$ between the upper and lower layers was 3.27 kg m^{-3} (Susanto et al., 2007). The water depth (h) in the study area was 800 m, based on the average bathymetric data from

BATNAS. A comparison of the ISW phase speed estimation results using satellite imagery and KdV theory is shown in Table 4.2.

While in-situ data are still required for validation, phase speed estimation results from satellite imagery can be used to predict the ISW amplitude, making it an important parameter to study. Table 4.2 shows that the four estimation results using multi-satellite and the KdV equation show that the phase speed in the NWM is faster than that in the SEM. In the estimation using the KdV equation, the SEM thermocline depth was shallower. The differences in thermocline depth play a significant role in explaining the observed variations in phase speed during the different seasons. The contrast depth of the thermocline produces a different pattern of thermal stratification which affects the ISW propagation characteristics. These estimation results follow the numerical model results, which show that the phase speed in the NWM is faster than that in the SEM period (Ningsih et al., 2008). Seasonal, interannual, and long-term climate change effects must be thoroughly studied using long-term time-series data.

4.3.2 Ocean color observation

The high spatial resolution (~250 m) of the SGLI ocean color products was used to observe the ISW patterns in the Lombok Strait. The ocean color products in the SGLI images used in this study showed a clear ISW pattern in both seasons. Figure 4.4 shows the Chl-a, SST, and AOT images from the SGLI sensor during the SEM and NWM periods. The Chl-a images showed the same pattern as the visible images (Figure 4.3). Interesting findings were observed in the SST and AOT images during the NWM period. The ISW pattern was only detected in the SST imagery in the northern Lombok Strait, whereas the AOT image detected two ISW packets. These findings require further investigation into the effects of atmospheric correction patterns. The ISW pattern detected in ocean color products still requires further study because the detected pattern may be caused by the influence of sunlight reflectance from the sea surface induced by ISW. Research on the interaction between nonlinear internal ocean waves and the atmosphere has shown that the surface roughness generated by internal waves has a distinct and profound impact on the physical characteristics and structure of the near-surface atmosphere (Ortiz-Suslow et al., 2019).

A unique phenomenon is observed in Figure 4.4(d), where a pattern of high Chl-a concentrations extends to the north, suggesting material propagation to the north. At first glance, this pattern resembles an upwelling phenomenon during the NWM period, but the SST image at the same time does not show any significant temperature difference. Figure

4.5 compares the Chl-a images in the same area at almost the same time. On the same day, the VIIRS and MODIS sensors passed through the same area as the SGLI sensors. These three sensors showed a high Chl-a pattern that appeared to propagate to the north; however, the pattern of light and dark lines due to surface roughness modification by ISW was not visible on the VIIRS and MODIS sensors due to cloud factors and sun-glint position.

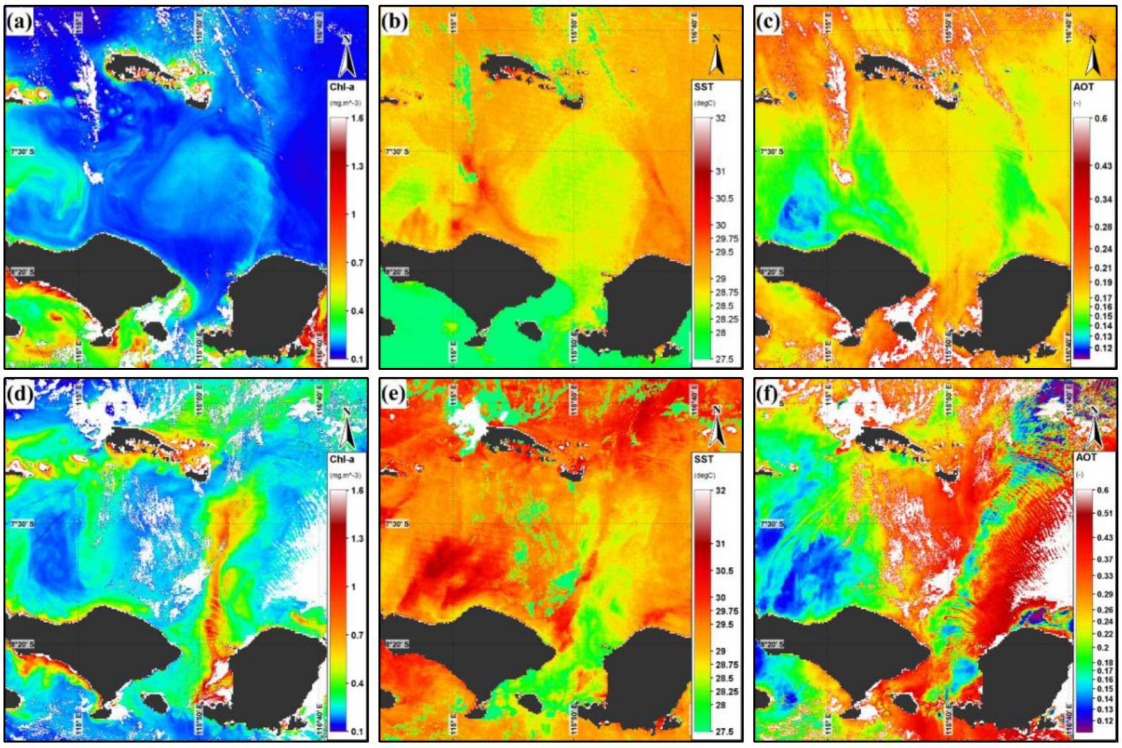

Figure 4.4. Ocean color products from SGLI sensors (a) Chl-a, (b) SST, (c) AOT in the SEM period, (d) Chl-a, (e) SST, (f) AOT in the NWM period.

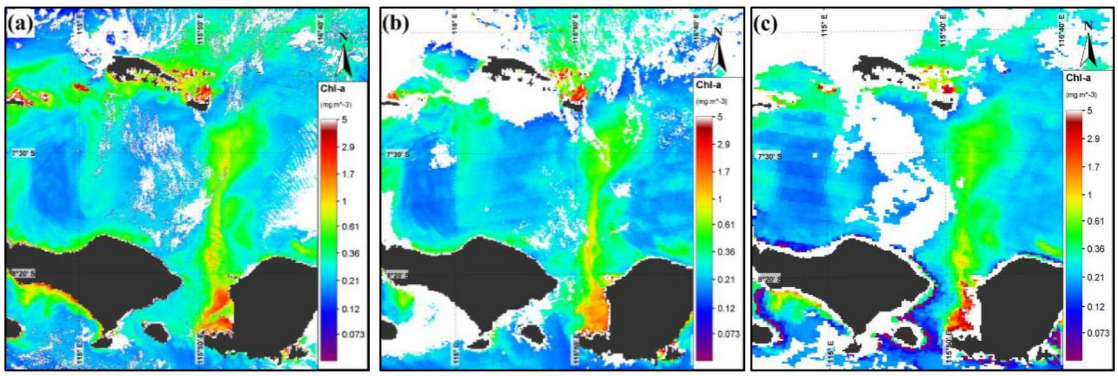

Figure 4.5. Chl-a images on 9 January 2019 from (a) the SGLI sensor (~250 m spatial resolution) at 10:35 WITA, (b) the VIIRS sensor (~750 m spatial resolution) at 13:48 WITA, and (c) the MODIS sensor (~1000 m spatial resolution) at 10:10 WITA.

More detailed investigations of remote sensing reflectance (Rrs) can be carried out using VIIRS and MODIS sensors. The spatial distributions of Chl-a, Rrs 443, and Rrs 555

from the two sensors are shown in Figure 4.6. The spatial distribution of the VIIRS and MODIS sensors showed a lower Rrs 443 and a higher Rrs 555 in the Chl-a bloom pattern area, indicating that the Chl-a concentration detected in this image may be biased by the condition of turbid water (Wirasatriya et al., 2021).

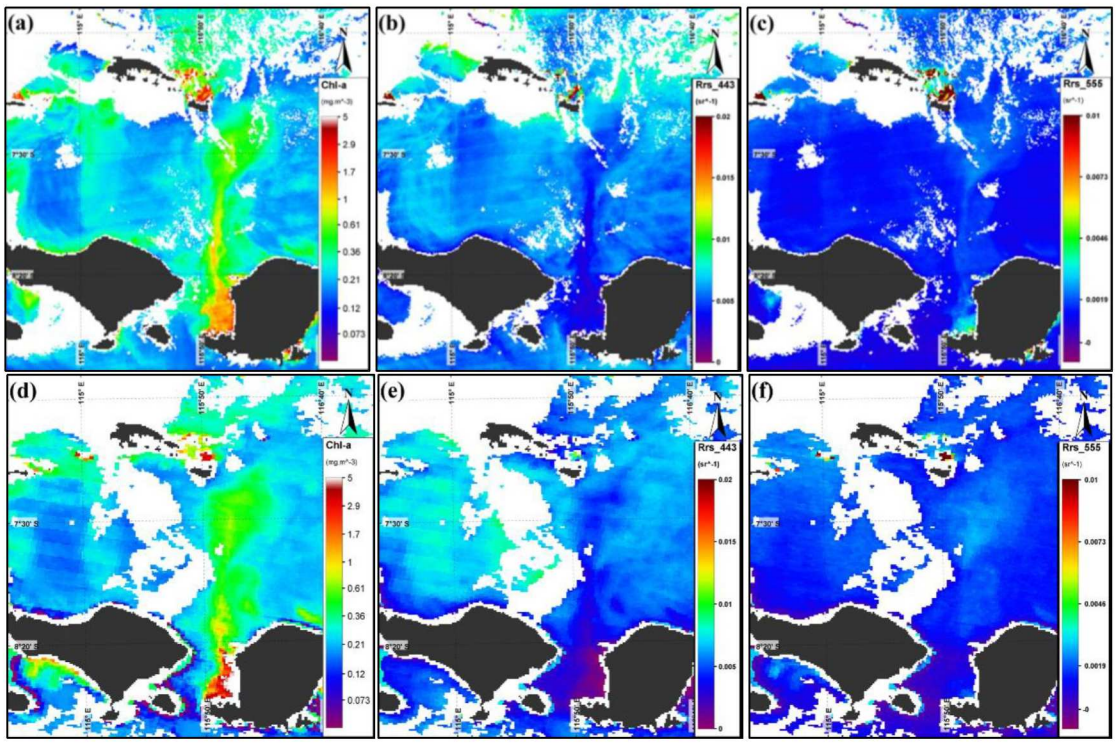

Figure 4.6. Spatial distribution of (a) Chl-a, (b) Rrs 443, and (c) Rrs 555 from the VIIRS sensor on 9 January 2019 13:48 WITA, and (d) Chl-a, (e) Rrs 443, and (f) Rrs 555 from the Terra/MODIS sensor on 9 January 2019 10:10 WITA.

4.4 Discussions

A rare phenomenon in the discussion of the previous results was confirmed by Sentinel-2/MSI and Terra/MODIS images on 8 January 2019 which showed river discharge due to flooding on Lombok Island (Figure 4.7). January is the peak month for rainfall in southern Indonesia (Prasetia et al., 2013).

Although the Chl-a bloom detected in this study was biased due to the river discharge phenomena on the Island of Lombok, the transport induced by ISW is interesting to study further. We assume that the distribution of turbid water propagating to the north is dominant because of the intense ISW activity in this area. Further investigation of the start time of the Chl-a bloom pattern employed Chl-a data on the days before and after the Chl-a bloom pattern appeared. Figure 4.8 shows the results of overlaying Chl-a images, extracting ISW patterns from Sentinel-1/SAR images on the same day, and daily northward current velocity.

The Chl-a bloom pattern was indicated to occur on 8 – 9 January 2019 because, on 5 January 2019 this pattern was not detected, and on 11 January 2019 the Chl-a bloom started to appear but had not spread to the north.

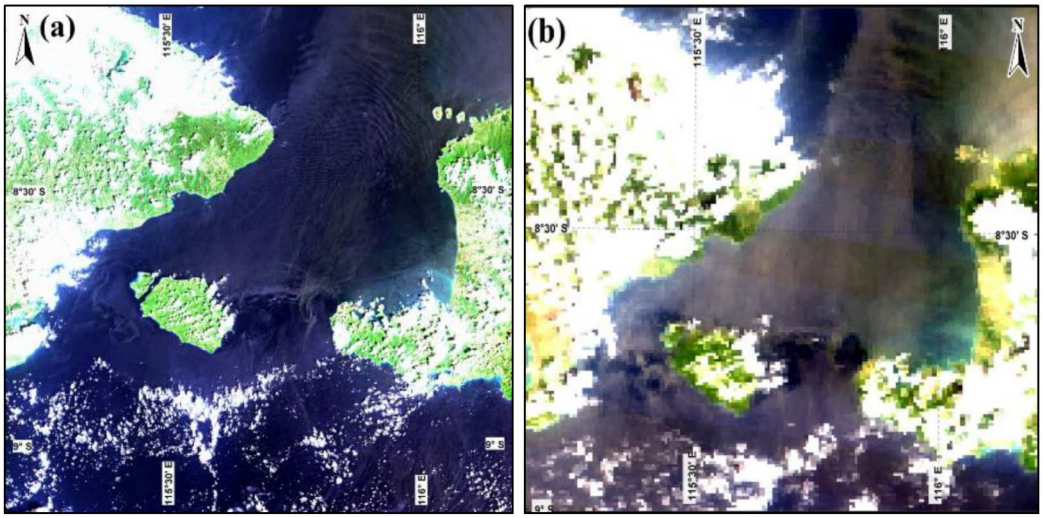

Figure 4.7. (a) Sentinel-2A/MSI true color image (~10 m spatial resolution) on 8 January 2019 at 10:20 WITA, and (b) Terra/MODIS true color image (~500 m spatial resolution) on 8 January 2019 at 11:05 WITA shows the river discharge pattern on the island of Lombok.

ISWs are generated in stratified water by the interaction among strong tidal flows, background currents, and rough bottom topography in the sill south of the Lombok Strait (Susanto et al., 2005). Convergence and divergence zones were identified in the SAR images through light and dark patterns, representing the first baroclinic mode. In this mode, the surface and deep-layer flows are in opposing directions, which could have implications for the impact of these waves on nearshore ecosystems (Woodson, 2018). A remarkable echogram of the water column obtained by an EK500 Echosounder captured internal waves with a wavelength of ~1.8 km passing under the ship at a speed of ~1.5 m s^{-1} in the Lombok Strait (Susanto et al., 2005). Higher backscatter values indicate higher plankton concentrations or large fish schools. A higher backscatter value at each depth indicates a higher concentration of plankton or a large school of fish, which shows the effect of IWs activity on the surrounding water conditions.

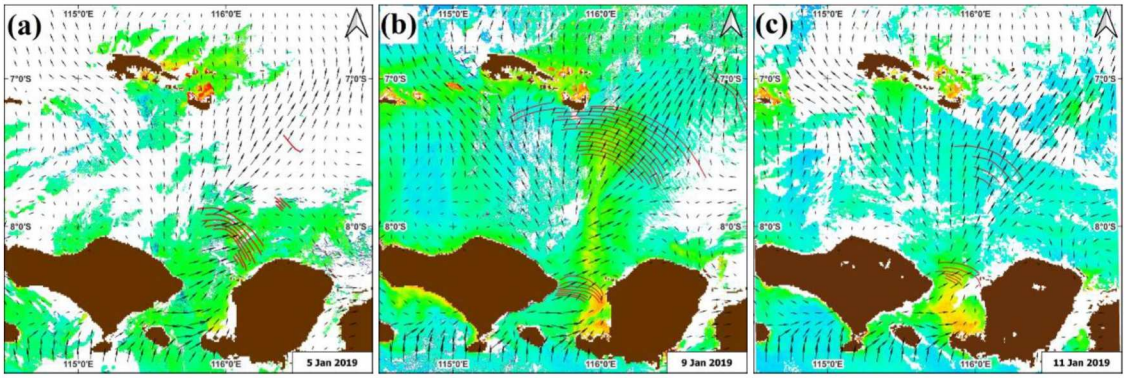

Figure 4.8. Chl-a image overlaid with ISW patterns extracted from the Sentinel-1/SAR and daily northward current velocities on (a) 5 January 2019 (b) 9 January 2019 and (c) 11 January 2019.

According to Heathershaw (1985), IWs directly influence sediment transport, causing an increase or decrease in the amount of sediment carried by tidal currents, depending on the direction of IW propagation. This study suggests that the impact of IWs is more significant when tidal currents are only slightly above the threshold required for sediment transport to occur. Figure 4.9 illustrates the vertical northward ocean current velocity profiles in the Lombok Strait on 5 January 8, and 11. The northward ocean velocity conditions were higher on 5 January and 8 than on 11 January and there was greater variability in the current gradients on 8 January. This study hypotheses that the higher variations in currents attributed to ISW activity in the Lombok Strait are responsible for the sediment transport anomalies observed.

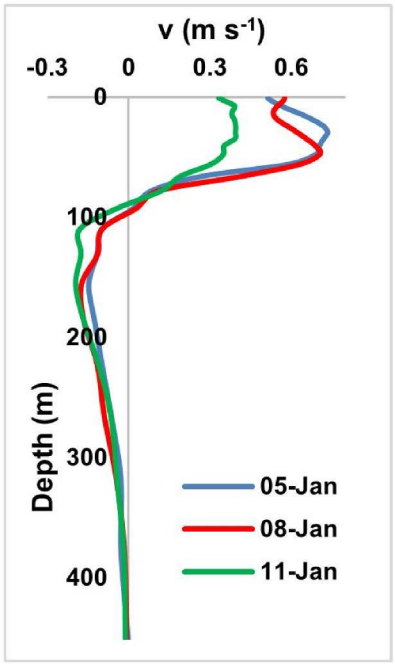

Figure 4.9. Vertical northward ocean current velocity profile in the Lombok Strait.

The study found that the quantity observed in the imagery was more strongly associated with the surface current gradients of the IWs than with the surface currents themselves (Alpers, 1985). Predicting the effects of IWs on the system is challenging, if not impossible, without a comprehensive understanding of how ISWs respond to variations in stratification, wind forcing, and thermocline depth.

4.5 Conclusion

The combination of radar and optical sensors has proven to be effective in studying ISWs in the Lombok Strait. The Sentinel-1/SAR, GCOM-C/SGLI, and Terra/MODIS sensors distinguished the characteristics of the ISWs observed during the two seasons. Sentinel-1/SAR detected a higher soliton number in the northward-propagating ISW during the NWM period than during the SEM period. The wavelength of the ISWs was wider during the SEM period, with two distinct packets in a single image. These findings were consistent with the observations from the optical sensors (SGLI and MODIS). Estimations of the ISW phase speed using multi-satellite images and the KdV equation revealed faster phase speeds during the NWM period. Seasonal variations in ISW parameters were closely associated with changes in the thermocline depth and density differences between layers. The SGLI ocean color products provided interesting findings in the SST and AOT images during the NWM period, but further investigation is required to fully understand the ISW patterns in these products. The presence of turbid water conditions biased the Chl-a pattern observed in the SGLI, MODIS, and VIIRS products during the NWM period, influenced by river discharge phenomena. The transport induced by ISWs presents an intriguing subject for further study, assuming that turbid water distribution propagates northward owing to intense ISW activity. This study contributes to the understanding of the impact of ISW on coastal interactions in the Lombok Strait by providing multi-satellite observations and highlighting recent progress in this field.

CHAPTER 5
Conclusions

5.1 Conclusions

This dissertation presents a comprehensive investigation of ISWs in the Lombok Strait using a multi-satellite remote sensing approach. This study integrated optical and radar data to explore the surface manifestation, propagation dynamics, seasonal variability, and climatic influences on ISWs, thereby contributing to a deeper understanding of their behavior and environmental impact. The key findings of this study are summarized as follows:

1. Surface manifestation of ISWs in optical imagery

   Analysis of the GCOM-C/SGLI optical data revealed that ISWs significantly altered ocean color parameters and thermal infrared signals. These manifestations are evident in the TOA radiance and SST anomalies, indicating a strong modulation of the rough sea surface. These findings suggest that ISWs can influence satellite-based oceanographic measurements and may interfere with large-scale estimations of ocean color and temperature.

2. Long-term dynamics and climate influence from Sentinel-1 SAR

   A nine-year archive of Sentinel-1 SAR imagery was used to estimate the ISW propagation speeds and occurrence frequencies. The results demonstrated that ISWs in the Lombok Strait exhibit a 54-month occurrence cycle and a 12-month cycle in propagation speed, reflecting both interannual and seasonal variations. Statistical analysis showed a moderate positive correlation between ISW occurrence and the IOD, while ENSO showed a moderate negative correlation with propagation speed and negligible influence on occurrence.

3. Seasonal characteristics from multi-satellite observations

   Seasonal comparisons using Sentinel-1, GCOM-C, and MODIS data revealed distinct ISW behaviors during the Northwest Monsoon (NWM) and Southeast Monsoon (SEM). More solitons and faster phase speeds were observed during the NWM, whereas wider wavelengths and multiple wave packets were more common in the SEM. These variations were closely linked to seasonal changes in the thermocline depth and upper-layer density structure. Additionally, the propagation of turbid water and high chlorophyll-a concentrations during the NWM suggested that ISWs play a key role in sediment transport and biogeochemical processes in the strait.

Overall, this study demonstrated the effectiveness of a multi-sensor remote-sensing strategy for monitoring and analyzing ISWs. This highlights the importance of considering both seasonal and long-term climatic variability when evaluating ISW behavior and its broader oceanographic implications.

5.2 Future Work

While this study provides valuable insights, several areas offer opportunities for future exploration and refinement.

1. Integration with in-situ measurements

   Incorporating in situ data (e.g. moorings, CTD profiles, and ADCP) would enhance the validation of remote sensing observations, particularly for vertical wave structure, thermocline depth, and current profiles. This would reduce reliance on indirect inferences and improve the accuracy of speed and amplitude estimation.

2. Application of deep learning and AI

   The development of automated detection and classification algorithms using machine learning or deep learning techniques could significantly improve the efficiency and consistency of ISW monitoring using satellite imagery. Time-series prediction models (e.g. LSTM) may also help forecast ISW activity.

3. High-resolution modeling and simulation

   Coupling observational data with numerical ocean models can help simulate ISW generation, propagation, and dissipation processes under various forcing conditions. Such models would support scenario-based studies on climate impact or anthropogenic influence on ISW dynamics.

4. Expanded geographic scope

   Applying this methodology to other key straits in the Indonesian Seas (e.g. Ombai and Halmahera Straits) would help determine whether similar ISW behaviors and climate interactions are observed elsewhere, thus contributing to regional and global internal wave research.

5. Air-sea interaction and ecological impacts

   Further studies should investigate the influence of ISWs on upper-ocean processes, such as air-sea gas exchange, nutrient upwelling, and phytoplankton blooms. This will deepen our understanding of how ISWs contribute to biophysical coupling and marine ecosystem variability in tropical seas.

REFERENCES

Aiki H., Matthews J. P., & Lamb, K. G. (2011). Modelling and energetics of tidally generated wave trains in the Lombok Strait: Impact of the Indonesian Throughflow. *Journal of Geophysical Research: Oceans*, *116*(3), 1–17. https://doi.org/10.1029/2010JC006589.

Alpers, W. (1985). Theory of Radar Imaging of Internal Waves. *Nature*, *314*(No. 6008), 245–247.

Alpers, W. (2014). Encyclopedia of Remote Sensing: Ocean Internal Waves. In E. G. Njoku (Ed.), *Encyclopedia of Remote Sensing* (pp. 433–437). Springer Reference.

Alpers, W., Member, S., & Huang, W. (2011). *On the Discrimination of Radar Signatures of Atmospheric Gravity Waves and Oceanic Internal Waves on Synthetic Aperture Radar Images of the Sea Surface*. *49*(3), 1114–1126.

Apel, J. R. (1988). *Principles of Ocean Physics* (R. Dmowska & J. R. Holton (eds.); Vol. 38, Issue 1). Academic Press. https://doi.org/10.1029/89EO00003.

Apel, J. R. (2002a). Oceanic Internal Waves and Solitons. In *An Atlas of Oceanic Solitary Waves*. Global Ocean Associates, Prepared for the Office of Naval Research –Code 322.

Apel, J. R. (2002b). Oceanic Internal Waves and Solitons. In C. S. Jackson (Ed.), *Synthetic Aperture Radar Marine User's Manual* (pp. 189–206). NOAA/ NESDIS.

Apel, J. R., Byrne, H. M., Proni, J. R., & Charnell, R. L. (1975). Observations of oceanic internal and surface waves from Earth Resources Technology satellite. *Journal of Geophysical Research*, *80*(6), 865–881. https://doi.org/10.1029/JC080i006p00865.

Apel, J. R., Holbrook, J. R., Liu, A. K., & Tsai, J. J. (1985). The Sulu Sea Internal Soliton Experiment. *Journal of Physical Oceanography*, *15*(12), 1625–1651. https://doi.org/10.1175/1520-0485(1985)015<1625:TSSISE>2.0.CO;2.

Apel, J. R., Thompson, D. R., Tilley, D. G., & Van Dyke, P. (1985). Hydrodynamics and Radar Signatures of Internal Solitons in the Andaman Sea. *Johns Hopkins APL Technical Digest (Applied Physics Laboratory)*, *6*(4), 330–337.

Atmadipoera, A., Molcard, R., Madec, G., Wijffels, S., Sprintall, J., Koch-Larrouy, A., Jaya, I., & Supangat, A. (2009). Characteristics and variability of the Indonesian throughflow water at the outflow straits. *Deep-Sea Research Part I: Oceanographic Research Papers*, *56*(11), 1942–1954. https://doi.org/10.1016/j.dsr.2009.06.004.

Brandt, P., Rubino, A., Alpers, W., & Backhaus, J. O. (1997). Internal waves in the Strait of Messina studied by a numerical model and synthetic aperture radar images from the ERS 1/2 satellites. *Journal of Physical Oceanography*, *27*(5), 648–663. https://doi.org/10.1175/1520-0485(1997)027<0648:IWITSO>2.0.CO;2.

Chonnaniyah, As-Syakur, A. R., Osawa, T., & Karang, I. W. G. A. (2023). Seasonal Variability of Internal Solitary Waves Phase Speed in the Lombok Strait Revealed by SenmodellingSAR. *2023 8th Asia-Pacific Conference on Synthetic Aperture Radar (APSAR)*, 1–5. https://doi.org/10.1109/APSAR58496.2023.10388730.

Chonnaniyah, As-Syakur, A. R., Raharja, I. M. D., & Osawa, T. (2025). Estimation of Internal Solitary Waves Propagation Speeds and Occurrence Using Long-Term Sentinel-1 SAR Data in the Lombok Strait, Indonesia. *IEEE Journal of Selected Topics in Applied Earth Observations and Remote Sensing*, *18*, 13770–13777. https://doi.org/10.1109/JSTARS.2025.3568845.

Chonnaniyah, Karang, I. W. G. A., & Osawa, T. (2021). Internal solitary waves propagation speed estimation in the northern-part of Lombok Strait observed by Sentinel-1 SAR and Himawari-8 images. *IOP Conference Series: Earth and Environmental Science 944*(1). https://doi.org/10.1088/1755-1315/944/1/012042.

Chonnaniyah, Osawa, T., As-Syakur, A. R., Karang, I. W. G. A., & da Silva, J. C. B. (2023). On the distinction of seasonal internal solitary waves characteristics in the Lombok Strait based on multi-satellite data. *International Journal of Remote Sensing*, *00*(00), 1–16. https https://doi.org/10.1080/01431161.2023.2242592.

Chonnaniyah, Osawa, T., Wayan Gede Astawa Karang, I., & As-Syakur, A. R. (2021). Variability of Internal Solitary Waves Detection in the Lombok Strait Observed by Sentinel-1 SAR: The Role of Monsoon, IOD, and ENSO. *2021 7th Asia-Pacific Conference on Synthetic Aperture Radar (APSAR)*, 1–5. https://doi.org/10.1109/APSAR52370.2021.9688341

Clavano, W. R. (2008). *Reflectance Change Due to Surface Roughness — With Applications to Ocean Optics* (Issue January). Cornell University.

Colosi, J. A., Kumar, N., Suanda, S. H., Freismuth, T. M., & MacMahan, J. H. (2018). Statistics of internal tide bores and internal solitary waves observed on the inner continental shelf off Point Sal, California. *Journal of Physical Oceanography*, *48*(1), 123–143. https://doi.org/10.1175/JPO-D-17-0045.1.

Craig, W., Guyenne, P., & Sulem, C. (2012). The surface signature of internal waves. *Journal of Fluid Mechanics*, *710*, 277–303. https://doi.org/10.1017/jfm.2012.364.

Da Silva, J. C. B., New, A. L., & Magalhaes, J. M. (2009). Internal solitary waves in the Mozambique Channel: Observations and interpretation. *Journal of Geophysical Research: Oceans*, *114*(5), 1–12. https://doi.org/10.1029/2008JC005125.

da Silva, J. C. B., New, A. L., Srokosz, M. A., & Smyth, T. J. (2002). On the observability of internal tidal waves in remotely sensed ocean colour data. *Geophysical Research Letters*, *29*(12), 10-1-10–14. https://doi.org/10.1029/2001GL013888.

Dwi Susanto, R., Ffield, A., Gordon, A. L., & Adi, T. R. (2012). Variability of Indonesian throughflow within Makassar Strait, 2004-2009. *Journal of Geophysical Research: Oceans*, *117*(9), 2004–2009. https://doi.org/10.1029/2012JC008096.

Farmer, D., & Armi, L. (1999). The generation and trapping of solitary waves over topography. *Science*, *283*(5399), 188–190. https://doi.org/10.1126/science.283.5399.188.

Farrar, J. T., Zappa, C. J., Weller, R. A., & Jessup, A. T. (2007). Sea surface temperature signatures of oceanic internal waves in low winds. *Journal of Geophysical Research: Oceans*, *112*(6), 1–19. https://doi.org/10.1029/2006JC003947.

Feng, M., Zhang, N., Liu, Q., & Wijffels, S. (2018). The Indonesian throughflow, its variability and centennial change. *Geoscience Letters*, *5*(1). https://doi.org/10.1186/s40562-018-0102-2.

Garrett, C., & Kunze, E. (2007). Internal Tide Generation in the Deep Ocean. *Annual Review of Fluid Mechanics*, *39*(1), 57–87. https://doi.org/10.1146/annurev.fluid.39.050905.110227.

Gill, A. E. (1982). *Atmosphere-Ocean Dynamics* (Vol. 30). Academic Press, New York.

Gong, Y., Xie, J., Xu, J., Chen, Z., He, Y., & Cai, S. (2022). Spatial asymmetry of nonlinear internal waves in the Lombok Strait. *Progress in Oceanography 202*(November 2021): 102759. https://doi.org/10.1016/j.pocean.2022.102759.

Gordon, A. (2005). Oceanography of the Indonesian Seas and Their Throughflow. *Oceanography*, *18*(4), 14–27. https://doi.org/10.5670/oceanog.2005.01.

Gordon, A. L., Sprintall, J., Van Aken, H. M., Susanto, D., Wijffels, S., Molcard, R., Ffield, A., Pranowo, W., & Wirasantosa, S. (2010). The Indonesian throughflow during 2004–2006 as observed by the INSTANT program. *Dynamics of Atmospheres and Oceans*, *50*(2): 115–128. https://doi.org/10.1016/j.dynatmoce.2009.12.002.

Hao, X., & Shen, L. (2020). Direct simulation of surface roughness signature of internal wave with deterministic energy-conservative model. *Journal of Fluid Mechanics*, *891*, R3. https://doi.org/10.1017/jfm.2020.200.

Helfrich, K. R., & Melville, W. K. (2006). Long Nonlinear Internal Waves. *Annual Review of Fluid Mechanics*, *38*(1), 395–425. https://doi.org/10.1146/annurev.fluid.38.050304.092129.

Hori, M., Murakami, H., Miyazaki, R., Honda, Y., Nasahara, K., Kajiwara, K., Nakajima, T. Y., Irie, H., Toratani, M., Hirawake, T., & Aoki, T. (2018). GCOM-C Data Validation Plan for Land, Atmosphere, Ocean, and Cryosphere. *Transactions of the Japan Society for Aeronautical and Space Sciences, Aerospace Technology Japan*, *16*(3), 218–223. https://doi.org/10.2322/tastj.16.218.

Jackson, C. (2007). Internal wave detection using the Moderate Resolution Imaging Spectroradiometer (MODIS). *Journal of Geophysical Research*, *112*(C11), C11012. https://doi.org/10.1029/2007JC004220.

Jackson, C., da Silva, J., Jeans, G., Alpers, W., & Caruso, M. (2013). Nonlinear Internal Waves in Synthetic Aperture Radar Imagery. *Oceanography*, *26*(2), 68–79.

https://doi.org/10.5670/oceanog.2013.32.

Jackson, C. R., & Alpers, W. (2010). The role of the critical angle in brightness reversals on sunglint images of the sea surface. *Journal of Geophysical Research: Oceans*, *115*(C9), 1–15. https://doi.org/10.1029/2009JC006037.

Jeon, C., Park, J.-H., Varlamov, S. M., Yoon, J.-H., Kim, Y. H., Seo, S., Park, Y.-G., Min, H. S., Lee, J. H., & Kim, C.-H. (2014). Seasonal variation of semidiurnal internal tides in the East/Japan Sea. *Journal of Geophysical Research: Oceans*, *119*(5), 2843–2859. https://doi.org/10.1002/2014JC009864.

Karang, I. W. G. A., Chonnaniyah, C., & Osawa, T. (2019a). Lombok Strait internal wave occurrence frequency derived from Sentinel-1A SAR images. In T. D. Pham, K. D. Kanniah, K. Arai, G. J. P. Perez, Y. Setiawan, L. B. Prasetyo, & Y. Murayama (Eds.), *Sixth International Symposium on LAPAN-IPB Satellite* (Issue January 2020, p. 49). SPIE. https://doi.org/10.1117/12.2540879.

Karang, I. W. G. A., Chonnaniyah, C., & Osawa, T. (2019b). Landsat 8 Observation of the Internal Solitary Waves in the Lombok Strait. *Indonesian Journal of Geography*, *51*(3), 251. https://doi.org/10.22146/ijg.42655.

Karang, I. W. G. A., & Nishio, F. (2011). Internal waves in the Lombok Strait revealed by ALOS PALSAR images. *IEEE Intern Geosci.Remote Sensing Symp. IGARSS 2011*, 17, 253–256.

Kida, S., & Wijffels, S. (2012). The impact of the Indonesian Throughflow and tidal mixing on the summertime sea surface temperature in the western Indonesian Seas. *Journal of Geophysical Research: Oceans*, *117*(9), 1–14. https://doi.org/10.1029/2012JC008162.

Kim, H., Son, Y. B., & Jo, Y.-H. (2018). Hourly Observed Internal Waves by Geostationary Ocean Color Imagery in the East/Japan Sea. *Journal of Atmospheric and Oceanic Technology*, *35*(3), 609–617. https://doi.org/10.1175/JTECH-D-17-0049.1.

Klemas, V. (2012). Remote Sensing of Ocean Internal Waves: An Overview. *Journal of Coastal Research*, *282*(May 2012), 540–546. https://doi.org/10.2112/JCOASTRES-D-11-00156.1.

Kurihara, Y., Murakami, H., Ogata, K., & Kachi, M. (2021). A quasi-physical sea surface temperature method for the split-window data from the Second-generation Global Imager (SGLI) onboard the Global Change Observation Mission-Climate (GCOM-C) satellite. *Remote Sensing of Environment*, *257*(February), 112347. https://doi.org/10.1016/j.rse.2021.112347.

Lindsey, D. T., Nam, S. H., & Miller, S. D. (2018). Tracking oceanic nonlinear internal waves in the Indonesian seas from geostationary orbit. *Remote Sensing of Environment*, *208*, 202–209. https://doi.org/10.1016/j.rse.2018.02.018.

Lukman, A., Atmadipoera, A. S., Nugroho, D., & Harsono, G. (2024). Characteristics of internal waves in the Bali Sea from Sentinel-1A data and ocean modeling. *IOP*

Conference Series: Earth and Environmental Science, *1350*(1). https://doi.org/10.1088/1755-1315/1350/1/012047.

Lund, B., Graber, H. C., Xue, J., & Romeiser, R. (2013). Analysis of Internal Wave Signatures in Marine Radar Data. *IEEE Transactions on Geoscience and Remote Sensing*, *51*(9), 4840–4852. https://doi.org/10.1109/TGRS.2012.2230635.

Marmorino, G. O., Smith, G. B., & Lindemann, G. J. (2004). Infrared imagery of ocean internal waves. *Geophysical Research Letters*, *31*(11), 1–4. https://doi.org/10.1029/2004GL020152.

Matthews, J. P., Aiki, H., Masuda, S., Awaji, T., & Ishikawa, Y. (2011). Monsoon regulation of Lombok Strait internal waves. *Journal of Geophysical Research: Oceans*, *116*(5), 1–14. https://doi.org/10.1029/2010JC006403.

Meng, J., Zhang, J., Song, W., & Yang, J. (2003). SAR imagery in studying internal waves in the northern South China Sea. *Ocean Remote Sensing and Applications*, *4892*, 440. https://doi.org/10.1117/12.466790.

Mitnik, L., Alpers, W., Chen, K. S., & Chen, A. J. (2000). Manifestation of internal solitary waves on ERS SAR and SPOT images: Similarities and differences. *International Geoscience and Remote Sensing Symposium (IGARSS)*, *5*(February), 1857–1859. https://doi.org/10.1109/igarss.2000.858146.

Mitnik, L., Alpers, W., & Hock, L. (2000). Thermal Plumes and Internal Solitary Waves Generated in the Lombok Strait studied by ERS SAR. *ERS-Envisat Symposium: Looking down to Earth in the New Millenium*, 1–9.

Muacho, S., da Silva, J. C. B., Brotas, V., Oliveira, P. B., & Magalhaes, J. M. (2015). Reprint of: Chlorophyll enhancement in the central region of the Bay of Biscay as a result of internal tidal wave interaction. *Journal of Marine Systems*, *147*, 85–93. https://doi.org/10.1016/j.jmarsys.2015.04.007.

Munk, W., & Wunsch, C. (1998). Abyssal recipes II: energetics of tidal and wind mixing. *Deep Sea Research Part I: Oceanographic Research Papers*, *45*(12), 1977–2010. https://doi.org/10.1016/S0967-0637(98)00070-3.

Murakami, H., Antoine, D., Vellucci, V., & Frouin, R. (2022). System vicarious calibration of GCOM-C/SGLI visible and near-infrared channels. *Journal of Oceanography*, *78*(4), 245–261. https://doi.org/10.1007/s10872-022-00632-x.

Ng, B., Cai, W., & Walsh, K. (2014). The role of the SST-thermocline relationship in Indian Ocean Dipole skewness and its response to global warming. *Scientific Reports*, *4*, 1–6. https://doi.org/10.1038/srep06034.

Ningsih, N. S., Rachmayani, R., Hadi, S., & Brodjonegoro, I. S. (2010). Internal Waves Dynamics in The Lombok Strait Studied by A Numerical Model. *International Journal of Remote Sensing and Earth Sciences (IJReSES)*, *5*(1), 17–33. https://doi.org/10.30536/j.ijreses.2008.v5.a1226.

Norel, M., Kałczyński, M., Pińskwar, I., Krawiec, K., & Kundzewicz, Z. W. (2021). Climate variability indices—a guided tour. *Geosciences (Switzerland)*, *11*(3), 1–27. https://doi.org/10.3390/geosciences11030128.

Nugroho, D., Koch-Larrouy, A., Gaspar, P., Lyard, F., Reffray, G., & Tranchant, B. (2018). Modelling explicit tides in the Indonesian seas: An important process for surface sea water properties. *Marine Pollution Bulletin*, *131*(June), 7–18. https://doi.org/10.1016/j.marpolbul.2017.06.033.

Ogata, K., Toratani, M., & Murakami, H. (2017). GCOM-C/SGLI Level 2 Ocean color products generation. *2017 IEEE International Geoscience and Remote Sensing Symposium (IGARSS)*, 5648–5649. https://doi.org/10.1109/IGARSS.2017.8128287.

Ortiz-Suslow, D. G., Wang, Q., Kalogiros, J., Yamaguchi, R., de Paolo, T., Terrill, E., Shearman, R. K., Welch, P., & Savelyev, I. (2019). Interactions Between Nonlinear Internal Ocean Waves and the Atmosphere. *Geophysical Research Letters*, *46*(15), 9291–9299. https://doi.org/10.1029/2019GL083374.

Osborne, A. R., & Burch, T. L. (1980). Internal solitons in the Andaman Sea. *Science*, *208*(4443), 451–460. https://doi.org/10.1126/science.208.4443.451.

Prasetia, R., As-syakur, A. R., & Osawa, T. (2013). Validation of TRMM Precipitation Radar satellite data over Indonesian region. *Theoretical and Applied Climatology*, *112*(3–4), 575–587. https://doi.org/10.1007/s00704-012-0756-1.

Purwandana, A., Cuypers, Y., & Bouruet-Aubertot, P. (2021). Observation of internal tides, nonlinear internal waves and mixing in the Lombok Strait, Indonesia. *Continental Shelf Research*, *216*(December 2020), 104358. https://doi.org/10.1016/j.csr.2021.104358.

Purwandana, A., Cuypers, Y., Surinati, D., Iskandar, M. R., & Bouruet-Aubertot, P. (2023). Observed internal solitary waves in the northern Bali waters, Indonesia. *Regional Studies in Marine Science*, *57*, 102764. https://doi.org/10.1016/j.rsma.2022.102764.

Ramp, S. R., Tang, T. Y., Duda, T. F., Lynch, J. F., Liu, A. K., Chiu, C. S., Bahr, F. L., Kim, H. R., & Yang, Y. J. (2004). Internal solitons in the northeastern South China Sea Part I: Sources and deep-water propagation. *IEEE Journal of Oceanic Engineering*, *29*(4), 1157–1181. https://doi.org/10.1109/JOE.2004.840839.

Robinson, I. S. (2010). *Discovering the Ocean from Space*. Springer - Praxis Publishing. https://doi.org/10.1007/978-3-540-68322-3.

Shroyer, E. L., Moum, J. N., & Nash, J. D. (2010). Energy transformations and dissipation of nonlinear internal waves over New Jersey's continental shelf. *Nonlinear Processes in Geophysics*, *17*(4), 345–360. https://doi.org/10.5194/npg-17-345-2010.

Sprintall, J., Gordon, A. L., Koch-Larrouy, A., Lee, T., Potemra, J. T., Pujiana, K., & Wijffels, S. E. (2014). The Indonesian seas and their role in the coupled ocean-climate system. *Nature Geoscience*, *7*(7), 487–492. https://doi.org/10.1038/ngeo2188.

Sprintall, J., Gordon, A. L., Wijffels, S. E., Feng, M., Hu, S., Koch-Larrouy, A., Phillips, H.,

Nugroho, D., Napitu, A., Pujiana, K., Dwi Susanto, R., Sloyan, B., Yuan, D., Riama, N. F., Siswanto, S., Kuswardani, A., Arifin, Z., Wahyudi, A. J., Zhou, H., … Setiawan, A. (2019). Detecting change in the Indonesian seas. *Frontiers in Marine Science*, *6*(JUN). https://doi.org/10.3389/fmars.2019.00257.

Sun, L., Liu, Y., Meng, J., Fang, Y., Su, Q., Li, C., & Zhang, H. (2024). Internal solitary waves in the central Andaman Sea observed by combining mooring data and satellite remote sensing. *Continental Shelf Research*, *277*(January), 105249. https://doi.org/10.1016/j.csr.2024.105249.

Susanto, R. D., Gordon, A. L., & Sprintall, J. (2007). Observations and proxies of the surface layer throughflow in Lombok Strait. *Journal of Geophysical Research: Oceans*, *112*(C03S92), 1–11. https://doi.org/10.1029/2006JC003790.

Susanto, R. D., Mitnik, L., & Zheng, Q. (2005). Ocean Internal Waves Observed in the Lombok Strait. *Oceanography*, *18*(4), 125–132. https://doi.org/10.5670/oceanog.2005.08.

Syamsudin, F., Kaneko, A., & Haidvogel, D. B. (2004). Numerical and observational estimates of Indian Ocean Kelvin wave intrusion into Lombok Strait. *Geophysical Research Letters*, *31*(L24307), 1–4. https://doi.org/10.1029/2004GL021227.

Syamsudin, F., Taniguchi, N., Zhang, C., Hanifa, A. D., Li, G., Chen, M., Mutsuda, H., Zhu, Z. N., Zhu, X. H., Nagai, T., & Kaneko, A. (2019). Observing Internal Solitary Waves in the Lombok Strait by Coastal Acoustic Tomography. *Geophysical Research Letters*, *46*(17–18), 10475–10483. https://doi.org/10.1029/2019GL084595.

Tao, M., Xu, C., Guo, L., Wang, X., & Xu, Y. (2022). An Internal Waves Data Set from Sentinel-1 Synthetic Aperture Radar Imagery and Preliminary Detection. *Earth and Space Science*, *9*(12). https://doi.org/10.1029/2022EA002528.

Tensubam, C. M., Raju, N. J., Dash, M. K., and Barskar, H. (2021). Estimation of internal solitary wave propagation speed in the Andaman Sea using multi–satellite images. *Remote Sensing of Environment*, *252*(October 2019), 112123. https://doi.org/10.1016/j.rse.2020.112123.

Vrećica, T., Pizzo, N., & Lenain, L. (2022). Airborne Observations of Shoaling and Breaking Internal Waves. *Geophysical Research Letters*, *49*(21), 1–10. https://doi.org/10.1029/2022GL100622.

Walsh, E. J., Pinkel, R., Hagan, D. E., Weller, R. A., Fairall, C. W., Rogers, D. P., Burns, S. P., & Baumgartner, M. (1998). Coupling of internal waves on the main thermocline to the diurnal surface layer and sea surface temperature during the Tropical Ocean-Global Atmosphere Coupled Ocean-Atmosphere Response Experiment. *Journal of Geophysical Research*, *103*(C6), 12613–12628.

Wang, C., Wang, X., & da Silva, J. C. B. (2019). Studies of internal waves in the Strait of Georgia based on remote sensing images. *Remote Sensing*, *11*(1). https://doi.org/10.3390/rs11010096.

Wang, X., Wang, J., Zhang, X., & Liu, J. (2025). SWOT observation revealed internal solitary wave characteristic variations in the Lombok Strait. *Journal of Oceanology and Limnology*, *2019*. https://doi.org/10.1007/s00343-025-5033-0.

Wirasatriya, A., Susanto, R. D., Kunarso, K., Jalil, A. R., Ramdani, F., & Puryajati, A. D. (2021). Northwest monsoon upwelling within the Indonesian seas. *International Journal of Remote Sensing*, *42*(14), 5437–5458. https://doi.org/10.1080/01431161.2021.1918790.

Woodson, C. B. (2018). The fate and impact of internal waves in nearshore ecosystems. *Annual Review of Marine Science*, *10*, 421–441. https://doi.org/10.1146/annurev-marine-121916-063619.

Zhang, S., Li, X., & Zhang, X. (2023). Internal Wave Signature Extraction from SAR and Optical Satellite Imagery Based on Deep Learning. *IEEE Transactions on Geoscience and Remote Sensing*, *61*, 1–16. https://doi.org/10.1109/TGRS.2023.3258189.

Zhang, Y., Hong, M., Zhang, Y., Zhang, X., Cai, J., Xu, T., & Guo, Z. (2023). Characteristics of Internal Solitary Waves in the Timor Sea Observed by SAR Satellite. *Remote Sensing*, *15*(11). https://doi.org/10.3390/rs15112878.

Zheng, Q., Susanto, R. D., Ho, C. R., Song, Y. T., & Xu, Q. (2007). Statistical and dynamical analyses of generation mechanisms of solitary internal waves in the northern South China Sea. *Journal of Geophysical Research: Oceans*, *112*(3), 1–16. https://doi.org/10.1029/2006JC003551.

Zhu, Q., & Wang, C. (2024). Contributions of Indo-Pacific Forcings to Interannual Variability of the Indonesian Throughflow in the Upper and Lower Layers. *Journal of Geophysical Research: Oceans*, *129*(1). https://doi.org/10.1029/2023JC020306.